VISION-BASED AUTONOMOUS ROBOT BODY ALIGNMENT FOR COPPER WIRE SPOOL PICK UP

MOHD RAZALI BIN DAUD
SHALFARINA BINTI SHAHRIMAN
AHMAD AFIF BIN MOHD FAUDZI
MOHD HERWAN BIN SULAIMAN
ADDIE IRAWAN BIN HASHIM
ZULKIFLI BIN MUSA

RESEARCH VOT NO:
RDU1703143

Faculty of Electrical & Electronics Engineering Technology
Universiti Malaysia Pahang

2019

ACKNOWLEDGEMENTS

Firstly, all praises and thanks to Allah S.W.T. for Allah's mercy and grace to me and all my life. Without His mercy, this thesis will not be completed.

I wish to express my profound gratitude to Research & Innovation Department, Universiti Malaysia Pahang their financial during the full term of this research.

This project would not be completed without help and guidance from fellow researchers, Shalfarina Binti Shahriman, Ahmad Afif bin Mohd Faudzi, Mohd Herwan Bin Sulaiman, Addie Irawan Bin Hashim and Zulkifli Bin Musa. Their comments, suggestions and encouragement give me a strength to carry out this research until the end. A very big thank to my students; Farah Adiba Binti Azman and Thilainaathan A/L Sivaraman for their endless effort in helping and completing this research.

Last but not least, I would like to thank the Faculty of Electrical & Electronics Engineering Technology (FTKEE) for allowing our team to use facilities and equipment related to this project.

ABSTRAK

PENJAJARAN BADAN ROBOT SECARA AUTOMATIK UNTUK MENGANGKAT KILI WAYAR TEMBAGA BERDASARKAN SISTEM PENGLIHATAN KAMERA

(Kata kunci: robot automatik, peg-in-hole, pengamatan kamera, Transformasi Bulatan Hough)

Sistem yang mudah, murah dan berkesan dalam melaksanakan tugas yang diperlukan adalah menjadi pilihan dalam industri. Tugas *peg-in-hole* digunakan secara meluas dalam proses pembuatan dengan menggunakan sistem penglihatan dan *sensor* yang tinggi kosnya dan memerlukan algoritma yang kompleks. Proses mengambil kili wayar tembaga yang disusun bersebelahan di atas satu rak juga menggunakan konsep *peg-in-hole.* Pada masa ini, robot seperti *forklift* yang dikawal secara berwayar digunakan. Walaubagaimnapun, agak sukar bagi pengendali untuk memastikan penarik dimasukkan dengan betul ke dalam lubang (masalah *peg-in-hole*) kerana struktur robot. Dalam kajian ini, sistem penglihatan dibuat untuk menyelesaikan masalah *peg-in-hole* dengan membolehkan robot untuk melaksanakan secara automatik kaedah pemasukan dan mengangkat kili tanpa menggunakan sebarang sensor kecuali kamera kos rendah. Kamera kos rendah digunakan untuk mengambil imej kili wayar tembaga dalam video masa nyata. Diilhamkan oleh bagaimana manusia melihat orientasi objek berdasarkan bentuknya, sistem dibuat untuk menentukan orientasi kamera berdasarkan bentuk kili dan sudut *yaw* dari pusat kamera (CFOV) ke CHS. Prestasi sistem yang dicadangkan dianalisa berdasarkan analisis kadar pengesanan. Projek ini dibangunkan dengan menggunakan perisian MATLAB. Analisis dilakukan dalam persekitaran terkawal dengan kadar jarak 50-110 cm kamera ke kili. Di samping itu, orientasi kamera dianalisa di antara kadar sudut *yaw* -20^{o} hingga 20^{o} . Untuk memastikan penarik tidak akan berlanggar dengan kili, persamaan matematik dibuat untuk mengira toleransi penarik. Dengan menggunakan sistem ini, sistem boleh menganggarkan kedudukan kili berdasarkan orientasi kamera dan pengiraan jarak. Penggunaan sistem ini adalah mudah dan kos efektif. Kaedah *Modified Circular Hough Transform* (MCHT) dicadangkan dan diuji dengan kaedah yang sedia ada iaitu kaedah *Circular Hough Transform* (CHT) untuk membuang bulatan yang salah. Hasil analisis menunjukkan kadar kejayaan pengesanan 96% berbanding dengan kaedah CHT. Sistem yang dicadangkan dapat mengira jarak dan orientasi kamera berdasarkan keadaan imej kili dengan kadar ralat yang rendah. Oleh itu, ia menyelesaikan masalah *peg-in-hole* tanpa menggunakan *Force/Torque sensor*. Sebagai kesimpulan, sejumlah 7 analisis yang terdiri daripada analisis pemprosesan imej, segmentasi imej, klasifikasi objek, perbandingan antara CHT dan MCHT, pengukuran pencahayaan, pengiraan jarak dan *yaw angle* telah diuji secara eksperimen termasuk perbandingan dengan kaedah yang sedia ada. Sistem yang dicadangkan dapat mencapai semua objektif.

Para Penyelidik : PM Dr. Mohd Razali bin Daud, Pn. Shalfarina binti Shahriman, Dr. Ahmad Afif bin Mohd Faudzi, PM. Dr. Mohd Herwan bin Sulaiman, Ir. Dr. Addie Irawan, En. Zulkifli bin Musa

Email: mrazali@ump.edu.my
Tel. No: 09-4246048
Vote No: RDU1703143

ABSTRACT

VISION-BASED AUTONOMOUS ROBOT BODY ALIGNMENT FOR COPPER WIRE SPOOL PICK UP

(Keywords: Autonomous robot, peg-in-hole, vision system, Circular Hough Transform)

A simple, inexpensive system and effective in performing required tasks is the most preferable in industry. The peg-in-hole task is widely used in manufacturing process by using vision system and sensors but costly and needs complex algorithm. Picking up process of copper wire spools which are arranged side by side on a rack is also applying peg-in-hole concept. Currently, a forklift-like robot controlled using wired controllers is used. However, it is difficult for the operator to ensure the stem is properly inserted into the hole (peg-in-hole problem) because of the structure of the robot. However, the holder design is not universal and not applicable to other companies. The spool can only be grasped and pulled out from the front side and cannot be grasped using robot arm and gripper. In this study, a vision system is developed to solve the peg-in-hole problem by enabling the robot to autonomously perform the insertion and pick up the spool without using any sensors except a low-cost camera. A low-cost camera is used to capture images of copper wire spool in real-time video. Inspired by how human perceive an object orientation based on its shape, a system is developed to determine camera orientation based on the spool image condition and yaw angle from the center of the camera (CFOV) to CHS. The performance of the proposed system is analyzed based on detection rate analysis. This project is developed by using MATLAB software. The analysis is done in controlled environment with 50-110 cm distance range of camera to the spool. In addition, the camera orientation is analyzed between -20º to 20º yaw angle range. In order to ensure the puller will not scratch the spool, a mathematical equation is derived to calculate the puller tolerance. By using this, the system can estimate the spool position based on the camera orientation and distance calculation. Application of this system is simple and cost-effective. A Modified Circular Hough Transform (MCHT) method is proposed and tested with existing method which is Circular Hough Transform (CHT) method to eliminate false circles and outliers. The results of the analysis showed detection success rate of 96% compared to the CHT method. The proposed system is able to calculate the distance and camera orientation based on spool image condition with low error rate. Hence, it solves the peg-in-hole problem without using Force/Torque sensor. In conclusion, a total of 7 analysis consist of image pre-processing, image segmentation, object classification, comparison between CHT and MCHT, illumination measurement, distance calculation and yaw angle analysis were experimentally tested including the comparison with the existing method. The proposed system was able to achieve all the objectives.

Key researchers : Assoc. Prof. Dr. Mohd Razali bin Daud, Mdm. Shalfarina binti Shahriman, Dr. Ahmad Afif bin Mohd Faudzi, Assoc. Prof. Dr. Mohd Herwan bin Sulaiman, Ir. Dr. Addie Irawan, En. Zulkifli bin Musa

Email: mrazali@ump.edu.my
Tel. No: 09-4246048

Vote No: RDU1703143

TABLE OF CONTENT

LIST OF TABLES

LIST OF FIGURES

LIST OF SYMBOLS

D_{bc}	Distance between BC center and SC center
R_1	Radius 1
R_2	Radius 2
X_1, Y_1	BC coordinate
X_2, Y_2	SC coordinate
x	Left and right moves
y	Front and back moves
z	Height of camera
θ_{real}	Yaw angle of camera
θ_{pixel}	Yaw angle of camera in pixel unit
FL	Focal length
ROH	Real object height
FH	Frame height
SH	Sensor height
OH	Object height
m	Horizontal resolution
n	Vertical resolution
D	Distance
DC_1	Distance between RC and BC
DC_2	Distance between RC and SC
t_f	Tolerance between puller and SC
P_d	Puller diameter
SC_d	SC diameter
P_r	Puller radius
SC_r	SC radius

LIST OF ABBREVIATIONS

ACED	Adaptive Canny edge detection
ANN	Artificial Neural Network
BC	Big circle
CACD	Curvature aided HT for circle detection
CFOV	Center line of camera FOV
CHS	Center hole of spool
CHT	Circular Hough Transform
DMP	Dynamic Motor Primitives
DOF	Degree of Freedom
EHT	Extended Hough Transform
F/T	Force/Torque
FOV	Field of View
HSV	Hue-Saturation-Value
IAS	Intuitive assembly strategy
MCHT	Modified CHT
PAP	Passive alignment principle
PD	Proportional derivatives
POI	Points of Interests
RANSAC	Random Sample Consensus
RC	Reference center
RCD	Randomized circle detection
RGB	Red-Green-Blue
S1	Switch 1
S2	Switch 2
S3	Switch 3
SC	Small circle
SURF	Speeded-up Robot Features
ToF	Time-of-Flight

CHAPTER 1

INTRODUCTION

1.1 Background of Study

All industries are moving toward automation either for quality improvement or cost down purposes. Robotic manipulator is broadly used in manufacturing process since it is a reliable system to maintain productivity and quality. Typically, tasks performed by the manipulators can be categorized into two types which are grasping and insertion (peg-in-hole). For the grasping tasks, the robot manipulator is required to grasp object on its outer side. On the other hand, the manipulator should hold an object using it's fingers and insert it into another object, such as inserting a few centimetres of a straight plug into an elastic rubber hose or inserting a shaft into O-ring. Almost all of the above mentioned tasks are performed by 6 to 8 Degree of Freedom (DOF) robot manipulator equipped with a force or torque sensors. Some of the grasping tasks utilized an expensive camera, or a camera with a laser range finder to confirm the orientation of the object. After the object has been grasped, force or torque sensor will be used to autonomously adjust the grasping force or adjust the position of the peg, in the case of insertion process. However, the sensors are very costly and requires complicated algorithm to be implemented. There are some grasping tasks without utilizing with any sensors and used stereo vision camera instead, to measure the distance between the robot and the object. The system requires depth image from two cameras to develop an algorithm. Problems such as lighting, occlusions, and distortions can be occurred by using a vision system (Tsarouchi et al., 2016). Hence, stereo vision camera also requires complex algorithm to be implemented.

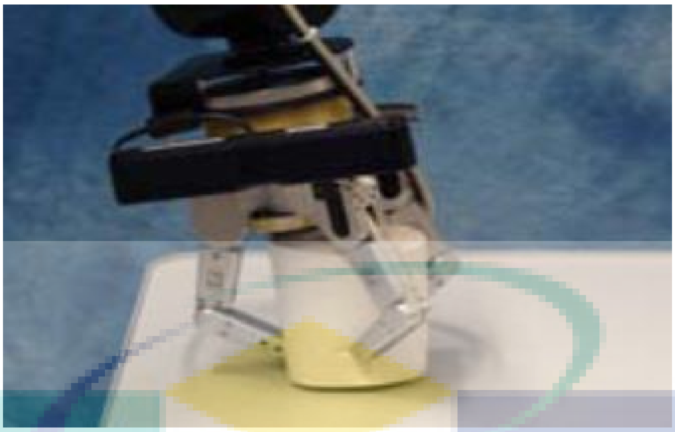

(a)

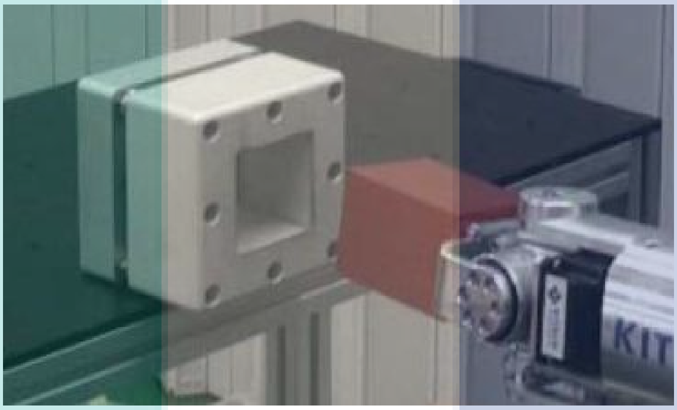

(b)

Figure 1.1 Robot manipulator tasks (a) Grasping tasks (b) Insertion (peg-in-hole)
Source: C. Eppner & O. Brock (2014) and H. Park et al. (2013)

This study focuses on peg-in-hole task because it is the most preferred assembly task performed by a robot manipulator and the industries are moving to autonomous robot system. The tasks performed by manipulator has the certainty of knowing the precise hole location compared to the task performed by operator. The manipulator inserts the peg into the hole with the calculated hole location. While an operator does not require the exact hole location (H. Park et al., 2013). However, the robot at Vacuumschmelze (M) Sdn. Bhd. (VAC) is remotely controlled by operator for copper wire spool picking process. The spool is in circular shape and surrounded with copper wires. Figure 1.2 (a) shows a manually controlled forklift as transporter in the picking up process of the spool from the shelf. Figure 1.2 (b) shows the illustration design on how the puller and holders grasped the spool from front view and side view. As can be seen from Figure 1.2 (b), there are three rods used to hold a spool. A puller is attached at the center of the three rods and will be inserted into the center hole of spool (CHS) to pick up the spool. The above process is considered as a peg-in-hole problem. The transporter is built without a vision system and did not use either force sensor or torque sensor. Therefore, the robot's puller and the holders need to be securely aligned with the CHS. This is to ensure that the puller and the holder will not hit the spool body which may cause the spool to drop. However, the spool is positioned so that it will be easily grasped and pulled out from the front side and cannot be grasped using aforementioned gripper designs.

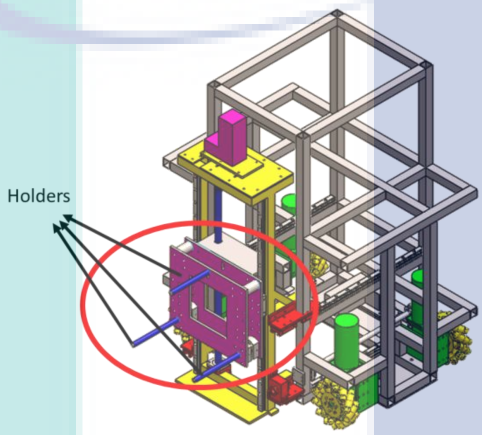

(a)

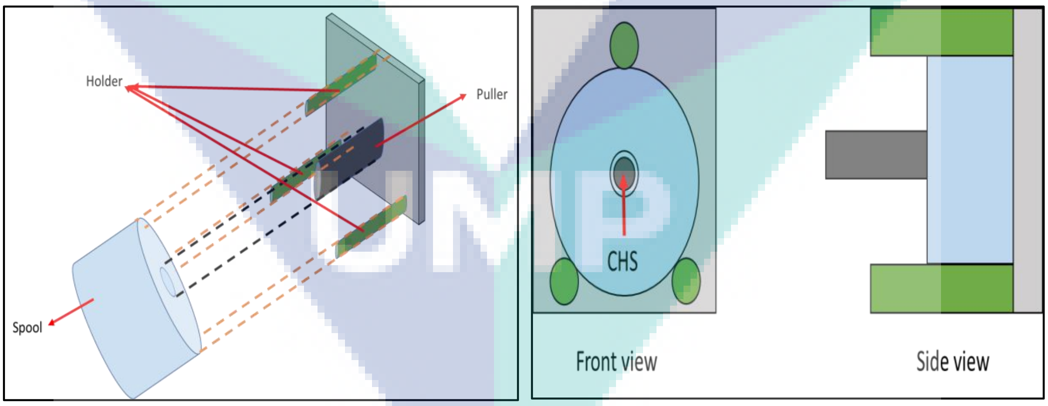

(b)

Figure 1.2 Mechanical design of the robot (a) Full mechanical design of the robot without its camera and puller (b) Illustration design for the puller and holders grasped the spool in front view and side view

With known camera orientation, position and distance will help the robot to take further action before it proceeds to pick up the spool. The position of the camera will be determined based on the distance between the center of the spool image and reference center (RC) plotted in image frame as shown in Figure 1.3. On the other hand, the orientation of the camera will be determined based on the spools' image condition whereby the distance of the camera to the spool will be calculated using distance equation. Once the spool is detected, then it will move forward while confirming the orientation of the spool and camera. In this study, a forklift-liked robot will be equipped with a vision system to ensure the puller inserted smoothly into the CHS with distance calculation and camera orientation calculation but without a force sensor or touch sensor.

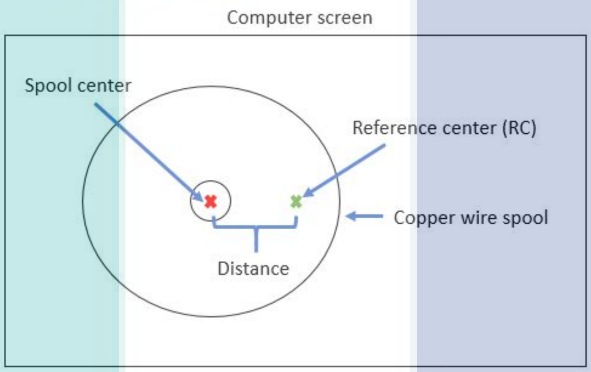

Figure 1.3 Illustration design to determine position of the camera

1.2 Problem Statement

Currently, the robot at Vacuumschmelze (M) Sdn. Bhd. (VAC) is remotely controlled by operator for spool picking process. The system used by VAC is not universal and not applicable for other companies. The main problem here is the conventional method will lead to human error because of the operator's limited capability to view and confirm the alignment of robots' puller and holders with the spool position. If the robot is not accurately aligned, the robot arm may scratch the copper wire and may drop the spool to the floor. However, most of the researches solve the peg-in-hole problem by using robot arm and gripper with utilising some sensors such as force sensor and torque sensor, which are quite expensive and required a complex algorithm. In addition, it needs high DOF mechanism with fine movement. The biggest challenge is the difficulty in image processing such as illumination and orientation checking of the spool and the camera. This research aims to seek the possibility of using a camera without Force/Torque sensor to solve the stated problem using image processing.

1.3 Research Objectives

The objectives of this research are:

i. To develop a vision system for camera orientation without using Force/Torque sensor for peg-in-hole system.

ii. To develop an algorithm for detection and determinate of camera orientation of spool image condition.

iii. To evaluate the performance of proposed vision system based on detection rate by using Modified Circular Hough Transform (MCHT).

1.4 Contribution

The main contribution of this research is the development of a vision system to solve peg-in-hole problem facing by an industry to pick up spools from a storage shelf to another location without damaging another spool at it sides and preventing other spools on the shelves from falling. The vision system assisted by a low-cost camera and the peg-in-hole solution are based on the camera's orientation and calculated distance.

1.5 Scope of Research

The focus of this study is the system development for detection and determination of camera orientation based on spools' image conditions by using MATLAB and Logitech C270 webcam. The scope of this work are:

i. Limited to vision system only in Robotic Lab at Faculty of Electrical & Electronics Engineering (FKEE), Universiti Malaysia Pahang (UMP) with controlled environment.

ii. The illumination value is limited to 98 lx-205 lx. Vision system will provide information about the position and orientation of the camera relative to the spool location only.

iii. Only one size of the spool to be used for experiment (diameter: 35 cm) and the color of the spool is black color.

iv. The distance used for this study is 50-110 cm.

v. The robot used is an existing robot and Modified Circular Hough Transform (MCHT) method is applied for this robot only.

1.6 Thesis Overview

This thesis consists of five chapters including this chapter. In Chapter 1, the introduction of robot manipulator for peg-in-hole task was explained. The problems faced by industry for peg-in-hole task are thoroughly discussed. The scope and objective of this research are mentioned clearly.

In Chapter 2, some reviews were explained. Review on relevant existing vision-based system with peg-in-hole task were surveyed. In addition, review on circular object detection was surveyed too. The advantages and disadvantages of these methods are discussed clearly.

In Chapter 3, the methodology used in this study are explained. The proposed algorithm for camera geometry determination based on circular's shape for peg-in-hole task was explained and developed. The proposed algorithm is described in this chapter includes the description of the approach and its implementation in detail.

In Chapter 4, the experimental results of proposed system for camera geometry determination based on circular's shape for peg-in-hole task were critically discussed. The proposed detection system analysis was explained into three stages which are image processing analysis, morphological analysis and object classification analysis. The proposed camera orientation analysis was presented into two stages which are distance calculation analysis and yaw angle analysis. The fourth chapter presents the results, analysis and discussions of experiments by using the proposed method.

Finally, Chapter 5 gives the concluding remarks from the discussion as well as recommends future works that could be performed.

CHAPTER 2

LITERATURE REVIEW

2.1 Introduction

This chapter reviews the contents of researches that are related to this study. The literature review also will present evidence that supports the need of this research in terms of circle detection, peg-in-hole task and vision-based robot. In general, this chapter presents a critical analysis of research paper on vision-based system, peg-in-hole task, image processing and circle detection. Furthermore, the characteristics, strengths, and weaknesses of the related mentioned area are discussed.

2.2 Vision-based System

There are a lot of methods used in vision system for object recognition. Vision system involves image processing stage which involve existence of dust, lighting, distortions, illumination and occlusions although in indoor environment. Some researchers applied single camera in order to perform the object recognition task. Tsarouchi et al. employs a high -resolution camera and performed the Points of Interest (POI) recognition and method for object detection. It shows that the method is robust against occlusions and lighting conditions when compared to Speeded-Up Robot Features (SURF) and Red-Green-Blue (RGB) color detection algorithm (Tsarouchi et al., 2016). Harada et al. presents a segmentation clustering process by using Asus Xtion whereas K. Cho et al. used a single camera. However, the distortion of captured image tends to be large and it is robust against occlusions. The method allows vision system to measure the position and orientation object by using 3D cloud data (Cho et al., 2013; Harada et al., 2014). A recognition method by using a wireless camera is proposed by R. Soans et al. and R. Deepu et al. Both research groups aimed to detects an object based on its color that needs color thresholding method performed on the system (Deepu et al., 2015; R. Soans et al., 2018). In order to prevent false detections, R. Deepu et al. proposed a method with laser source based on thresholding algorithm whereas R. Soans et al. applied thresholding and morphology opening algorithm to remove unwanted regions. Y. Suzuki et al. employed a Kinect sensor to decrease the false detections and increase the robustness towards lighting and occlusions (Suzuki et al., 2015). H. Ali et al. proposed a thresholding and bounding box method by using web camera. It is able to detect the object based on its color and shape (Ali et al., 2018).

Figure 2.1 Asus Xtion sensor
Source: https://www.asus.com/us/3D-Sensor/Xtion_PRO_LIVE/

Figure 2.2 Kinect sensor
Source: https://electronics.howstuffworks.com/microsoft-kinect2.htm

Some researchers used stereo vision system on a robot for object tracking and recognition in order to measure the distance between robot and object. F. Suligoj et al. and K. Mironov et al. proposed circular object tracking by using Circular Hough Transform (CHT) and other additional methods such as HSV, SURF and Random Sample Consensus (RANSAC) method (K. Mironov, 2017; Šuligoj et al., 2014). However, the precisions requirement is not satisfied although the system used additional sensors. The distance is measured by using Euclidian distance equations.

(Šuligoj et al., 2014). Next, J. Shim et al. opines that by using two surveillance cameras, the object can be detected. The method does not require additional sensors. The object is detected by using HSV color thresholding method. However, it is less accurate in terms of detection (Shim & Cho, 2015). H. Ukida et al. highlights that binocular stereo camera able to track an object by using template matching method. In addition, it is able to estimate the position of the object. Next, A. Cangelosi highlights that Bumblebee stereo camera able to track an object and measure distance by using image processing techniques (Cangelosi et al., 2016). The blob analysis method is used to track an object is presents by T. Luu et al. It produces a good detection for simple color images (Luu & Tran, 2015).

Figure 2.3 Bumblebee camera (Stereo head A) on 2 DOF robot
Source: A. Cangelosi et al. (2016).

Some of the researchers used distance measurement to track an object. Stereo vision system is widely used to measure distance between robot and object. Stereo vision needs a good calibration between two cameras. It is because vision system is dealing with noise, light and occlusions. However, stereo vision system needs to deal with the digital calibration as it can produces error to distance measurement (Luu & Tran, 2015). The calibration process is a process to find and correct the parameters of the camera such as lens distortions and lens misalignment (Cangelosi et al., 2016). Additionally, single camera also can measure distance between object and robot. R. Deepu measured the distance by using laser beam and it involves the focal length of the camera (Deepu et al., 2015). Another approach is presents by A. Troppan et al. to measure the distance without using any sensors. A Kalman filter is used to detect the spherical object based on color thresholding method. The distance can be calculated by assuming that the robot is at the origin of the coordinates and the object is on the ground plane. The aforementioned relationship between object's contact point and ground plane is able to calculate the distance (Troppan et al., 2013). In addition, there are distance formula on education website to calculate the distance between object and robot by using single camera. However, there are no prior analysis regarding that formula is used for research purposes.

As summary, most of the researchers used single or stereo camera for object recognition. Some of them employ a sensor and laser beam to increase the accuracy of detection. By using a sensor, it increases the project cost. There are disadvantages using a stereo camera which is it needs calibration process from both cameras because vision system needs to deal with occlusions and distortion problems. It can produce less accuracy if the calibration produces an error. Next, detection based on object color making the system less reliable because lighting or illumination factor can affect the color itself. Most of the researchers applied thresholding method in order to remove unwanted image and noise. Generally, an expensive camera with high resolution able to track an object accurately compared to low resolution camera. However, there are low cost camera such as webcam can performed this task accurately depends on its algorithm and the environment factor. All the summary of the literature review for vision-based system is summarizes in Table 2.1.

Table 2.1 Summary table for vision-based system

Title	**Author/Year**	**Technique**	**Results**	**Gaps**
A Method for Detection of Randomly Placed Objects for Robotic Handling.	Tsarouchi et al. (2016).	-SURF and RGB. -2D vision sensor. -MATLAB.	-Robust against occlusions and lighting conditions for object recognition task.	-Color detection method. -High resolution camera.
Project on Development of a Robot System for Random Picking.	Harada et al. (2014).	-Low cost camera sensor (Asus Xtion). -3D cloud data.	-Robust against occlusions. -Distortion of captured image tends to be large.	-Camera with sensor.
Path Generation for Robot Navigation using a Single Camera.	R. Deepu et al. (2015).	-Using single wireless camera and a laser source. -Thresholding method. -Static environment.	-Able to detect obstacles, floor flaws and depth is estimated through single camera.	-Use laser beam to detect an obstacle.

Object tracking robot using adaptive color thresholding.	R. Soans et al. (2018).	-Single camera and ultrasonic sensor. -Opening & thresholding, method. -MATLAB and Arduino.	-The various problems that arise and leads to false object identification. -Lightning conditions problems.	-Ultrasonic sensor.
Unknown-color spherical object detection and tracking.	A.Troppan et al. (2013).	-Kalman filter and HSV. -Thresholding method. -Single camera.	-Can detect spherical shape without using ay sensor.	-Color detection method.
Grasping Strategy for Moving Object using Net-Structure Proximity Sensor and Vision Sensor.	Y. Suzuki et al. (2015).	-Proximity sensor and Kinect sensor. -RGB.	-Robust and responsive.	-Use sensors. -Color detection method.
Vision-based Robot Manipulator for Industrial Applications.	H. Ali et al. (2018).	-Thresholding and bounding box method. -Web camera. -MATLAB, Scorbase and Visual basics.	-Successfully perform pick-and-place operation based on size, color and shape.	-Offline image processing..
Object Tracking with a Multiagent Robot System and a Stereo Vision Camera.	F. Šuligoj et al. (2014).	-Stereo vision and sensor. -CHT, HSV and SURF method. -OpenCV.	-Precisions requirement is not satisfied.	-Stereo vision camera. -Utilises sensor.
Transport by robotic throwing and catching: Accurate stereo tracking of the spherical object.	K. Mironov (2017).	-HSV, SURF, CHT and RANSAC. -Canny edge detection.	-Precisions requirement is not satisfied.	-Stereo vision camera.
A Mobile Robot Localization using External Surveillance Cameras at Indoor.	J. Shim & Y. Cho (2015).	-2D mapping, HSV and thresholding. -2 remote ceiling-mounted cameras.	-Successfully maneuverer to destination position using only the 2D map without help of any other sensors.	-2 remote ceiling-mounted cameras.
Object tracking system by adaptive pan-tilt-zoom cameras and arm robot.	H. Ukida et al. (2012).	-Template-matching. -Stereo camera. -OpenCV.	-Able to estimate the position of the object.	-Stereo camera.
Stereo Vision	A. Cangelosi	-Bumblebee	-Able to measure	-Stereo vision

based Object Tracking Control for a Movable Robot Head.	et al. (2016).	stereo camera – Fuzzy logic and color thresholding. -MATLAB.	distance by using camera. -Less computational time.	camera.
3D vision for mobile robot manipulator on detecting and tracking target.	T. Luu & T. Tran (2015).	-Blob analysis and color thresholding. -Stereo camera.	-Can adapt distance measurement in an expected range with high accuracy.	-Stereo vision camera.

2.3 Peg-in-Hole Task

The peg-in-hole problems are widely discussed in robotic research due to complexity in applying control algorithm that requires position and force feedback. The peg-in-hole task usually performed by 6 to 7 DOF manipulator robot with use of Force and Torque (F/T) sensor. There are two shapes of peg commonly used in industries which are circular peg and square peg. Abdullah et al. proposed a peg-in-hole task for circular peg by using two high speed cameras and F/T sensor. The vision system is done by thresholding method and it produces 40% accuracy estimation of angles (Abdullah, Roth, Weyrich, & Wahrburg, 2015). Y. Zheng et al. presents a 3D point clouds and Time-of-Flight (ToF) sensor in order to detect the potential risk of collisions in static scenario. The system able to achieve the objectives without using vision system (Zheng et al., 2017). Next, Y. Kim et al. proposed a shape recognition algorithm so that the system can estimate the shape and location of the hole. The method produces 6% error rate and it can be applied to circular and square peg (Kim et al., 2012). Some of researchers avoid using vision system and employ F/T sensor for both arms by using dual arm robot. Therefore, the robot does not need to measure the position and orientation of the robot. I. Jasim et al. highlights a peg-in-hole task using Cartesian and Torque forces for circular peg (Jasim et al., 2014). D. Ortega et al. used a gripper and Artificial Neural Network (ANN) to perform the peg-in-hole task. The location of the peg was unknown and the information from the environment minimal without using vision system (Ortega-Aranda et al., 2017). D. Park et al. highlights a contact phase estimation by using F/T sensor. However, the contact phase estimation is estimated by using threshold values for F/T sensor produces low accuracy (D. Park et al, 2012). J. Takahashi et al. presents that the novel mating technique based on passive alignment principle (PAP) produces 97.8% success rate for peg-in-hole task (Takahashi et al., 2016). In addition, Y. Zheng et al. proposed peg-in-hole assembly based on hybrid vision or force guidance and dual-arm coordination. The method has been tested on round, triangle and square shaped parts and it produce 90% success rate. This method also performed by multiple cameras which are on the upper part of the robot, left and right arm of the robot (Zheng et al., 2017).

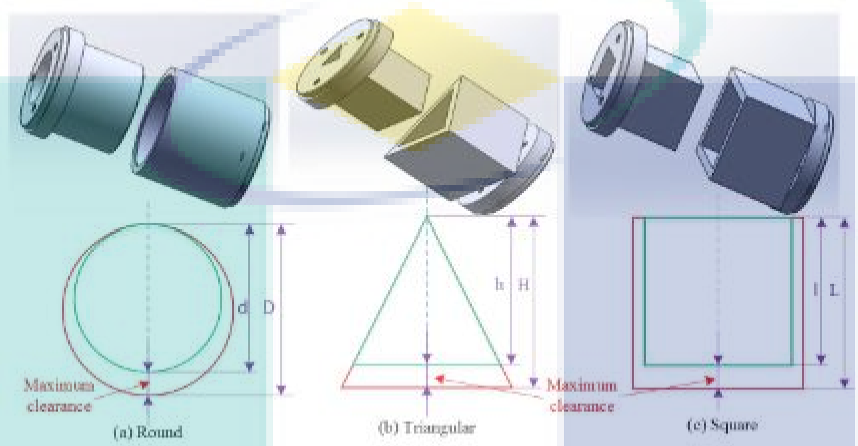

Figure 2.4 Three kinds of parts for peg-in-hole assembly tasks
Source: Y. Zheng et al. (2017).

Next, K. Zhang et al. highlighted that states and jamming analysis with force control strategies can solve peg-in-hole problem for flexible dual peg-in-hole assembly. However, it cannot used for high speed assembly task although force sensor is applied on the robot gripper (Zhang et al., 2018). Performances of matrices and systematic data analysis strategy is proposed by M. Culleton et al. The system used 6 DOF manipulator with F/T sensor to solve the insertion task at a comparable level (Culleton et al., 2018). The use of F/T sensor indeed increases the accuracy of peg-in-hole task. However, it increases the budget at once. This encourages further research to solve the problem without using any sensor and reduce the budget at once. H. Park et al. proposed a peg-in-hole assembly method without passive compliance mechanisms and sensors to overcome the unavoidable positional uncertainty of the hole incurred in the recognition process. The experiment was succeed using an 8 DOF anthropomorphic arm, single camera and CHT method for cylindrical peg (H. Park et al., 2017). L. Lin et al. opines that by using multiple cameras such as Bumblebee, Kinect and stereo camera, it produces high success rate of insertion task. The insertion task is relying on Dynamic Motor Primitives (DMP) method and does not require any sensors (L. Lin et al., 2015).

W. Chang et al. used two fixed cameras and performed the insertion task by using feature extraction process. It is able to solve the assembly task with high success rate (Chang & Wu, 2017).

R. Jain et al. presents a proportional derivatives (PD) controller to actuate the gripper to get desired force. The system is performed by using two cameras which are attached to front and back of the robot. The performance for peg-in-hole assembly is improved by using this method (Jain et al., 2013). In addition, S. Huang et al. employ two high speed cameras and it produces 85% success rate by using image feature extracting algorithm. The failures mainly resulted from the noises of the image (Huang et al., 2013). Meanwhile, J. Bae et al. proposed an intuitive assembly strategy (IAS) that does not need a precise location of hole. The method employs a hybrids force/position control and passive compliance control to perform the assembly task. The method produces 100% success rate in unlimited time (H. Park et al., 2013). L. Debortoli et al. presents a peg-in-hole task solution by using UR5 robot equipped by standard gripper without using any sensor. The method produces 96.7% success rate for insertion task with three trials (Debortoli et al., 2017). Another approach by using simulation platform is presents by N. Liu et al. by using machine learning method. The simulation platform based on ROS and Gazebo. ROS is a robot middleware whereas Gazebo is a well-designed robot simulator. The peg-in-hole task can be collected in real-time by using Gazebo with F/T sensor (Liu et al., 2018). J. Xu et al. used model driven deep deterministic policy gradient (MDDPG) algorithm to perform multiple peg-in-hole assembly tasks although the contact force simulator cannot accurately estimate the contact forces. The simulation training results cannot be applied in realistic experiments because the results are totally different. It shows that the peg-in-hole task must be perform in real-time experiments to ensure the success rate (Xu et al., 2018).

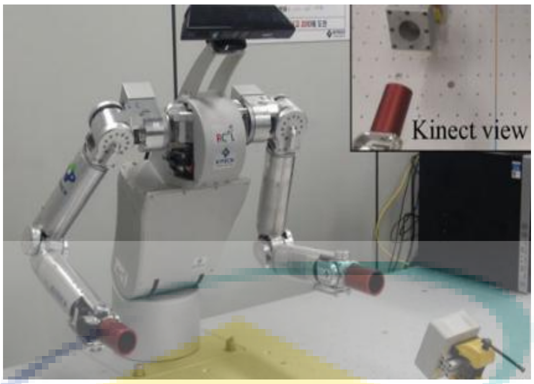

Figure 2.5 8 DOF anthromorphic arm
Source: H. Park et al. (2017).

From the literature review, there are lots of research in using an F/T sensor for the peg-in-hole task to increase the accuracy of the insertion task. However, using additional sensors increases the cost of the project. Therefore, some research did not use any sensor to perform the peg-in-hole task. The selection of the camera also affects the performance of the peg-in-hole task. Thus, some research used a stereo camera. As mentioned in the previous literature review, a stereo camera has a complex algorithm as it needs to calculate the depth image from two cameras. There are a few researches used a single camera to perform a peg-in-hole task. However, as far as this literature research has been conducted, there is no literature discussing on peg-in-hole task using aforementioned gripper designs as mentioned in Chapter 1. Most of the peg-in-hole task performed by robotic arm, dual-arm and gripper. All the summary of the literature review for peg-in-hole task is summarizes in Table 2.2.

Table 2.2 Summary review on peg-in-hole task

Title	Author/Year	Technique	Results	Gaps
An approach for Peg-in-Hole Assembling using Intuitive Search Algorithm Based on Human Behaviour and Carried by Sensors Guided	Abdullah et al. (2015).	-Using Force/ Torque sensor and web camera. -Thresholding method. -Peg-in-hole assembling task use robot arm.	-40% accuracy because of the 0.1 mm tolerance.	-Use 6 DOF industrial robot. -Hold a peg using its' fingers and insert into hole.

Industrial Robot.				
Peg-in-hole Assembly based on Hybrid Vision/Force Guidance and Dual-arm Coordination.	Y. Zheng et al. (2017).	-Based on vision/force guidance and dual-arm coordination. -ROS and Ubuntu system.	-90% success rate. -Tested on round-shaped, triangle-shaped and square-shaped parts.	-Use force/torque sensor. -Use dual-arm for peg-in-hole task.
Hole Detection Algorithm for Square Peg-in-Hole using Force-based Shape Recognition.	Y. Kim et al. (2012).	-Shape recognition based on 6 axis F/T sensor and hole detection algorithm. -Use robotic arm.	-Can be implemented on circular peg. -Error within 5% to 8%.	-Use Force/Torque sensor. -Hold a peg using its' fingers and insert into hole.
Position Identification in Force-Guided Robotic Peg-in-Hole Assembly Tasks.	I. Jasim et al. (2014).	A position identification strategy (Cartesian force and torque). -KUKA lightweight robot (robotic arm).	-Excellent performance of the hole position identification.	-Use Cartesian force and torque sensor. -Hold a peg using its' fingers and insert into hole.
Towards Learning Contact States during Peg-in-hole Assembly with a Dual-Arm Robot.	D. Ortega-Aranda et al. (2017).	-ANN and fuzzy logic. -F/T sensor. - Motoman SDA-20 dual-arm robot.	-Industrial manipulators can learn contact states during manipulative tasks using only contact force information.	-Use force/torque sensor. -Use dual-arm robot equipped with gripper.
Assembly phase estimation in the square peg assembly process.	D. Park et al. (2012).	-Contact phase estimation by using F/T sensor. -Thresholding. -Robot arm.	-Low accuracy.	-F/T sensor. -Use robot arm for peg-in-hole task.
Passive Alignment Principle for Robotic Assembly between a Ring and a Shaft with Extremely Narrow Clearance.	J. Takahashi et al. (2016).	-Novel mating technique based on passive alignment principle (PAP). -Force sensor. -6 DOF manipulator.	-Success rate 97.8%.	-Use force sensor. -6 DOF manipulator. -Use gripper to perform peg-in-hole task.
Jamming Analysis and Force Control for Flexible Dual Peg-in-Hole Assembly.	K. Zhang et al. (2018).	-Based on contact states, contact forces, and jamming states analysis. -Use ABB robotic arm.	-The successful rate of 100% for 50 trials.	-Cannot be used for high speed assembly task. -Dual peg-in-hole task. -Hold a peg using its' fingers and

				insert into hole.
Comparative Peg-in-Hole Testing of a Force-Based Manipulation Controlled Robotic Hand.	M. Culleton et al. (2018).	-A peg-in-hole test method with associated metrics. -6 DOF robot manipulator with F/T sensor.	-Increase the performance of peg-in-hole task.	-F/T sensor. -6 DOF manipulator. -Use robotic hand to perform peg-in-hole task.
Compliance-based Robotic Peg-in-Hole Assembly Strategy without Force Feedback.	H. Park et al. (2017).	-8 DOF anthropomorphic arm. -Does not use tactile/force sensor.	-Able to find a suitable ratio between assembly force and position control gain.	-Use 8 DOF anthropomorphic arm.
Peg-in-Hole Assembly Under Uncertain Pose Estimation.	L. Lin et al. (2015).	-Vision-based pose estimation using Dynamic Motor Primitives (DMP). -Use Kinect, Bumblebee stereo and high-resolution cameras.	-The proposed DMP method improved the performance of the challenging peg-in-hole task.	-Use multiple cameras and sensors. -Use robotic hand to perform peg-in-hole task.
SCARA based Peg-in-Hole Assembly using Compliant IPMC Micro Gripper.	R. Jain et al. (2013).	-Use proportional-derivative (PD) controller. -Use two cameras. -Use SCARA robot.	-The vision system shows that compliant IPMC micro gripper helps in correction of error and achieving assembly.	-Use two cameras (mounted at the front and bottom assembly. -Use SCARA robot (gripper).
Fast Peg-and-Hole Alignment using Visual Compliance.	Huang, Murakami et al. (2013).	-Using two high speed cameras and a 3 DOF active peg. -Using 4 DOF robotic arm.	-The success rate about 85%.	-Use two cameras. -Use robotic arm.
Intuitive Peg-in-Hole Assembly Strategy with a Compliant Manipulator.	H. Park et al. (2013).	-Intuitive peg-in-hole assembly strategy (IAS). -Hybrid force/position control. -Using robotic arm.	-100% success rate with unlimited time.	-Force feedback. -Robotic arm.
Peg-in-hole operation using a robot without using external sensors.	L. Debortoli (2017).	-UR5 robot with gripper. -No sensor.	-96.7% success rate.	-Use gripper to insert peg.
A Containerized Simulation	N. Liu et al. (2018).	-Simulation platform for robot	-Provide precise contact force	-Use Gazebo Force/Torque

Platform for Robot Learning Peg-in-Hole Task.		learning PIH task (ROS and gazebo). -Use robotic arm.	clearly.	sensor. -Not applied in real-time. -Use robotic arm.
Feedback Deep Deterministic Policy Gradient with Fuzzy Reward for Robotic Multiple Peg-in-hole Assembly Tasks.	J. Xu et al. (2018).	-Use model-driven deep deterministic policy gradient (MDDPG) algorithm. -Dual peg-in-hole task. -Use 6 DOF robotic arm.	-Can perform multiple peg-in-hole assembly tasks. -The contact force simulator cannot accurately estimate the contact forces.	-Cannot be applied in realistic experiments. -Use robotic arm.

2.4 Image Processing

An image processing method is a cheap algorithm that is widely used for a vision system. Among these image processing techniques are filtering, morphological, thresholding, color detection and many more. Image processing involves 5 stages which are image acquisition, image pre-processing, image segmentation, feature extraction and object classification. Image processing needs to deal with some factors such as noise in image, occlusions and illumination. Hence, image pre-processing and image segmentation stage is the important stage in order to remove unwanted noise in image.

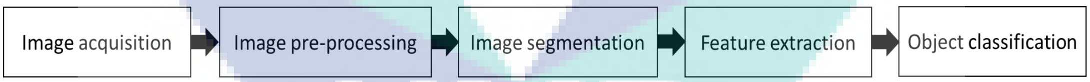

Figure 2.6 Steps for image processing
Source: Norsyahirah et al. (2015).

In pre-processing stage, all the noise is removed prior to processing step. An enhancement and improvement of the images are done in this stage. The process for image denoising includes image filtering and color processing (Fu & Han, 2012). Color processing requires complex algorithm and the detection is very limited because it depends on the color of the object. Hence, image filtering is most preferred compared in order to remove noise in image. Some researchers proposed Unsharp filter to remove noisy background in image. V. Hari et al. presents Unsharp filter with Canny edge detection to enhance the fingerprints image whereas M. Bhuyan proposed an Unsharp filter to highlights edge, corners and fine details of image. The proposed method gives quite reliable and consistent results for different modalities of images (Hari et al., 2013; Bhuyan et al., 2018). Another approach by using Unsharp filter is presents by S. Lin et al. for color image enhancement. Results of enhanced images had shown that greater sharpness were obtained from the adaptive gain approach. Unsharp filter is validated in terms of edge preservation in the presence of noise (S. Lin et al., 2016).

Next, N. Ghandi highlighted that noise can be removed by using Gaussian filtering in Mean Shift Technique. The techniques can detect the circle smoothly compared to Circular Hough Transform (CHT) method (Gandhi et al., 2014). Gaussian filter being the most widely used filter for noise denoising. R. Schranzer et al. proposed an image processing techniques by using Gaussian filter. However, it leads to considerable blurring the certain part of the images (Schranzer et al., 2018). W. Cai et al. used Gaussian filter to achieve good balance between noise suppression and edge detection (Cai et al., 2019). W. Dong et al. presents a hyperspectral image sharpening using Gaussian filter whereas J. Qu et al. used Average filter and Guided filter. Guided filter is an improved method by using Gaussian filter (Dong et al., 2018; Li et al., 2018). Some researchers used Median filter to smoothing noise and preserving edge of the image. However, Median filter is suitable for salt and pepper (SAP) noise (Erkan et al., 2018; Gao et al., 2019). H. Gao et al. compared the performance of Median filter with Average and Gaussian filter. It shows that Median filter achieves best performance in low resolution with strong JPEG compression (Gao et al., 2019).

Figure 2.7 Image with salt and peppper noise (SAP).
Source: U. Erkan et al. (2018).

Next, the purpose of image segmentation is to extract the objects from the background by selecting the best threshold value for the image. The threshold value can be select by using color threshold or binary threshold. The most preferred method in this stage is morphology. There are 4 types of mathematical morphology which are dilation, erosion, opening and closing as shown in Table 2.3.

Table 2.3 Mathematical morphology

Morphology	**Formula**	**Application**
Dilation	$A \oplus B = \bigcup_{b \in B} A_b$	Grow or thicken objects
Erosion	$A \ominus B = \bigcup_{b \in B} A_{-b}$	Shrink or thin objects
Opening	$A \circ B = (A \ominus B) \oplus B$	Remove small objects, protrusions and connections
Closing	$A \bullet B = (A \oplus B) \ominus B$	Remove small holes and gaps

Source: Z. Fu & Y. Han (2012)

E. Rodrigues et al. highlighted that morphology method operates when the image is in binary image. Dilation is an operation that “thickens” object in binary image. Additionally, dilation is applied in binary image and the output pixel is set to 1 whenever any of the pixels is set to the value 1. Next, erosion is an operation that “thins” object in binary image. In a binary image, the output pixel is set to 0 whenever any of the pixels is set to the value 0. For instance, opening is a combination of erosions and dilations, while closing is the opposite, a combination of dilations and erosions, respectively using the same structuring element The opening is used for removing small objects, protrusions and connections of an object in image whereas closing is used to remove small holes and gaps (Fu & Han, 2012; Rodrigues et al., 2018). Z. Fu et al. presents an opening and contour detection to eliminate some details in round shape image. G. Landini et al. used opening and closing method to split the background image (Landini et al., 2019). D. Li et al. used erosion method whereas R. Soans et al. used opening method to prevent false detection (D. Li et al., 2017; Soans et al., 2018).

From the literature review, the important steps in image processing is image pre-processing and image segmentation stage. Most of the researchers used filtering and morphology method in order to remove unwanted details in image. There are 4 types of filtering mostly used by researchers which are Median, Gaussian, Average and Unsharp filter. In addition, the thresholding part is always used for segmentation process before applied the morphology method. Basically, the selection of morphology method is depending on the tested image. Hence, the method is selected according to the purpose of the image being processed. All the summary of the literature review for peg-in-hole task is summarizes in Table 2.4.

Table 2.4 Summary review on image processing

Title	Author/Year	Technique	Results	Gaps
A Circle Detection Algorithm Based on Mathematical Morphology and Chain Code.	Z. Fu & Y. Han (2012).	-Opening. -Contour detection -Area filling.	-Eliminate the details of an image.	-Suitable for standard round shape.
Unsharp masking using quadratic filter for the enhancement of fingerprints in noisy background.	V. Hari et al. (2013).	-Unsharp filter. -Canny edge detection.	-Eliminate images from noisy background.	-Tested on fingerprints image.
An optimized non-subsampled shearlet transform-based image fusion using Hessian features and unsharp masking.	M. Bhuyan et al. (2018).	-Unsharp filter. -Canny edge detection. -Hessian features.	-Reliable and consistent for different modalities of image.	-Complex algorithm (Hessian features).
Intensity and edge based adaptive	S. Lin et al. (2016).	-Unsharp filter. -Dilation method.	-Enhance the image quality.	-Tested on panoramic scenes.

unsharp masking filter for color image enhancement.				
Mean shift technique for image segmentation and Modified Canny Edge Detection Algorithm for circle detection.	N. Ghandi et al. (2014).	-Gaussian filter. -Canny edge detection. -Mean shift technique.	-Remove noise successfully. -Able to detect circle smoothly by using CHT.	-Complex algorithm (Mean shift technique)..
Noise reduction in FLAIR2 images using total generalized variation, Gaussian and Wiener filtering.	R. Schranzer et al. (2018).	-Gaussian filter. -Wiener filter.	-Leads to considerable blurring.	-Complex algorithm (Wiener filter).
Research on image processing of intelligent building environment based on pattern recognition technology.	W. Cai et al. (2019).	-Gaussian filter. -Otsu method.	-Achieve good balance between noise suppression and edge detection.	-Applied on building image taken from Google maps.
Hyperspectral pansharpening based on guided filter and Gaussian filter.	W. Dong et al. (2018).	-Gaussian filter.	-Able to remove noise in image.	-Applied on hyperspectral image.
Fusion of hyperspectral and panchromatic images using an average filter and a guided filter.	J. Qu et al. (2018).	-Guided filter (improved Gaussian filter). -Average filter.	-Able to remove noise and obtain spatial information of the image.	-Applied on hyperspectral image.
Different applied median filter in salt and pepper noise.	U. Erkan et al. (2018).	-Median filter.	-Able to remove noise in image.	-Suitable for salt and pepper noise.
Robust detection of median filtering based on combined features of difference image.	H. Gao et al. (2019).	-Median filter.	-High performance for noise removal compared to Average and Gaussian filter.	-Applied for forensic images.

2.5 Circular Object Detection

There are many methods based on image processing used in previous research to detect a circular object. The most popular method used to detect circular objects and locate analytic curves in binary image favoured for its tolerance to noise is Circular Hough Transform (CHT) and its variants. The CHT method can be described as transformation to the parameter space from X, Y- plane. The mathematically equation of a circle in X, Y-plane is given by Equation 2.1.

$$r^2 = (x - a)^2 - (y - b)^2 \quad 2.1$$

As it can be seen the circle got three parameters, r, a and b. Where a and b are the center of the circle in the x and y direction respectively and where r is the radius. The parametric representation of the circle is shown in Equation 2.2 and 2.3. Thus, the parameter space for a circle will belong to R^3. Each point in geometric space in Figure 2.6 (a) generates a circle in parameter space in Figure 2.6 (b). The circles in parameter space intersect at the (a, b) that is the center in geometric space as shown in Figure 2.6 (b).

$$x = a + r\cos\theta \quad 2.2$$

$$y = b + r\sin\theta \quad 2.3$$

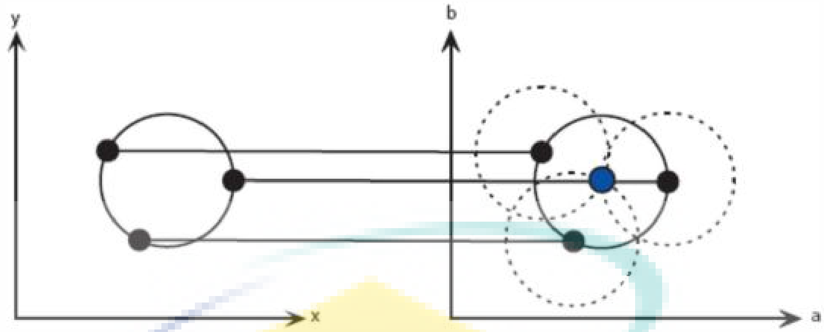

(a) (b)

Figure 2.8 Parametric space representation of a constant radius circle (a) CHT from the x-y space (b) CHT from the parameter space

Source: V. Yadav et al. (2014).

R. Hussin et al.and C. Kim et al. employed the CHT and color segmentation method to detect the circle. However, lighting intensity affects the original color of the object and produces false circles. Input image with less noise prevents the brightness problem. Median filter is used to eliminate noise and smoothing the image (Hussin et al., 2012; C. Kim et al., 2017). V. Yadav et al. highlighted that applying the concept of CHT and local maxima and considering the nature of the image will reduce the occurrence of false circles (Yadavet al., 2014). J. Ni et al. proposed a method based on CHT and contour detection method. These methods increase the detection accuracy and solve the problem of detachment of random circle shape (Ni et al., 2016). Addition of filters in pre-processing stage can minimize the noise of an image and prevent false detection. To increase the accuracy of circles detection, D. Lestriandoko et al. presented a CHT and Mexican Hat filter method whereas Y. Meng et al. proposed a circular detection method by using local adaptive Canny edge detection (ACED) and Gaussian filter to filter noise and increase the accuracy of circles detection. However, there are still errors in the mean diameter of the circle. The method also needs improvement for circles shape with any noise (Lestriandoko & Sadikin, 2017; Meng et al., 2018). Previous research improves CHT method to increase the detection accuracy. R. Lo et al. highlights the improvement of CHT method by using Extended Hough Transform (EHT) method. Furthermore, the method does not require pre-processing stage hence, it is robust against noise and occlusions (Lo & Hsu, 2016). Z. Yao et al. presents a novel curvature aided Hough Transform (HT) for circle detection (CACD). Although the circle detection is more precise, error during edge detection could lead wrong results (Yao & Yi, 2016). D. Li et al. opines that randomized HT (RHT) with circle features and gradient algorithm is effective for incomplete images circle detection or short arc. Median filter is applied in order to remove noise and preserve the edge information of the image (D. Li et al., 2017). Moreover, L. Jiang et al. improved the RHT method with randomized circle detection (RCD) for circular shape detection. The method produces high detection accuracy and robustness. However, the thresholding method need to be improved (Jiang et al., 2018). S. Li et al. presents a gradient-based CHT method although there are some limitations of contour detection. The method proves that it is robust against noise, illumination and localization accuracy (S. Li & Tie, 2010).

Next, some researchers used segmentation-based method for circular detection. J. Luo et al. opines that high detection rates is achieved by using threshold segmentation method according to Helmholtz principle (Luo et al., 2017). The segmentation algorithm is combined with Freeman chain code is presents by J. Road et al. It is proved that the method has strong adaptability and high efficiency towards its noise and occlusions. The threshold value can be adjusted depends on its environment factor (Road & District, 2013). M. Nahangi et al. used cluttered point cloud scans based on local data level curvature estimation, clustering and features matching to identify the pipe spool. The complex algorithm has successfully extracted the pipe spool from point cloud (Nahangi, 2016). In addition, L. Jia et al. employ a parallel operator and Gaussian filter to detect single circles and multiple circles despites the presence of noise (Jia & Peng, 2012). K-means algorithm with application of center-based clustering method is proposed by R. Scitovski et al. to solve the multiple circle detection problem (Scitovski & Marošević, 2015).

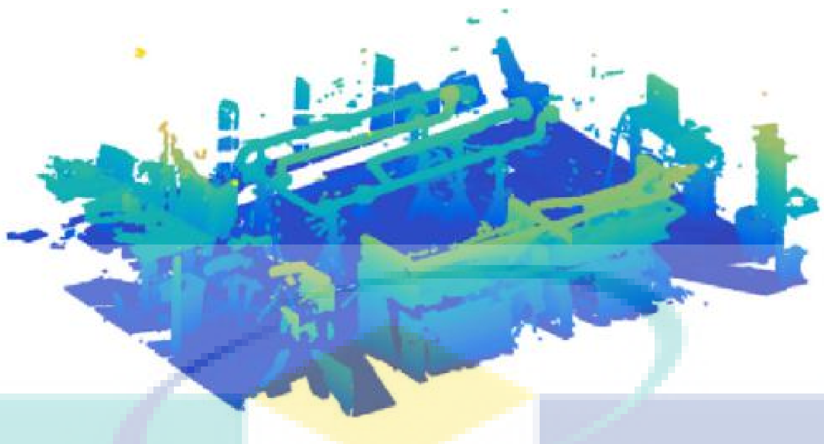

Figure 2.9 Examples of cluttered point cloud scan
Source: M. Nahangi et al. (2016)

From the literature review, most of the circle detection is detect by using CHT-based method and improvement of CHT method. It shows that CHT method is mostly preferred to use for circle detection. The circle detection method is performing with image processing techniques such as thresholding, filtering and morphology to remove unwanted image. Some of the method are robust against noise, occlusions, lighting and illumination factor. However, it is depending on its algorithm and the environment factor. In addition, the segmentation-based method produces a complex algorithm because it involves some mathematical analysis to increase the detection accuracy. Hence, the CHT method is most preferable to detect circular shape. All the summary of the literature review for peg-in-hole task is summarizes in Table 2.5.

Table 2.5 Summary review on circular object detection

Title	Author/Year	Technique	Results	Gaps
Digital Image Processing Techniques for Object Detection from Complex Background Image.	R. Hussin, M. Johari et al. (2012).	-Grayscale and CHT. -Color image processing (RGB).	-The object cannot be detected accurately due to lighting intensity that affect the original color of the object.	-Color image processing. -Offine image processing.
Automatic Detection of Defective Welding Electrode Tips Using Color Segmentation and Hough Circle	C. Kim et al. (2017).	-Color segmentation (YCbCr) and CHT.	-Possible to classify which defects, among burr, chip and contamination.	-High time consuming. -Acquire input image with less noise. -Angle of the light and brightness problem.

Detection.				
Approach to Accurate Circle Detection: CHT and Local Maxima Concept.	V. Yadav, S. Batham et al. (2014).	-CHT and Local Maxima concept. -Canny edge detection.	-Reduction in false circles.	-Offline image processing. -Algorithm sometime contains false circles.
Automatic Detection and Counting of Circular Shaped Overlapped Objects Using CHT and Contour Detection.	J. Ni, Z. Khan et al. (2016).	-HT and Contour Detection methods. -Canny edge detection and contour method.	-Increase the accuracy of circle detection. -Solve the problem of detachment of random shaped cells attached with the circular shaped cells.	-Suitable to apply to the cell segmentation and counting in human blood.
Circle Detection based on Hough Transform and Mexican Hat Filter.	N. Lestriandoko et al. (2017).	-HT with Mexican Hat Filter. -Sobel edge detection.	-It increases the accuracy of circle detection.	-Need improvement for circles shape with any noise. -Offline image processing.
Automatic Detection of Particle Size Distribution by Image Analysis Based on Local Adaptive Canny Edge Detection and Modified CHT.	Y. Meng et al. (2018).	-Gaussian filter, local ACED and CHT.	-The robust algorithm can measure the particles with high precision.	-Have small errors in regards of detected number and mean diameter.
A Circular Band Extraction Method Based on Extended Hough Transform.	R. Lo & H. Hsu (2016).	-Extended Hough Transform (EHT).	-Robust against noise, occlusions and discontinuities in binary images. -Does not require pre-processing stage.	-Direct input from binary image. -Suitable for parallel computing using CUDA.
Curvature Aided Hough Transform for Circle Detection (CACD).	Z. Yao &W. Yi (2016).	-CACD method (estimates the circle radius from curvature).	-More precise circle detection. -Less time consuming.	-Error during edge detection would lead to wrong results.
Circle Detection of Short Arc Based on Randomized Hough Transform.	D. Li et al. (2017).	-Randomized HT with the circle features and gradient algorithm. -Median filter.	-Less time consuming. -Accurately locating the arc to be detected.	-Effective for incomplete images circle detection (short arc).
Fast circle detection	L. Jiang et al. (2018).	-Randomized circle detection	-Thresholding method need to be	-Suitable for ellipse detection

algorithm based on sampling from difference area.		(RCD).	improved.	for random sampling.
A robust high-precision circular target detection method based on Hough Transform.	S. Li et al. (2010).	-Gradient-based CHT method.	-Robust against noise and illumination.	-Limitations on contour detections.
A Fast Circle Detection Method Based on Threshold Segmentation and Validity Check for FPC Images.	J. Luo et al. (2017).	Threshold segmentation method and a validation check (Helmholtz principle).	High detection rates and good accuracy.	It can be used to detect circles in images with simple graphic patterns.
Circle And Circular Arc Detection Algorithm Research Based on Freeman Chain Code.	J. Road et al. (2013).	-Segmentation algorithm is combined with Freeman chain code. -Binarization, and thresholding.	-High efficiency towards its noise and occlusions.	-Complex algorithm.
Pipe spool recognition in cluttered point clouds using a curvature-based shape descriptor.	M. Nahangi et al. (2016).	-Cluttered point cloud scans based on local data level curvature estimation, clustering and features matching.	-Extract pipe spool successfully using point cloud.	-Complex algorithm.
A new circle detection method based on parallel operator.	L. Jia et al. (2012).	-Parallel operator to detect single circles and multiple circles. -Gaussian filter.	-Good accuracy despite of the presence of different noises.	-Offline image processing. -Complex algorithm.
Multiple circle detection based on center-based clustering.	R. Scitovski et al. (2015).	-K means algorithm and clustering method.	-Multiple circle detection problem recognized.	-Complex algorithm.

2.6 Summary

Based on the reviewed literatures, peg-in-hole task usually performed by vision-based autonomous robot and dual-arm robot. However, there is no literature discussing on an object that has a circular shape and located in a situation that it can be grasped or pulled out only from front side and cannot be grasp using aforementioned gripper designs in VAC. Hence, a system intended for a vision-based autonomous self-aligned robot to pick up the objects. The peg-in-hole task are mostly performed by using expensive camera, additional sensors and stereo camera which is it produces complex algorithm. Although the use of single camera is not much, it proves that the method is successful and can be applied thus, reducing the project cost and needs a high DOF mechanism with fine movement. Moreover, it can solve one of the industry problems for peg-in-hole-task using single camera. Considering that the spool is in circular shape, the spool can be detected by using CHT method. However, there is no proper investigation has been done so far to propose an algorithm for pre-analysis prior to reliable system development.

CHAPTER 3

METHODOLOGY

3.1 Introduction

This chapter presents in detail the research methodology for the for camera orientation to enable the puller inserted to the CHS. This system is divided into two parts which are spool detection and the camera orientation. The system will identify the spool and estimate the distance between spool and camera. The orientation of the camera related to the spool front surface will be determined by using some mathematical equations developed in this study. The proposed system is simulated by using MATLAB software in real-time.

3.2 System Overview

The process of tracking and checking the orientation of the spool and camera only will be guided by a web camera and MATLAB software. The spool detection system is compared between existing method and proposed method which are CHT and Modified CHT (MCHT). The camera and puller are mounted on a robot at 106 cm and 100 cm height. The center hole of spool (CHS) height from the floor is 100 cm which is the camera is mounted higher 6 cm from the CHS height because in the real situation, the camera will be put at 106 cm height to avoid the collision of camera and puller. The distance of camera to spool is analyzed from 50-110 cm. Lastly, the diameter of spool is fix to 35 cm. Figure 3.1 shows the experimental setup for the proposed system.

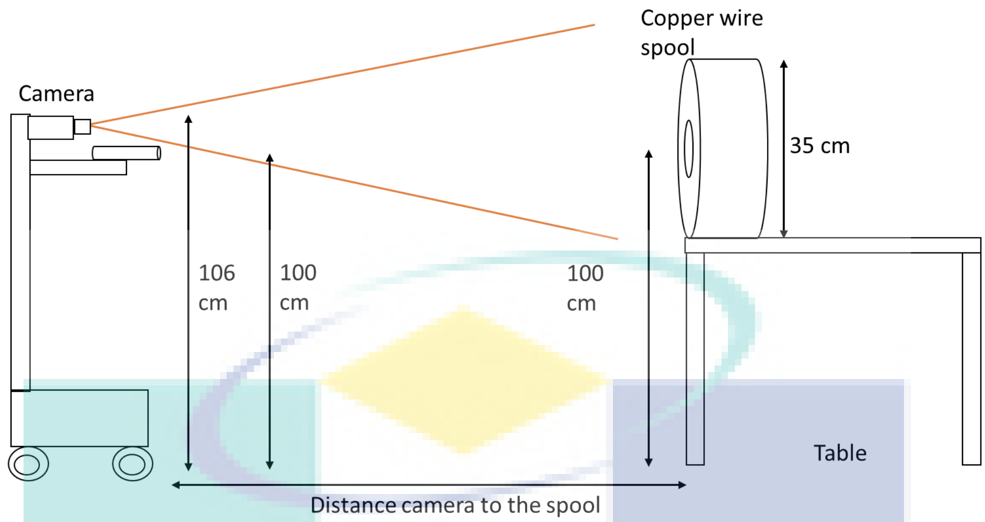

Figure 3.1 Experimental setup for proposed algorithm

For spool detection, there are two circles to be detected which are big circle (BC) and small circle (SC) as shown in Figure 3.2 below. BC and SC are presented in red and blue color as a standard color used to display in MATLAB. The detection of BC is to check the existence of the spool whereas the detection of SC is to check the camera orientation with the spool. The hardest part to do in this study is to remove as much as noise in image for spool detection. Noise and outliers in this system is the unwanted detection that occur in image processing system. The video is preview with reference center (RC) in green color because it is easy to see with human view. The RC coordinate is fix to (80,50) pixel. If the spool is moved to another location, the system need to analyzed again the new coordinates for RC based on camera's height and spool's height. The parameter of this study is fixed except for the distance as shown in Figure 3.1. The illustration design for RC, BC and SC are shown in Figure 3.2.

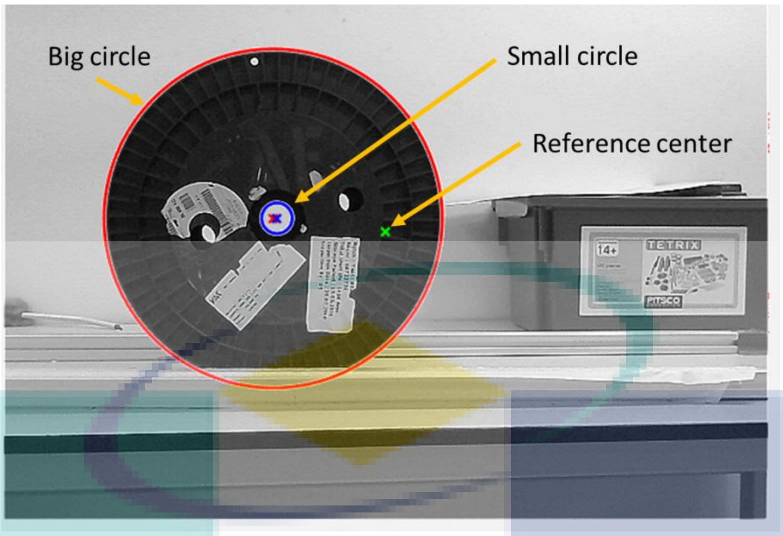

Figure 3.2 Illustration design for RC, BC and SC

Based on the images taken from video, the vision system guides the camera to stop at correct position. Referring to the isometric projection perspective as shown in Figure 3.3, the correct position is where the front and back circles (rims) of the spool are sharing same center. From the side view of isometric projection, they overlapped each other and seen as only one circle.

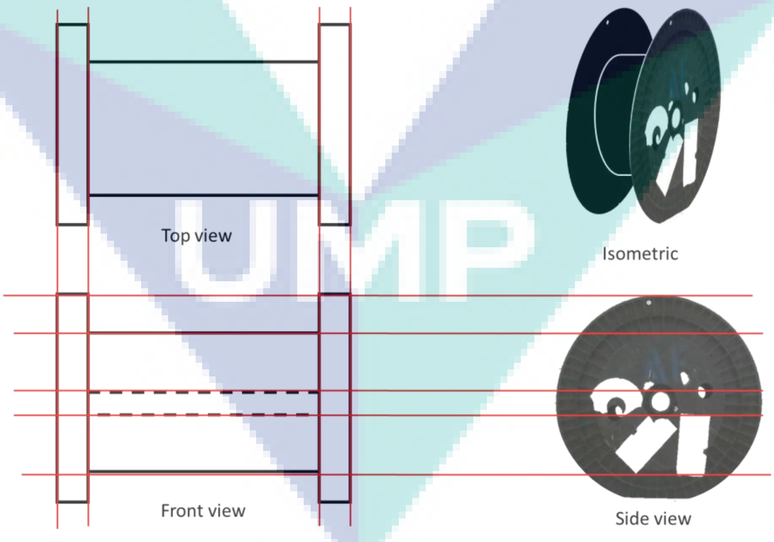

Figure 3.3 Isometric projection of spool

While the camera moves to the location where the spools are located, it is scanning its side and search for the spool. The spool will be detected starting from the point when it enters the field of view (FOV) of the camera. The robot orientation is depending on the camera orientation. As the spool reaching the center of the FOV, the centers of the BC and SC will become overlapping and finally sharing the same center point, as illustrated by Figure 3.4. In implementation of the system, a RC with coordinate (80,50) is plotted at the center of the image frame of the camera. The camera is in the correct position if the BC and SC of the spool are overlapped by the RC and the camera can move forward. While moving forward, the camera orientation (yaw angle, θ) is confirmed by determining the position of the spool on the frame image as shown in Figure 3.4. The yaw angle is considered 0° (parallel to spool) if the spool is at the center of the frame image. The spool image will change to the right-hand side of the image frame if the yaw angle is positive and likewise for the negative yaw angle.

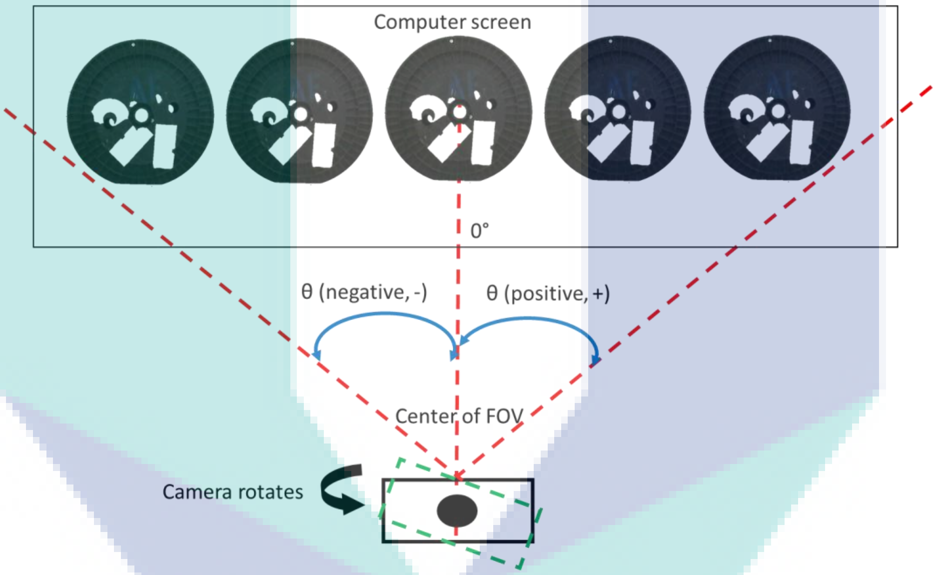

Figure 3.4 Camera orientation and spool orientation on captured image

The illumination value also analyzed in this system because illumination is one of the common issues when it comes to image processing. There are three switches used in the lab which are Switch 1 (S1), Switch 2 (S2) and Switch 3 (S3). Additional information based on previous studies, this study has been done with illumination value which is 202.3 lx in average. This means that S1, S2 and S3 are used. The illumination value is measured by using Lux Meter application on Android. The illumination value is analyzed with four conditions as shown in Figure 3.5.

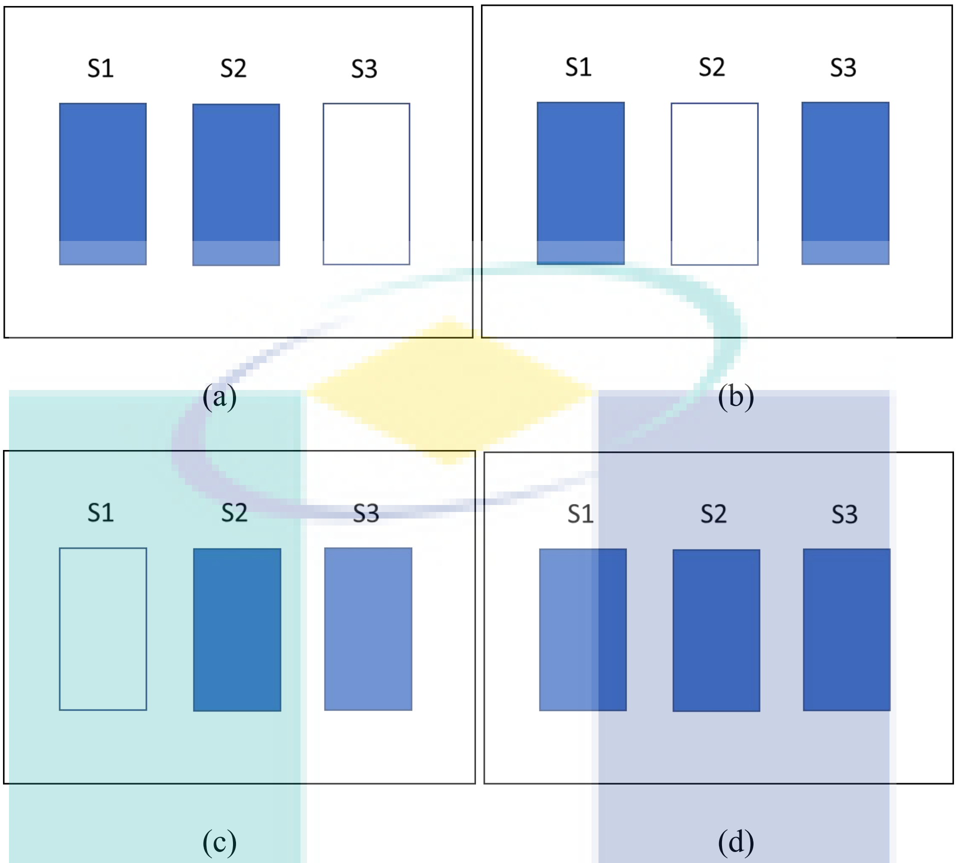

Figure 3.5 Illumination switch conditions (a) S1 and S2 are turned on (b) S1 and S3 are turned on (c) S2 and S3 are turned on (d) S1, S2 and S3 are turned on

3.3 Spool Detection System

The spool detection algorithm was developed based on five steps which will be described in this subchapter. The steps are image acquisition, image pre-processing, morphological processing, feature extraction and object classification. The overview of the whole process in this system is shown in Figure 3.6.

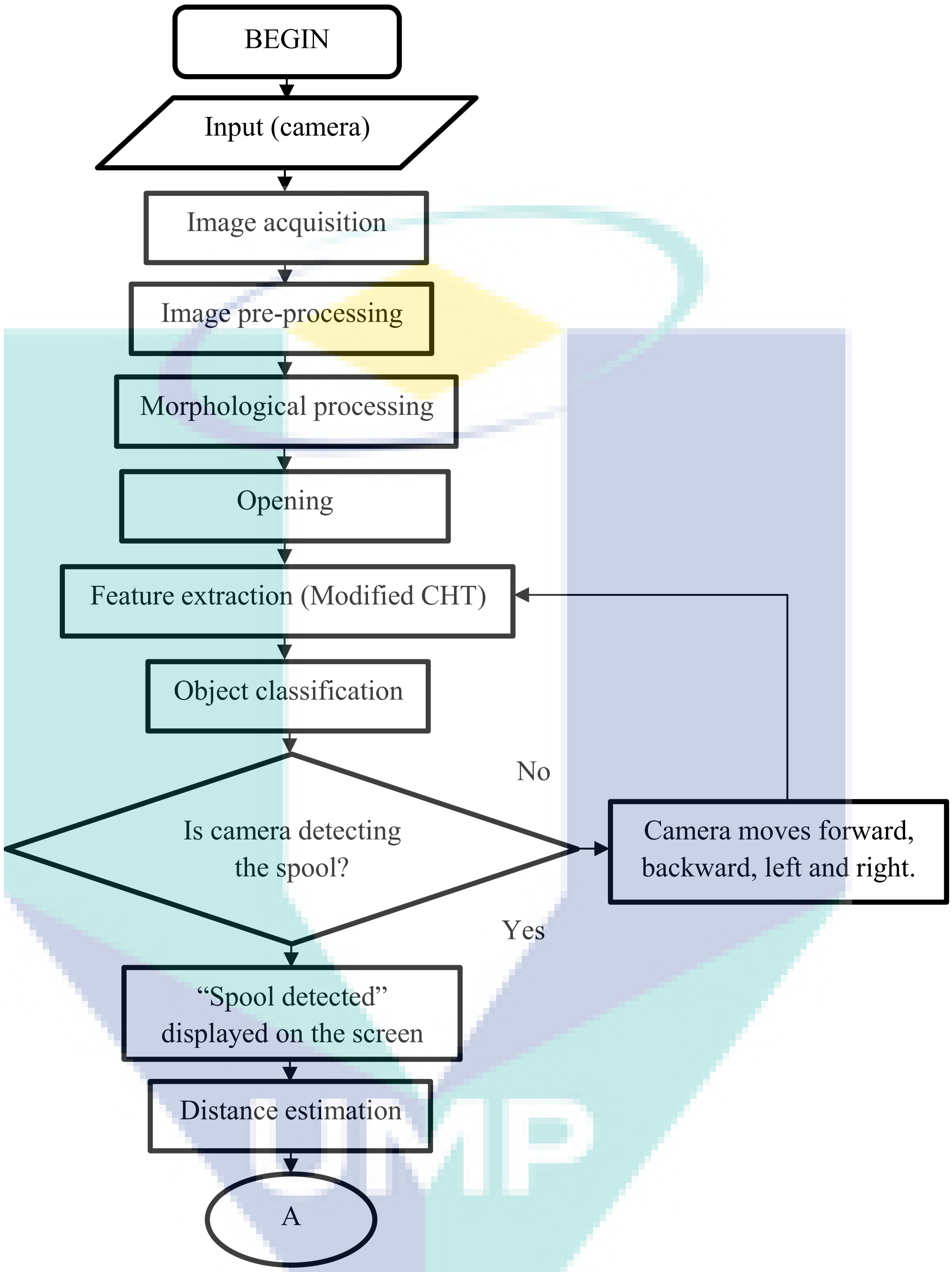
BEGIN
Input (camera)
Image acquisition
Image pre-processing
Morphological processing
Opening
Feature extraction (Modified CHT)
Object classification
Is camera detecting the spool?
No
Camera moves forward, backward, left and right.
Yes
"Spool detected" displayed on the screen
Distance estimation
A

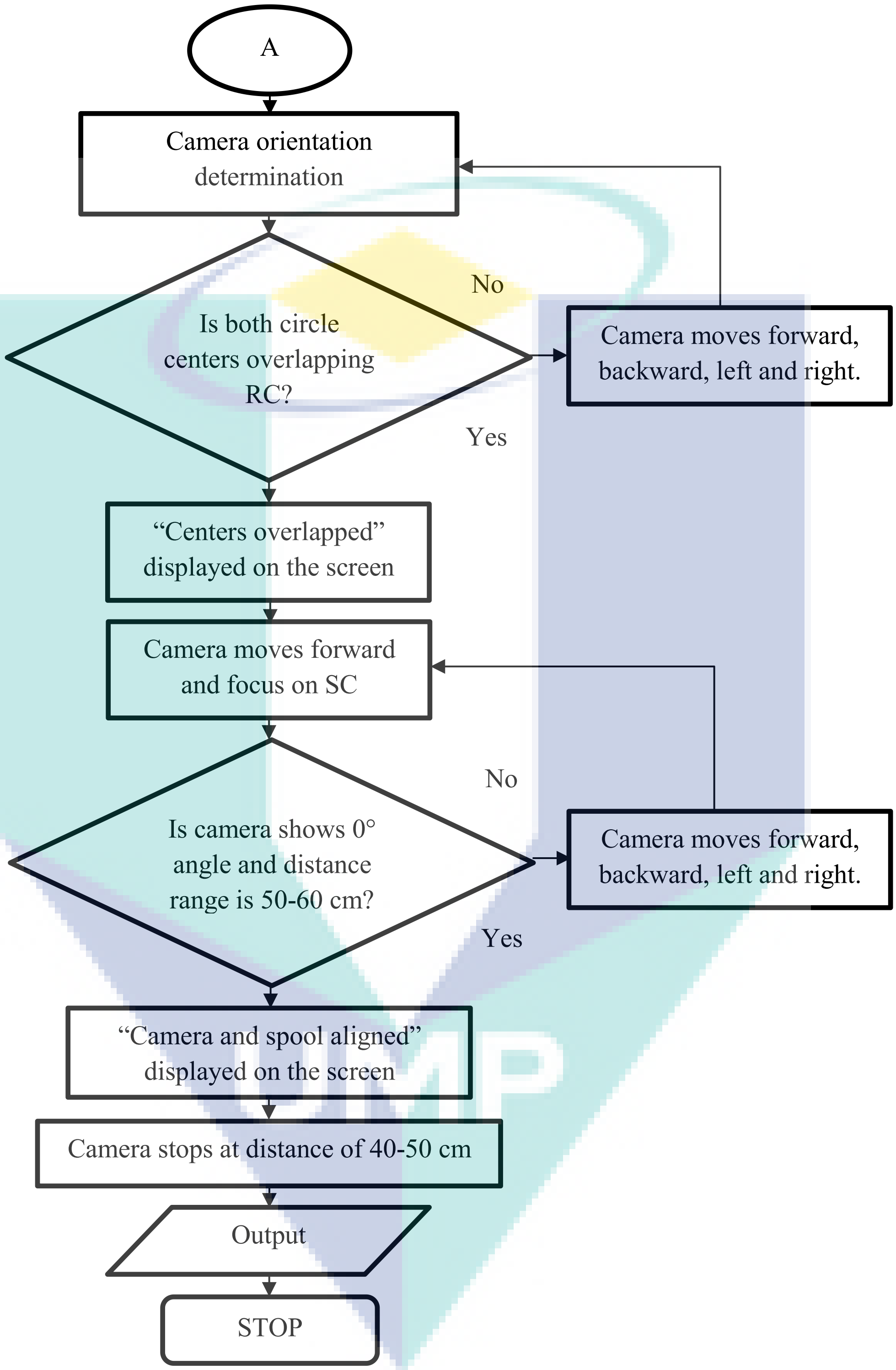

Figure 3.6 The flowchart of spool detection and camera orientation system

3.3.1 Image Acquisition

The first stage of image processing system is image acquisition. The video input is captured by using Logitech C270 camera by using MATLAB software as shown in Figure 3.7. The video input is called by using 'winvideo' syntax. MATLAB is received input from the camera and displayed on the MATLAB figure window in 160×120 resolution. The type of image acquisition is real-time data in color image as shown in Figure 3.8. In this study, the height of the camera remains constant which is 106 cm.

Figure 3.7 Logitech C270 camera
Source: www.logitech.com/en-my

Table 3.1 Specification of Logitech C270 camera

Feature	Description
HD requirement	2.4GHz Intel Core 2Duo = CPU 2GB = RAM
USB type	USB 2.0
Focus type	Fixed
Focal length	4.0 mm
Frame rate (max)	30 fps@640×480
Field of view	60°
Cable length	5 feet, 1.5 m

Source: www.logitech.com/en-my

Figure 3.8 Original image acquisition

3.3.2 Image Pre-Processing

All noises need to be removed during image pre-processing stage. An enhancement and improvement of the images are done in this stage. The pixel value of the image is explored. The real-time image is shown in a good quality without the need of camera changing. The image taken from the camera is converted and previewed in grayscale as shown in Figure 3.9.

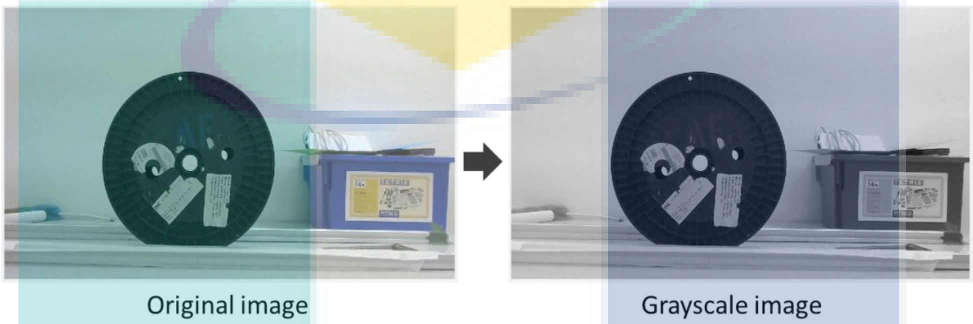

Figure 3.9 Image comparison between original and grayscale images.

Next, filter method is applied to reduce the noise and enhance the image. A comparison of filter is made between Gaussian filter, Unsharp filter, Median filter and Average filter. All filters have its own capabilities. For Gaussian filter, it returns a rotationally symmetric Gaussian lowpass filter of size with standard deviation sigma (positive). In other words, it filters image with a 2-D Gaussian smoothing kernel. For Median filter, the value of an output pixel is determined by the median of the neighborhood pixels, rather than the mean. In addition, the median is less sensitive than the mean to extreme values (outliers). Thirdly, Unsharp filter is used to unsharp contrast enhancement filter. Lastly, Average filter acts like Median filter which is remove noise in image. It returns an averaging filter of size of the filter. All filters have been tested in order to determine which one suits this study. There are 30 image samples analyzed for filter analysis. In this study, Gaussian filter is able to remove these outliers without reducing the sharpness of the image. Gaussian filter is used rather than other filters because other filters produce more noise and false detections compared to Gaussian filter. In addition, some researchers used Gaussian filter to reduce noise in circular image. The most important part of choosing the filter is to make sure the filter does not effect the SC image which are the CHS. Figure 3.10 shows the filtering process applied on a grayscale and binary image.

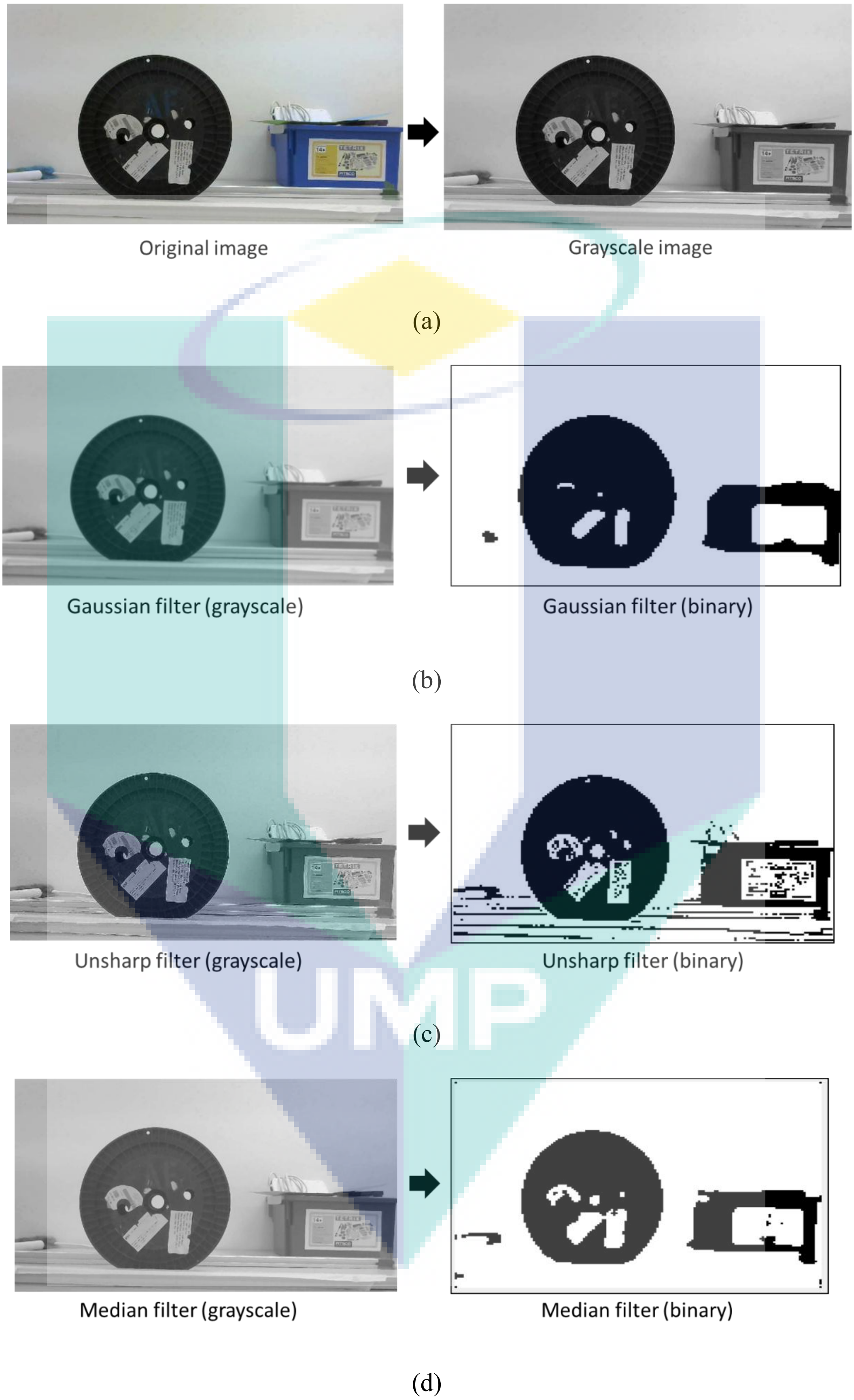
Original image
Grayscale image
(a)
Gaussian filter (grayscale)
Gaussian filter (binary)
(b)
Unsharp filter (grayscale)
Unsharp filter (binary)
(c)
Median filter (grayscale)
Median filter (binary)
(d)

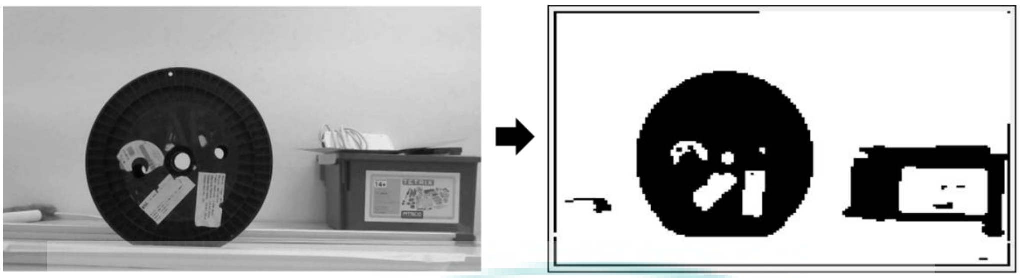

(e)

Figure 3.10 Steps for filtering process (a) Original and grayscale image (b) Gaussian filter (c) Unsharp filter (d) Median filter (e) Average filter

3.3.3 Image Segmentation

Image segmentation stage is to split up background from the target object in the image. In this system, this stage is to ensure the SC image is clearly presented without merge with another pixel that can cause difficulties to detect SC image. There are three process used in this stage which are binarization, area opening and selected morphology method. Each pixel for binary images stored as a single bit which are 0 (black) or 1 (white). For binarization process, the threshold binary value (0-1) is analyzed in order to determine the threshold value. In this stage, the threshold value must fulfill certain conditions. Firstly, the binarization process must not remove the spool image including SC image. Secondly, the spool image can be detected within 50-110 cm distances range. Lastly, the average pixel value to binarize the spool image within 13307-15938 pixels. Figure 3.11 shows the threshold values are compared between 0.25, 0.35 and 0.45 because those values are the closest value that can fulfill the conditions. In this study, the threshold value is set to 0.35 pixel to fulfill all binarization process conditions for better noise removal process. There are 40 image samples analyzed for threshold value analysis. Next, all connected components fewer than 30 pixels are removed as shown in Figure 3.12. In Figure 3.12, there are some white dots pixel in the image and it is removed by using area opening method. Next, a comparison of morphology method is made between opening, dilation and erosion. Morphology apply a structuring element to an input image, creating an output image of the same size. In this study, opening method are used.

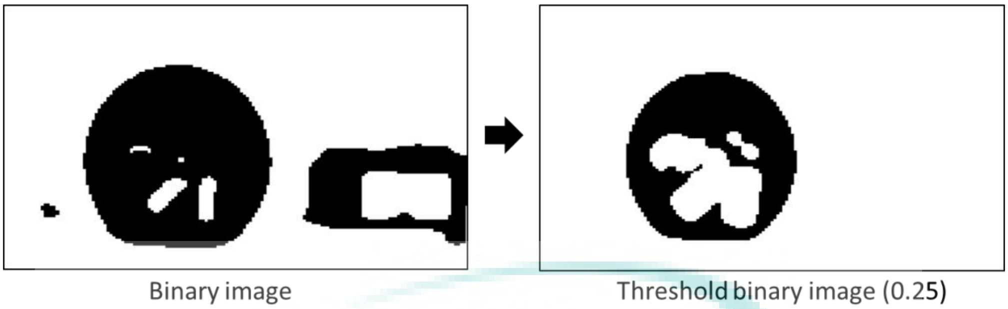

(a)

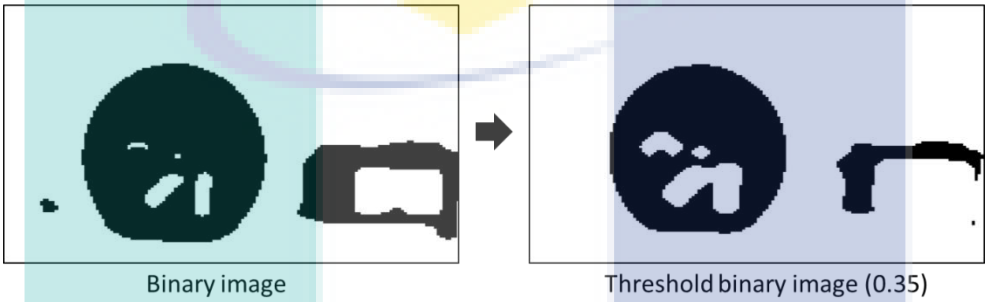

(b)

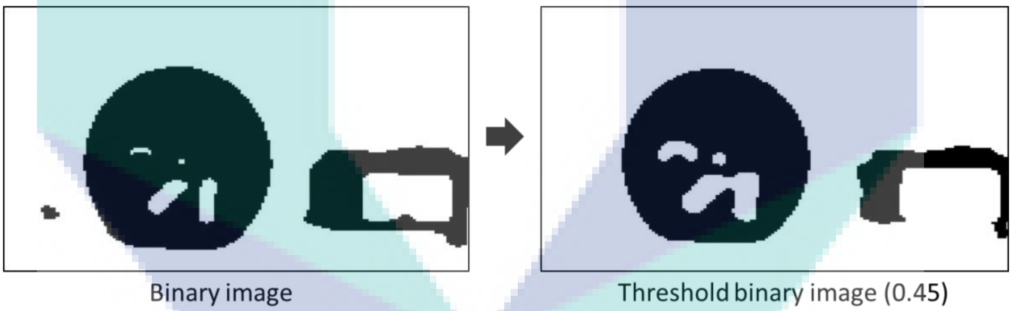

(c)

Figure 3.11 The comparison of thresholding binary image (a) 0.25 (b) 0.35 (c) 0.45

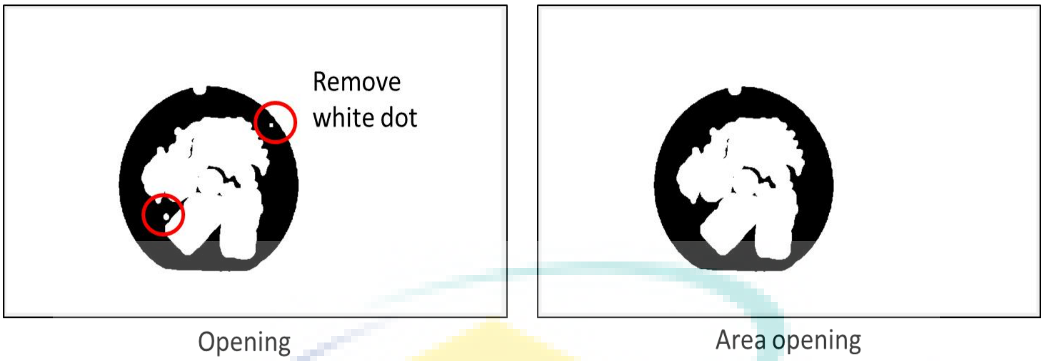

Figure 3.12 The difference between binary and area opening method

The morphology operation is applied after the binarization process and area opening is applied after the morphology operation is applied. Morphology operation is to remove the imperfections of the binary image and maintain the SC image. In this study, opening, dilation and erosion are analyzed. It shows that all morphology method applied can detect BC image. However, some morphology method such as the erosion method removes the SC image. Therefore, erosion method is not suitable to apply in this study. In this study, opening method is applied rather than dilation method because dilation method merges SC image with other pixel compared to opening method. There are 40 samples used for morphology analysis. Figure 3.13 shows the morphology process applied on a binary image.

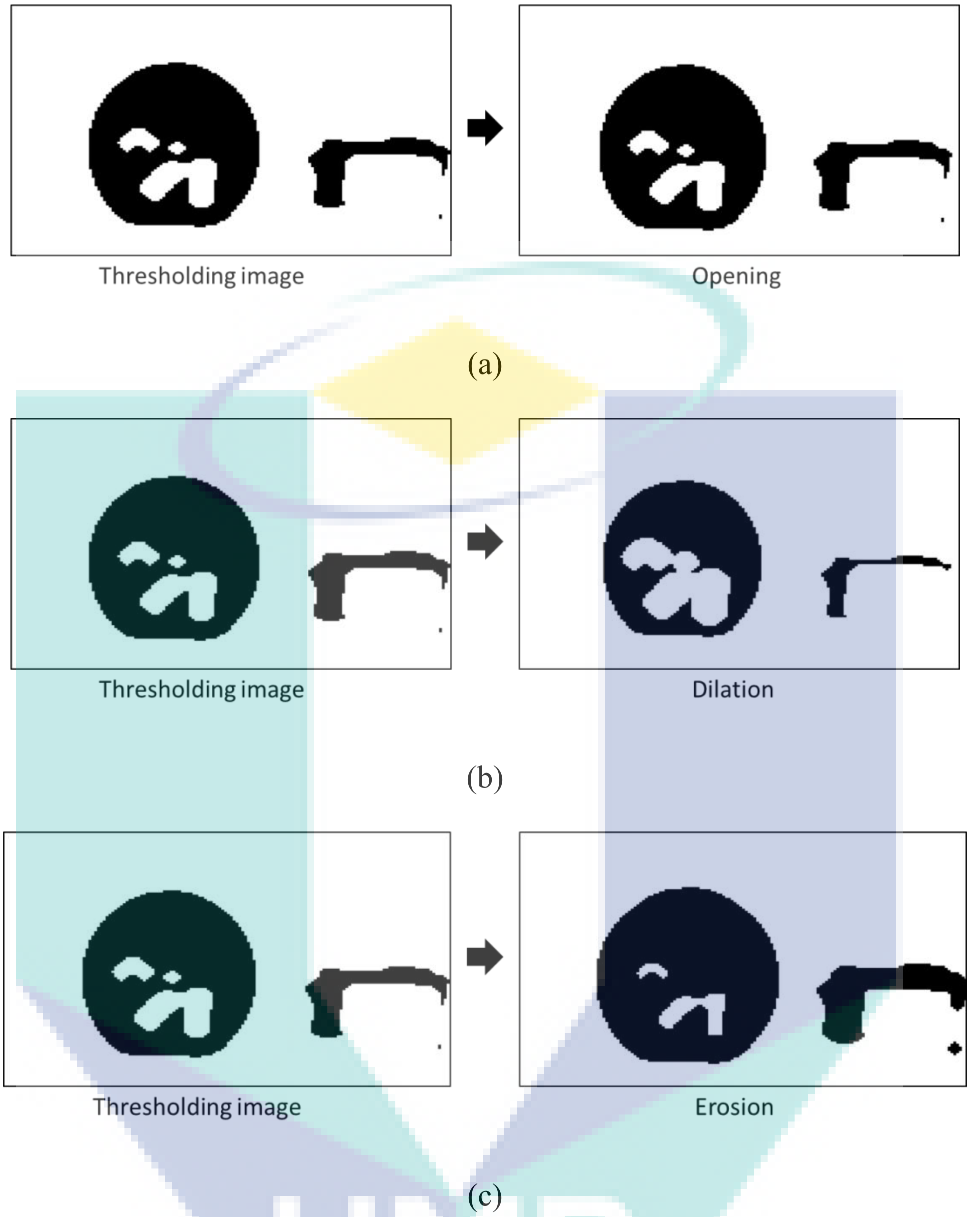

Figure 3.13 The comparison of morphology process (a) Opening (b) Dilation (c) Erosion

3.3.4 Feature Extraction

In this stage, the input data has been transforming into set of features. The set of features will extract relevant information accordingly to the desired task. All the data pixels that represent and describes the desired features are grouped in this stage. Besides, this stage will extract the spool features by Modified Circular Hough Transform (MCHT). This method is derived from Circular Hough Transform (CHT) method and modified by using Equation 3.1 shown below. The steps of the feature extraction stage are as shown in Figure 3.14.

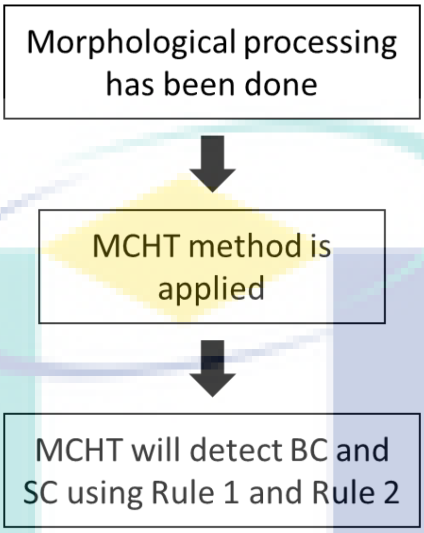

Figure 3.14 Steps of feature extraction process

Spool detection is extracted by using Rule 1 and Rule 2 shown below. There are two radii to be detected which are Radius 1 (R_1) and Radius 2 (R_2). R_1 for BC detection and R_2 for SC detection. R_1 value is from 35-65 pixels whereas R_2 is from 3-15 pixels. FA Azman et al. presents a spool detection method by using CHT method with different resolutions which is 640×480 pixels. The value of circle radii depends on the camera resolution and the distance between the camera and the spool. (FA Azman et al., 2017). The values are selected so that the camera can detect the spool within distance 50-110 cm.

$$\text{Rule 1} = \begin{cases} 1\ (\text{TRUE}), 35 \leq R_1 \leq 65 (\text{BC}) \\ 1\ (\text{TRUE}), 3 \leq R_2 \leq 15 (\text{SC}) \\ 0\ (\text{FALSE}), \text{otherwise} \end{cases}$$

MCHT is applied to identify the characteristics of spool. MCHT method cannot be applied on RGB image. It can be applied on grayscale, binary or edge images. The system will detect BC and SC by using Rule 1 and Rule 2. A RC with coordinate (80,50) is displayed once the program is run. Rule 2 is created based on Equation 3.1 in order to calculate distance between BC and SC center (D_{bc}). Equation 3.1 is a new mathematical equation created in order to classify true SC and remove outliers in image. From Equation 3.1, (X_2, Y_2) is referred to SC center coordinate and (X_1, Y_1) is referred to BC center coordinate. The D_{bc} range is from -2 to 2 pixels to prevent the false circle detections.

$$D_{bc} = ((X_2 - X_1),(Y_2 - Y_1)) \quad 3.1$$

$$\text{Rule 2} = \begin{cases} 1\ (\text{TRUE}), & -2 \leq D_{bc} \leq 2 \\ 0\ (\text{FALSE}), & \text{otherwise} \end{cases}$$

As mentioned in the previous subchapter, the noises in the spool image are difficult to be removed and causing difficulty in identifying the true circles. Therefore, MCHT method is applied to classify the true circles. The CHT method is improved by using MCHT method.

3.3.5 Object Classification

In this stage, the data that have been grouped will be classified. The decision in judging whether it is a spool or not will be made based on Rule 1 and Rule 2. The steps for object classification are as follows along with Figure 3.15.

i. First classification is BC detection. When BC is detected, the circle will display in red color on the screen.

ii. Second classification is SC detection. When SC is detected, the circle will display in blue color on the screen.

iii. When both circles or BC are detected, "Spool detected" will display on the screen. No message will display on the screen when BC and SC not detected.

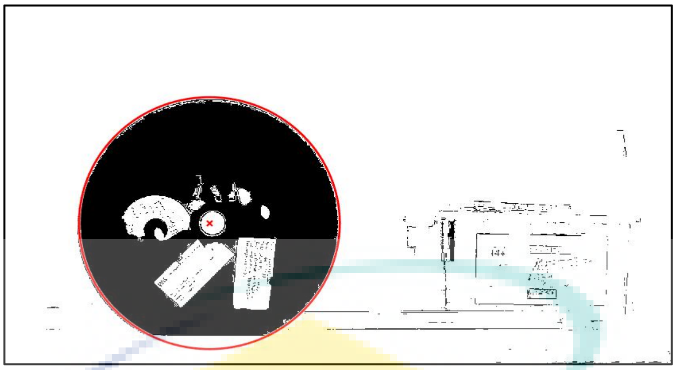

(a)

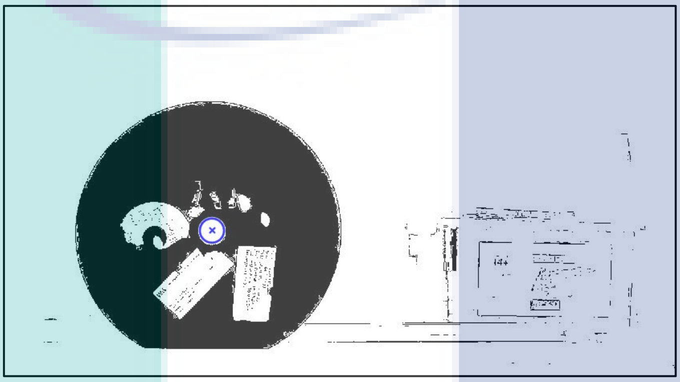

(b)

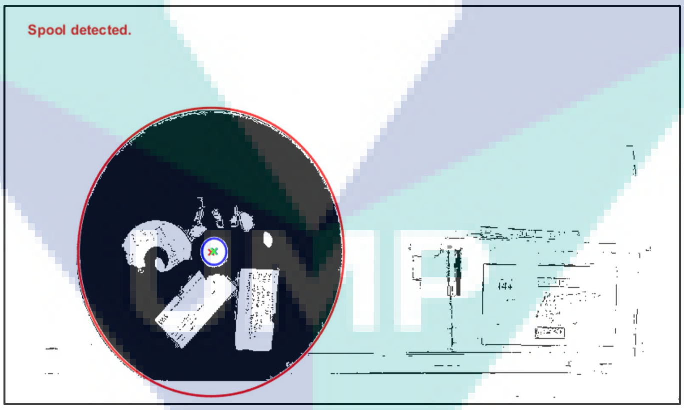

(c)

Figure 3.15 Steps of object classification (a) BC detected (b) SC detected (c) “Spool detected” is displayed on the screen

3.4 Camera Orientation System

This subchapter will explain how the system determined the camera orientation with respect to spool's front surface. There are three topics covered in this subchapter which are distance estimation from camera to spool, yaw angle estimation and overlapping center determination. The spool considered detected when both circles are detected. This subtopic explains briefly the calculations to get the spool distance from the camera and also the orientation of the camera. The camera will move in *x* (left and right), *y* (front and back) direction. The camera will stop when the center of the circles overlapping the RC while considering the spool is at the center of the frame. Next, the camera will move in *x* direction (front), and the camera will focus on the SC center. The overview of camera's movement is shown in Figure 3.16.

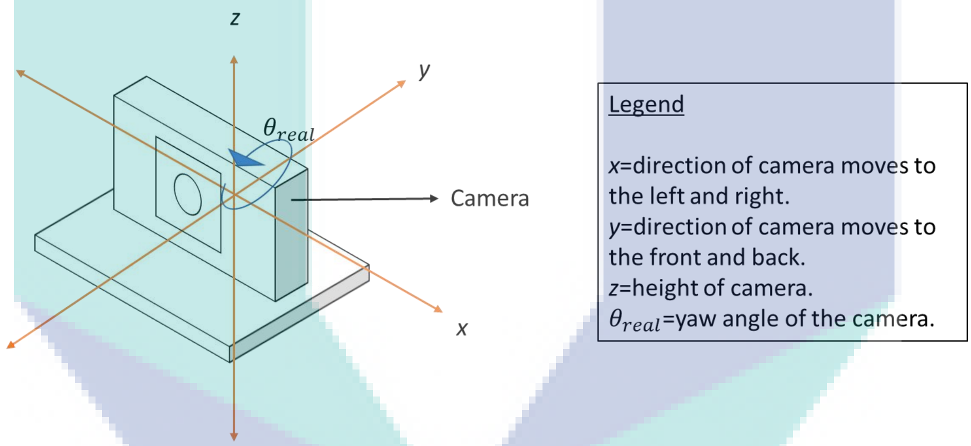

Figure 3.16 Illustration of the direction of camera's moving in *x, y* direction

Figure 3.16 shows the direction of camera in *x* and *y* direction. The *x* and *y* direction stands for the camera moving to the left and right and forward and backward, respectively. The camera is placed 106 cm from the floor. Moreover, the camera is mounted on the existing robot-like to move the camera in *x* and *y* direction. For θ_{real} direction, it shows the yaw angle of the camera.

3.4.1 Distance Calculation from Camera to Spool

Calculated distance of the camera from the spool is displayed when the system detects the spool. The system will measure the distance between camera and spool as illustrated in Figure 3.17 by using Equation 3.2.

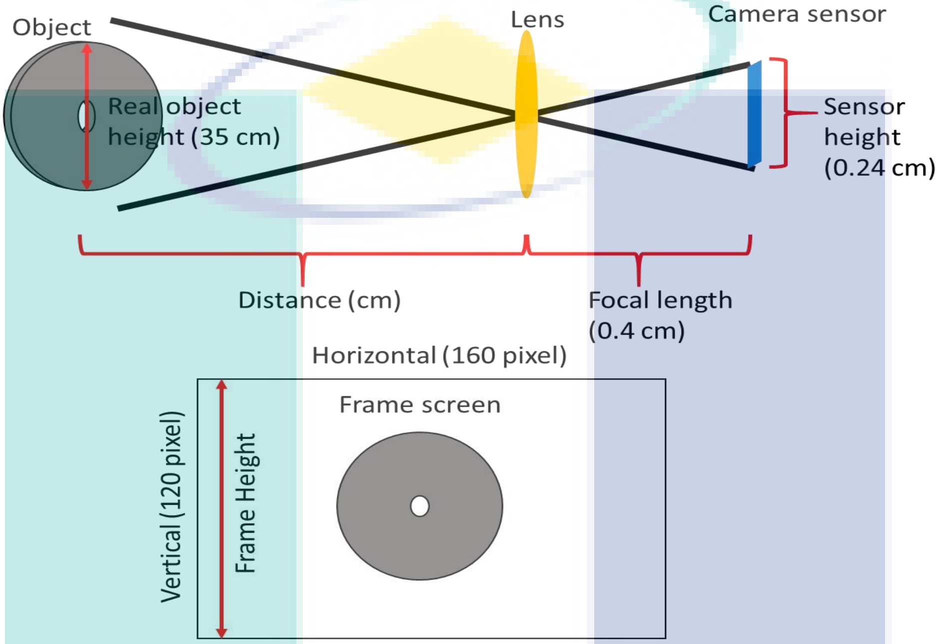

Figure 3.17 Illustration design for distance calculation from camera to spool

$$Distance, D(cm) = \frac{FL\ (cm) \times ROH\ (cm) \times FH(pixel)}{SH\ (cm) \times OH\ (pixel)} \quad 3.2$$

Source: https://photo.stackexchange.com/questions/12434/how-do-i-calculate-the-distance-of-an-object-in-a-photo

Where;

i. *FL* (Focal length) = 0.4 cm (Logitech C270 specifications).

ii. *ROH* (Real object height) = 35 cm (spool diameter)

iii. *FH* (Frame height) = 120 pixels (resolution of the vertical frame).

iv. *OH* (Object height) = radius detected in the system (diameter) × 2

v. *SH* (Sensor height) = 0.24 cm

$$SH(cm) = \frac{FL\ (cm) \times ROH\ (cm) \times FH(pixel)}{Measured\ distance\ (cm) \times OH\ (pixel)} \quad 3.3$$

Equation 3.2 shows the formula for distance calculation from camera to spool. The formula is not cited on any paper but, the effectiveness of the formula is tested and proved. The *FL* and *ROH* are stated clearly on above. In this study, the resolution of frame screen is 160×120 pixels (horizontal × vertical). Therefore, *FH* is 120 pixels. The OH value is using the value of the spool diameter in a pixel unit. The value is obtained from the system algorithm. Lastly, the sensor height value is determined by using Equation 3.3 by using real distance value (measured distance value). The measured distance value is measured by using measuring tape. The sensor height value is needed to fulfill Equation 3.2 which requires sensor height value. The analysis for sensor height value is shown in Appendix B.

3.4.2 Yaw Angle Estimation

The yaw angle of the camera, θ_{real} as illustrated in Figure 3.18 is determined based on Equation 3.4 and 3.5. Where, *m* and *n* are horizontal resolution and vertical resolution respectively. The distance between RC to BC center (DC_1) is measured in pixel. The yaw angle is measured from center field of view (CFOV) camera to BC center. The FOV of the camera is 60° given in the Logitech C270 specifications. The effectiveness of the formula is tested and proved.

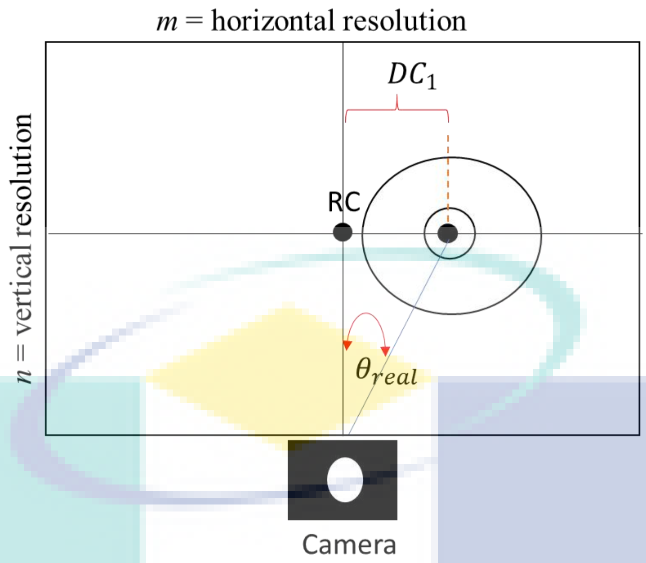

Figure 3.18 Illustration for yaw angle mathematical formula

$$\theta_{pixel}\,(^\circ) = \frac{FOV}{\sqrt{m^2 + n^2}} \quad 3.4$$

$$\theta_{real}(^\circ) = \theta_{pixel} \times DC_1 \quad 3.5$$

Source: https://stackoverflow.com/questions/17499409/opencv-calculate-angle-between-camera-and-pixel

Figure 3.19 shows the path indicator for camera movement to ensure the camera is at the right position before the puller is inserted to CHS. The path indicator verification is needed to ensure the system calculation for θ_{real} value is same with the path indicator value. It shows that Equation 3.5 is able to calculate the yaw angle and the accuracy of path indicator is proved by using Equation 3.5. The path indicator consists of 0°, 5°, 10°, 15°, 20°, -5°, -10°, -15° and -20°. Theoretically, there are three conditions that show the camera in aligned position. Firstly, the camera orientation is at 0°. Secondly, both centers are overlapped the RC. Lastly, the distance between camera and spool is between 50-60 cm. The length of the puller estimation is more than 50 cm because the puller needs to pull the neighbouring spools after the one in front is picked up. There are 27 data samples used to analyzed yaw angle estimation. The path indicator value is used as reference value. The yaw angle was analyzed in various distance from 80-100 cm. The experimental value is calculated by using Equation 3.5.

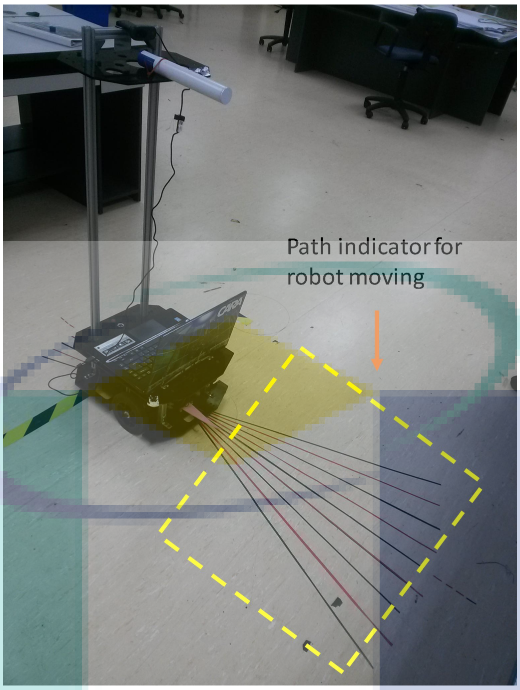

(a)

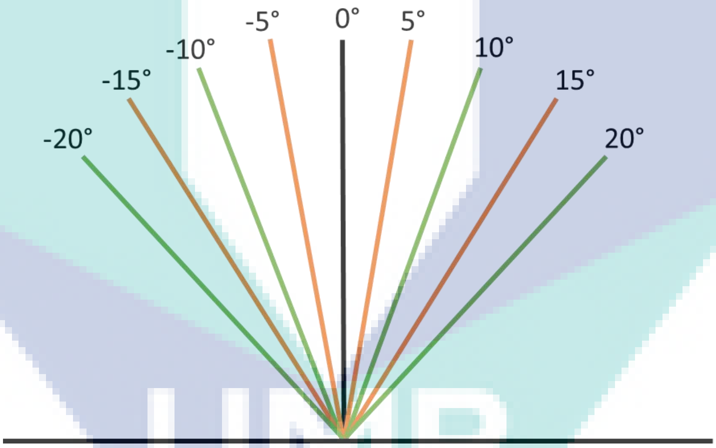

(b)

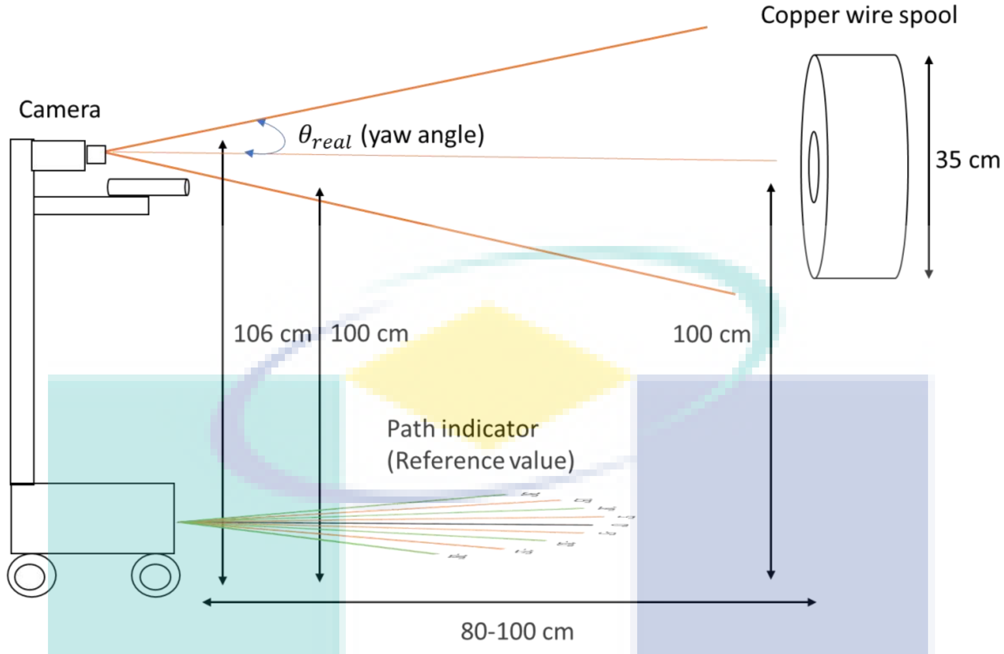

(c)

Figure 3.19 Path indicator (a) Path indicator for camera moving (b) Illustration of path indicator (c) Camera orientation experimental setup

In order to ensure the yaw angle estimation, both circle centers must overlap the RC. Theoretically, the yaw angle is considered 0° (parallel to spool) if the spool is at the center of the frame image. The RC (80,50) must overlap both circle centers (BC and SC) and the difference between the center should be (0,0). Therefore, a mathematical formula is created in order to determine the overlapping centers. However, the accepted distance between the center can be accepted within -2 to 2 pixels. The screen will display "Center overlapped" when the system detects the overlapping centers. Rule 3 below shows how the system decides the spool is at the center of the frame by using Equation 3.6 and 3.7.

$$\text{Rule 3} = \begin{cases} 1\ (\text{TRUE}),\ -2 \leq DC_1 \leq 2(BC) \\ 1\ (\text{TRUE}),\ -2 \leq DC_2 \leq 2(SC) \\ 0\ (\text{FALSE}), \text{otherwise} \end{cases}$$

DC_1 and DC_2 is calculated by using mathematical formula in Equation 3.6 and 3.7. The coordinate for the center of BC and SC is (X_1, Y_1) and (X_2, Y_2), respectively. Figure 3.20 shows the illustration design of DC_1 and DC_2 for further understanding.

$$DC_1 = ((80 - X_1),(50 - Y_1)) \quad 3.6$$

$$DC_2 = ((80 - X_2),(50 - Y_2)) \quad 3.7$$

Source: FA Azman et al. (2017)

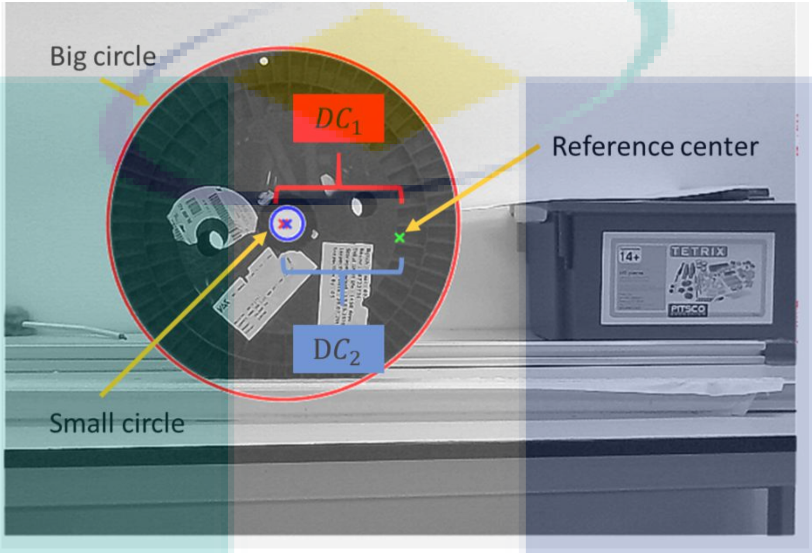

Figure 3.20 Illustration design of DC_1 and DC_2

The RC must overlap the BC and SC center because intuitively, when the centers overlapped, it means the spool center is aligning with center of the camera. However, the overlapping center cannot ensure the camera and the spool are aligned with each other. The camera is considered align with the spool when it fulfill two conditions which are:

i. The camera's yaw angle is at 0° by using Equation 3.5. The angle can be accepted within the range -0.25° to 0.25°.

ii. The distance calculation from camera to spool is within 50-60 cm distance range.

For first condition, it is crucial to get 0° even by using real-time robot. Therefore, the tolerance between puller and SC, t_f is used to determine the maximum and minimum angle which can be considered as aligned at 0°. For information, this system is evaluated until yaw angle estimation only. The puller diameter, P_d is 3.1 cm and the

SC diameter, SC_d is 3.6 cm. The explanation of the parameters used to determine the yaw angle is at 0° is shown in Figure 3.21.

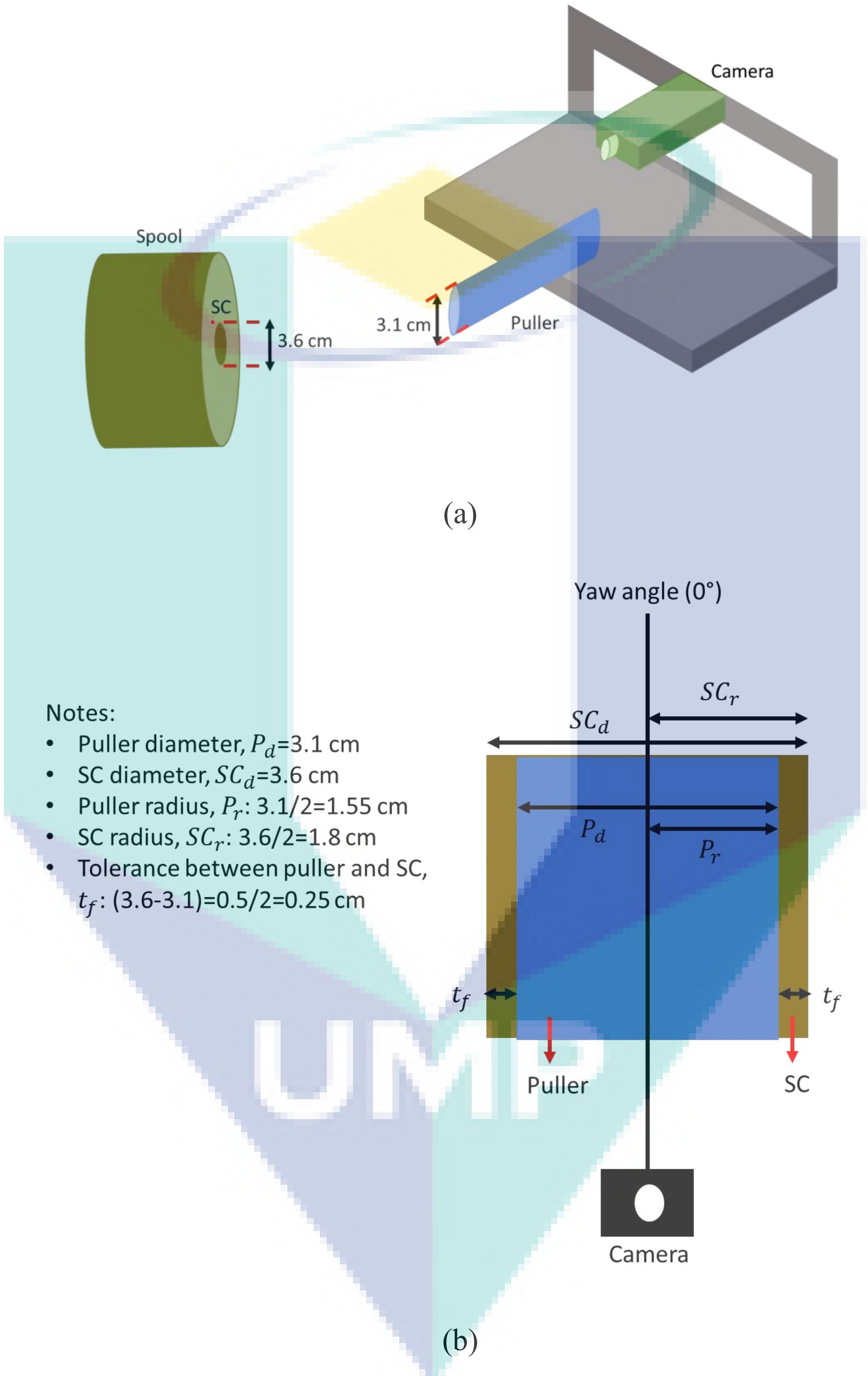

Figure 3.21 Illustration design for yaw angle at 0° (a) Puller diameter and SC diameter (b) Parameters used to determine yaw angle at 0°

The tolerance between puller and SC is 0.25 cm. From the analysis, the maximum yaw angle value can be accepted as aligned is 0.25°. The calculation is explained in Figure 3.22 and Equation 3.8. Equation 3.8 is a new mathematical equation created in order to prove the theoretical value for tolerance value, t_f. In order to ensure that the puller is not scratch the spool, the value of tx_r must be equal or less than t_f value which is 0.25 cm.

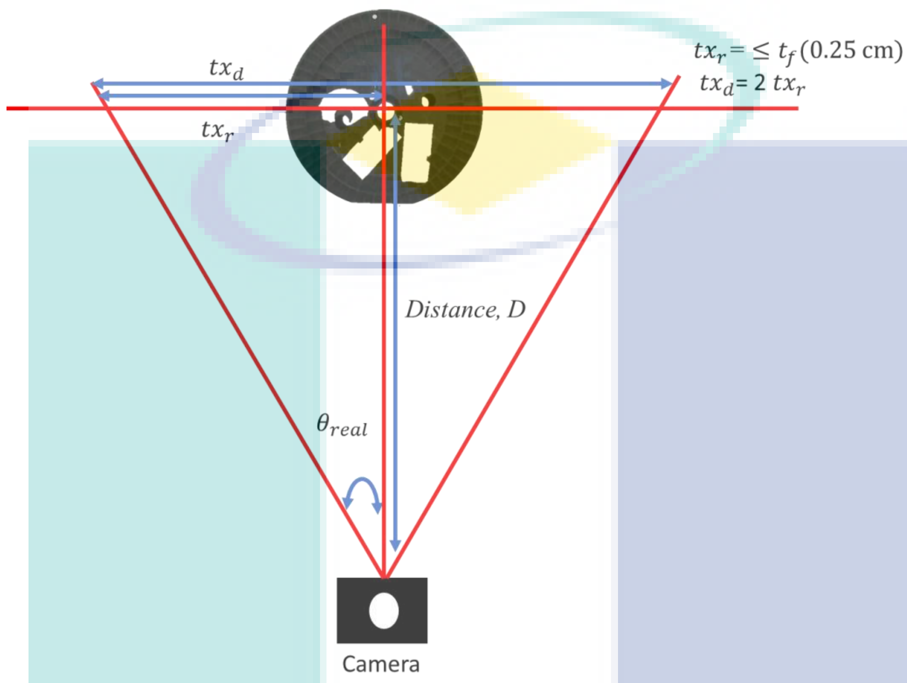

Figure 3.22 Illustration design for determining yaw angle in align position

$$tx_r = D \times |tan\ \theta_{real}| \quad 3.8$$

The θ_{real} value has positive and negative value as shown in path indicator value. In this study, the maximum distance value to determine whether the spool is aligned with the camera is 60 cm. Next, the minimum and maximum yaw angle value can be considered as aligned is -0.25° and 0.25°. Therefore, the value is used to calculate Equation 3.8.

3.5 Summary

This chapter has deliberated on the methods that is applied in this study to reach the objectives. The process of spool detection can be categorized in two main parts which are image processing and classification process. In image processing part, the original image captured by camera is previewed in grayscale image and filtered by using Gaussian filter. Next, the image transformed to binary image with 0.35 binary value. In order remove an unwanted image, opening and area opening method is applied. The main concern of image processing parts is to have a clear image of BC (outer circle parts of spool) and SC (hole of the spool) for spool detection. In feature extraction part, MCHT is applied to detect the BC and SC detection to prevent detection of false circles. Image is classified as BC in red color and SC in blue color in classification part. Next, the distance from camera to the spool is calculated once the spool is detected. The spool can be detected within the 50-110 cm distance range. In order to ensure the camera is aligned with the spool is based on the spools' image conditions. A mathematical equation is used to confirm the camera orientation. The camera orientation is calculated based on the center CFOV camera to BC center. The next chapter will discuss every part of the results and analysis obtain by using the methodology.

CHAPTER 4

RESULTS AND DISCUSSION

4.1 Introduction

This chapter has deliberated on the methods that are applied to achieve the objectives of this study. The training images used in this analysis are 40 data samples with different positions but same environment. The crucial part of this study includes the spool detection system and camera orientation system which involves the image processing techniques and MCHT. The next subchapter will discuss every part of the results and analysis obtained by using the methodology.

4.2 Proposed Detection System Analysis

The experimental results of detection system and camera orientation system is shown to give more details of this study and a simple understanding about this chapter. All the training images is taken at distance within 50-110 cm range and different angle with constant illumination value which is 202.3 lx. The same data samples used for proposed detection system analysis which is 40 data samples (V1-V40). This chapter will describe in detail the analysis of the techniques used in the development of the proposed system.

4.2.1 Image Pre-processing Analysis

In image pre-processing stage, 4 types of filtering test are carried out and analyzed. The filters used are Gaussian filter, Unsharp filter, Median filter and Average filter. The images are taken from different distance and different angles to show the reliability of each filters in order to maintain the SC image. In this analysis, the original image is converted to grayscale image and the filters are applied one by one to evaluate the performance. Figure 4.1 shows the data analysis from data samples V1-V40. In this analysis, all BC image can be detected. But, unlike BC, SC was hard to be detected effectively. Figure 4.1 shows that Gaussian and Unsharp filter can maintain the small circle (SC) image smoothly compared to Median and Average filter. There are some data samples cannot be filtered through the filtering method because it erased the SC image such as V11, V13, V14, V30 and V31. However, most of the data samples can extract the BC and SC image.

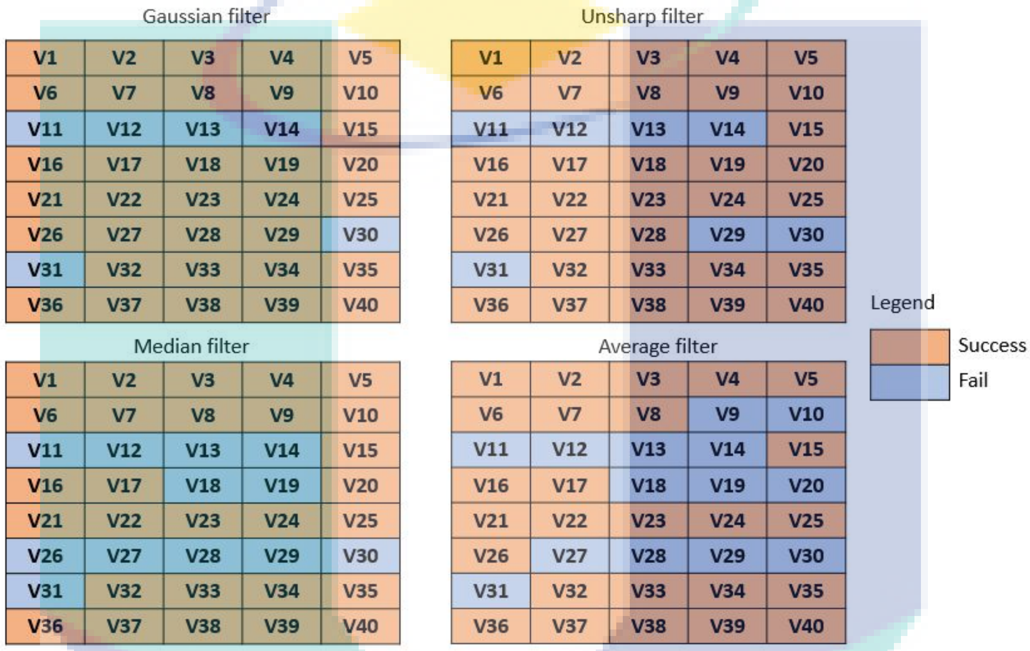

Figure 4.1 Comparison of filter methods

The filtering success rate analysis is made in Figure 4.2 (a). This analysis used 40 samples of images (V1-V40) to analyze each filter. In Figure 4.2 (a), there are two highest percentages for filtering success rate analysis which are Gaussian and Unsharp filter followed by Median and Average filter. Average filter has the lowest percentage compared to others. Median and Average filter has the lowest percentage with 70% and 65%. Gaussian filter has the highest success rate detection with 85%. Therefore, Gaussian filter is able to maintain the SC image compared to other filters. Gaussian filter blurs the image by decreasing the edge between pixels of the image which can improve the accuracy of spool detection. Gaussian filter has the best filtering success rate compared to others and it is the most suitable filter to use in this study. Figure 4.2 (b) shows the pixel value for filtering analysis sort from the smallest value to the largest value. In average, the pixel value for all filtering methods is done from 11671-15662 pixel. Based on Figure 4.2 (a), Gaussian filter has highest percentage for success rate analysis. In conclusion, Gaussian filter is able to maintain BC and SC image with 12252-15584 pixel.

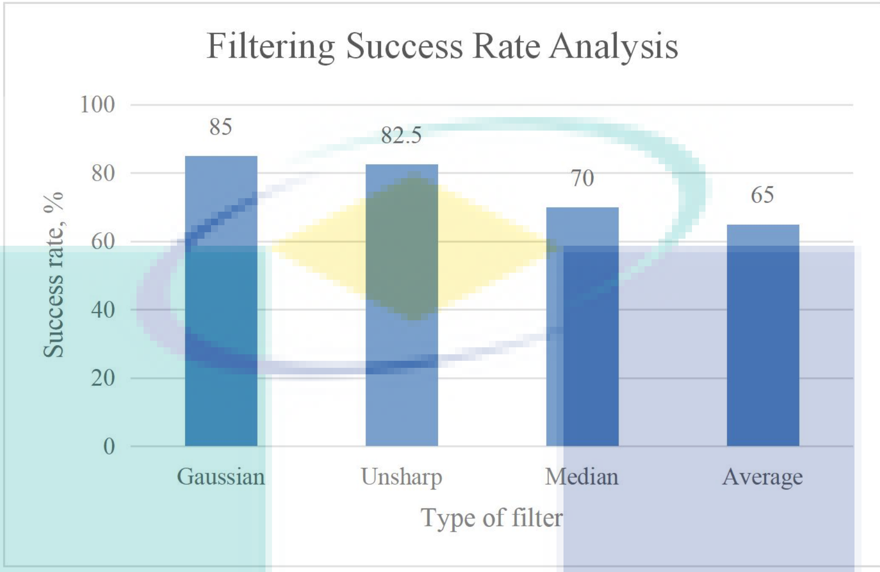

(a)

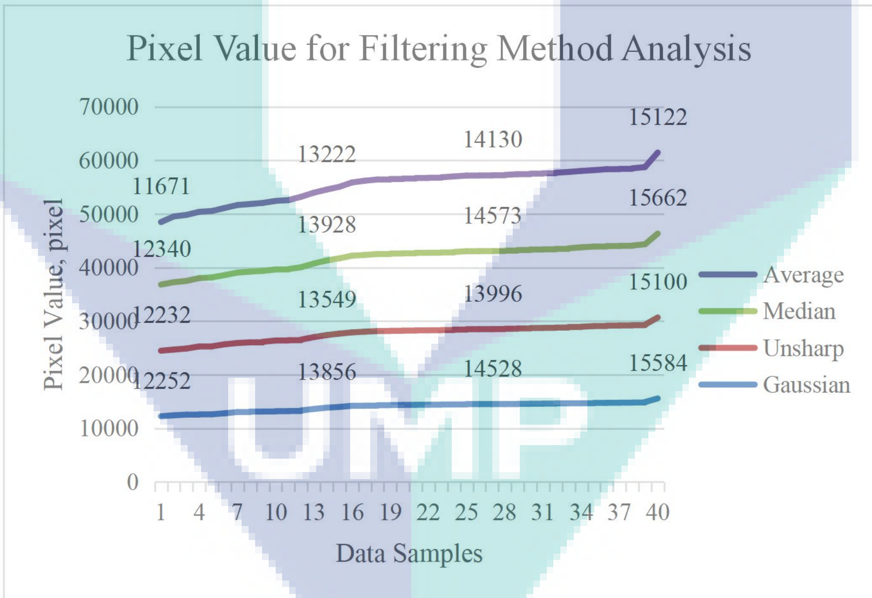

(b)

Figure 4.2 Filtering method analysis (a) Filtering success rate analysis (b) Pixel value for filtering method analysis

4.2.2 Image Segmentation Analysis

In this subchapter, the analysis of threshold binary value and morphological method will be discussed. In image processing parts, it involves binarization, opening and area opening method. In this subchapter, the threshold binary value and the morphology detection success rate is tested and analyzed. This analysis is to increase the accuracy of SC detection after filtering method. The threshold binary value used in this analysis is 0.35 which is determined based on trial and error. The threshold binary values are compared between 0.2, 0.25, 0.3, 0.35, 0.4 and 0.45. However, in this study, the threshold binary values used to analyse are 0.25, 0.35 and 0.45 because those values are the closest value that can fulfill the conditions. The other analysis is shown in Appendix F. The total samples used for this threshold value analysis is 40 samples. Figure 4.3 shows that the threshold binary value can increase the accuracy of SC detection by using 0.35 binary value.

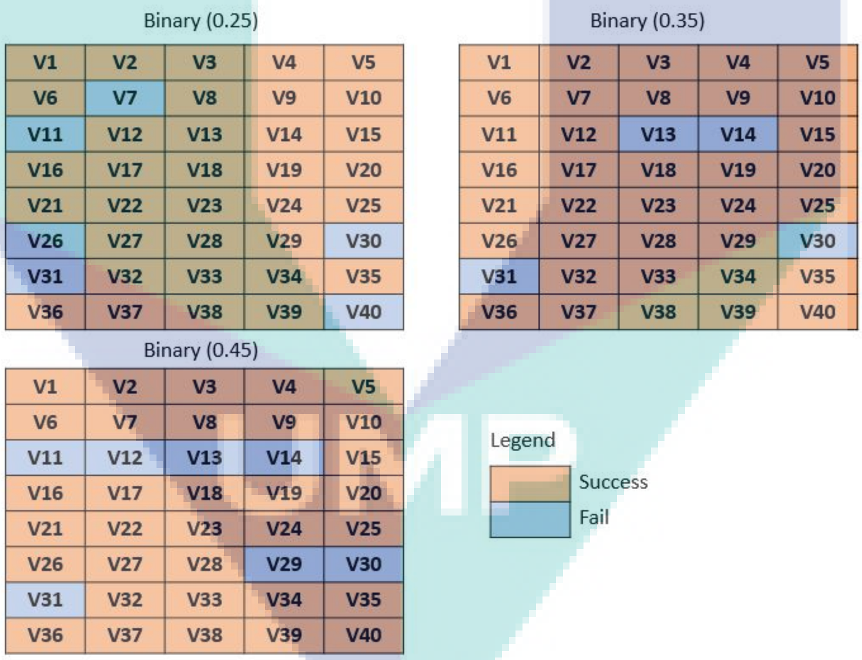

Figure 4.3 Comparison of threshold binary value

The binarization success rate analysis is shown in Figure 4.4 (a). The analysis has been done with the same samples from Figure 4.3. It shows that 0.35 binary value has the highest percentage which are 90%. For 0.45 binary value, it shows that it has lowest percentage which is 82.5%. The success rate analysis for 0.35 binary value increased 5% compared to Gaussian filtering method. Therefore, the threshold value is set to 0.35 pixel to fulfill all binarization process conditions for better noise removal process in image hence, increase the accuracy of SC detection. Next, Figure 4.4 (b) shows that the average pixels for 0.25, 0.35 and 0.45 binary value. The pixel value range for the three binary values are from 14252-16290, 13307-15938 and 12664-15274 pixels. In addition, the average pixels value for the three binary values are 15874.8, 14892.9 and 14434.9 pixels. Therefore, the binary value used in this system is 0.35 with 14892.9 average pixels value.

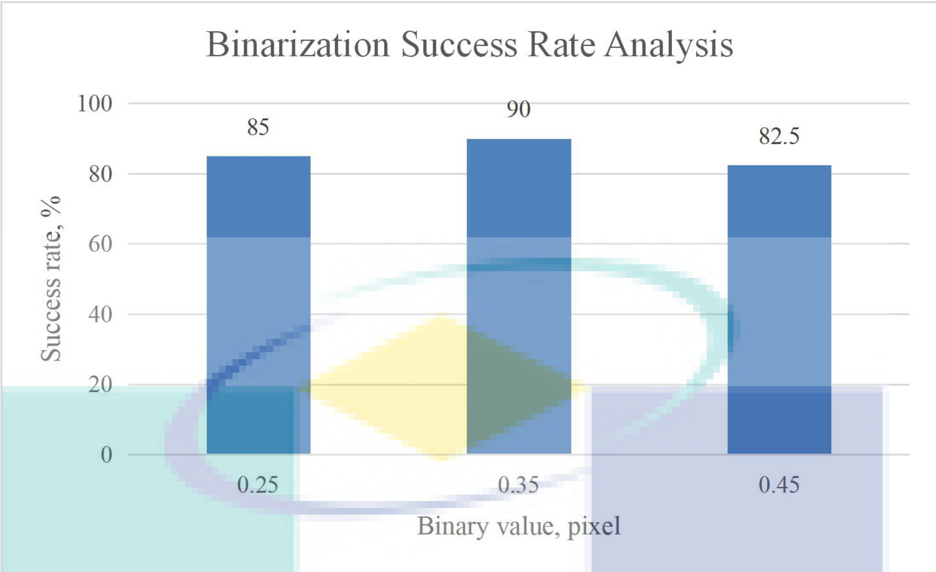

(a)

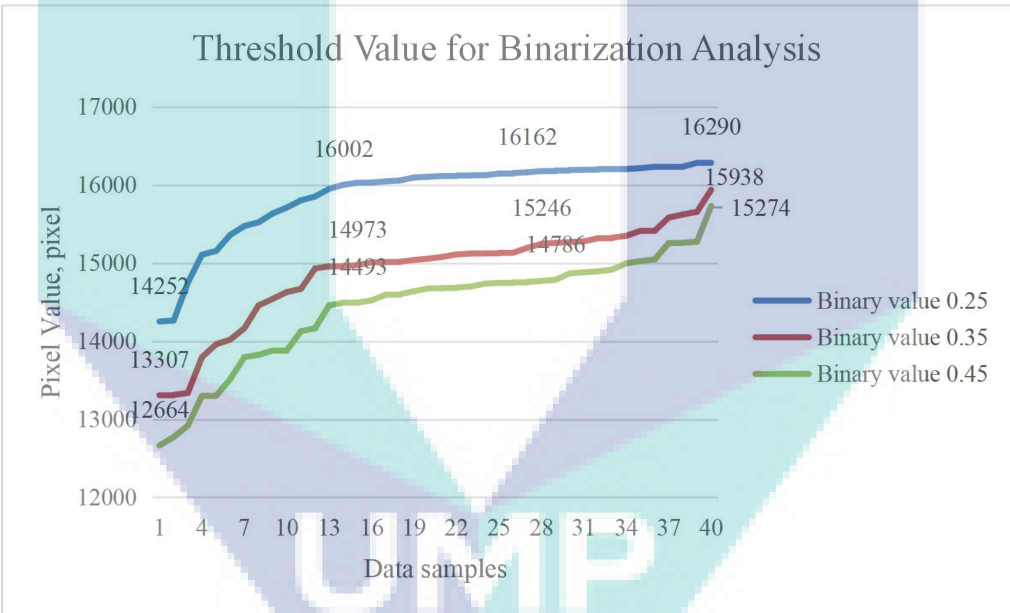

(b)

Figure 4.4 Binarization analysis (a) Binarization success rate analysis (b) Threshold value for binarization analysis.

Next, the analysis between opening, dilation and erosion method. Figure 4.5 shows the comparison for morphology methods. From Figure 4.5, it shows that dilation and erosion method is not suitable to be used in this study because it effects the SC image after both methods are applied. In addition, the possibility of SC image is merged with outliers' image thus produced false circle detections is higher. Therefore, opening method is suitable in this study compared to others in order to prevent false circle detections.

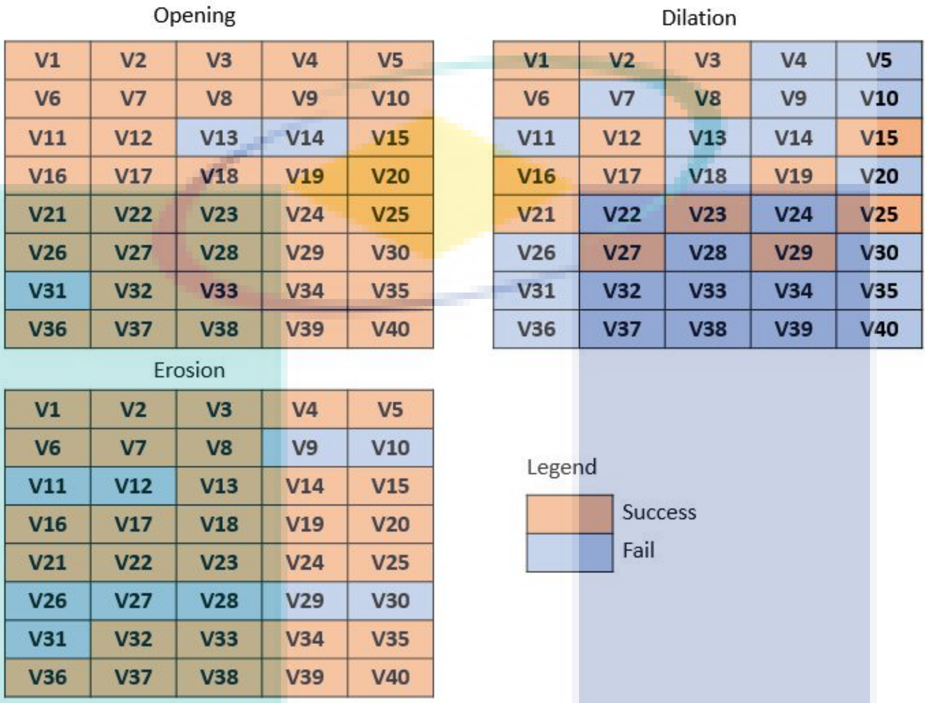

Figure 4.5 Comparison of morphology method.

The morphology success rate analysis is discussed and shown in Figure 4.6 (a). The total data sampling used for this analysis is 40 samples. From the graph shown in Figure 4.6 (a), it shows that opening method has the highest percentage which is 92.5% compared to others. Dilation method has the lowest percentage which is 37.5% and 75% for erosion method. Therefore, it is proven that opening method has the highest success rate for BC and SC detection compared to others and it is the most suitable morphology method to use in this study. Next, Figure 4.6 (b) shows that the pixel value for morphology method. Based on Figure 4.6 (a), opening method has highest percentage for success rate analysis. As conclusion, opening method is able to maintain BC and SC image with 13178-15911 pixel.

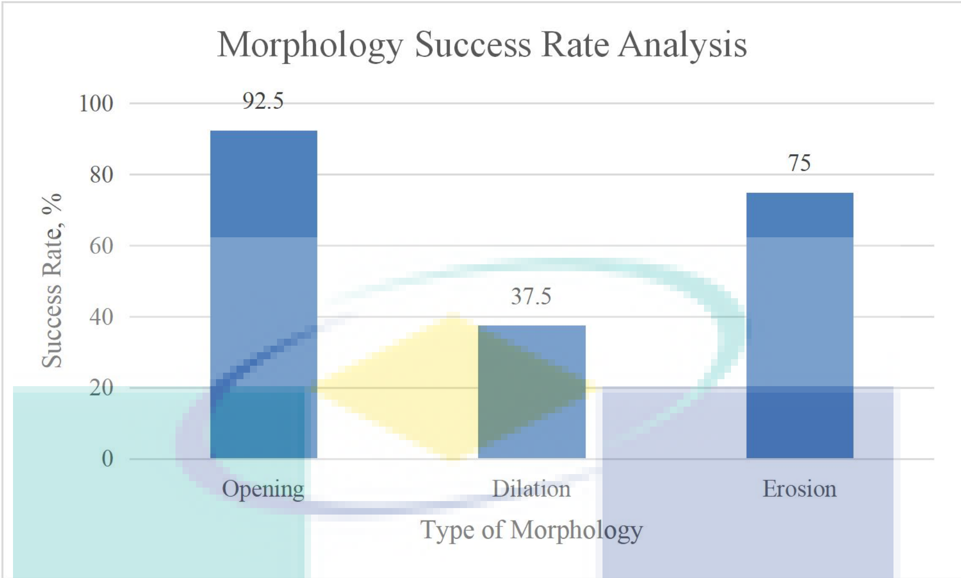

(a)

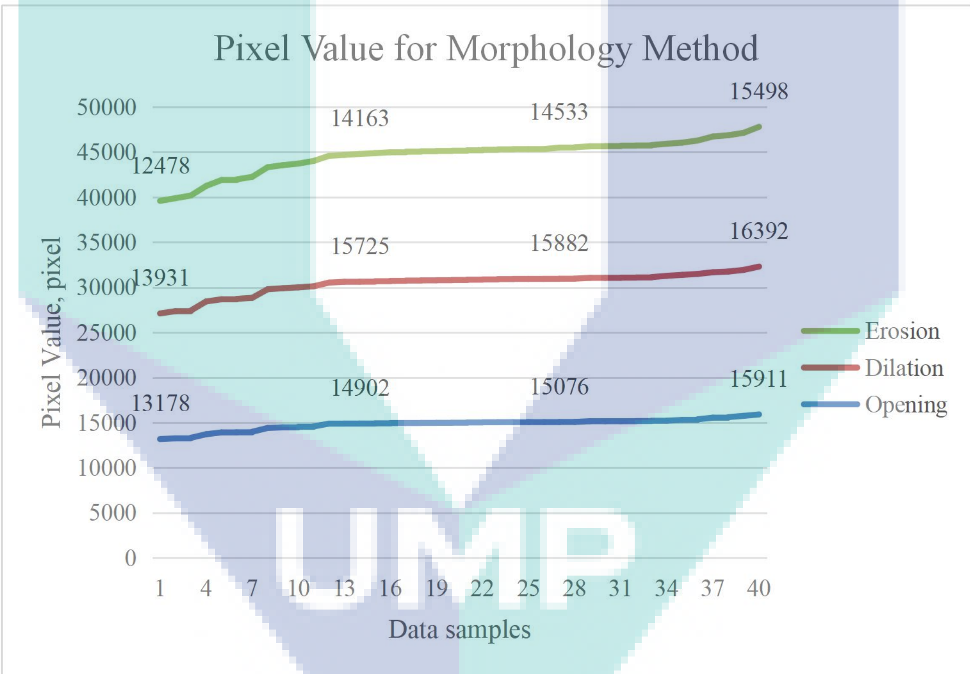

(b)

Figure 4.6 Morphology analysis (a) Morphology success rate analysis (b) Pixel value for morphology method

4.2.3 Object Classification Analysis

In this subchapter, the object classification process will classify BC in red color and SC in blue color. When both circles or BC are detected, "Spool detected" will display on the screen. No message will display on the screen when BC and SC not detected. The data samples used for this analysis is 40 samples. Figure 4.7 shows the MCHT method can detect BC accurately with 100% percentage whereas 90% for SC detection.

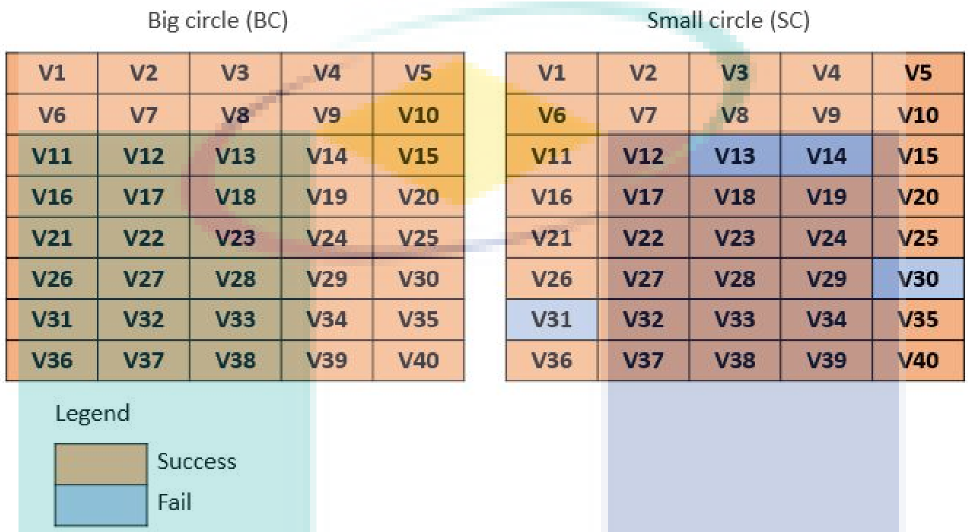

(a)

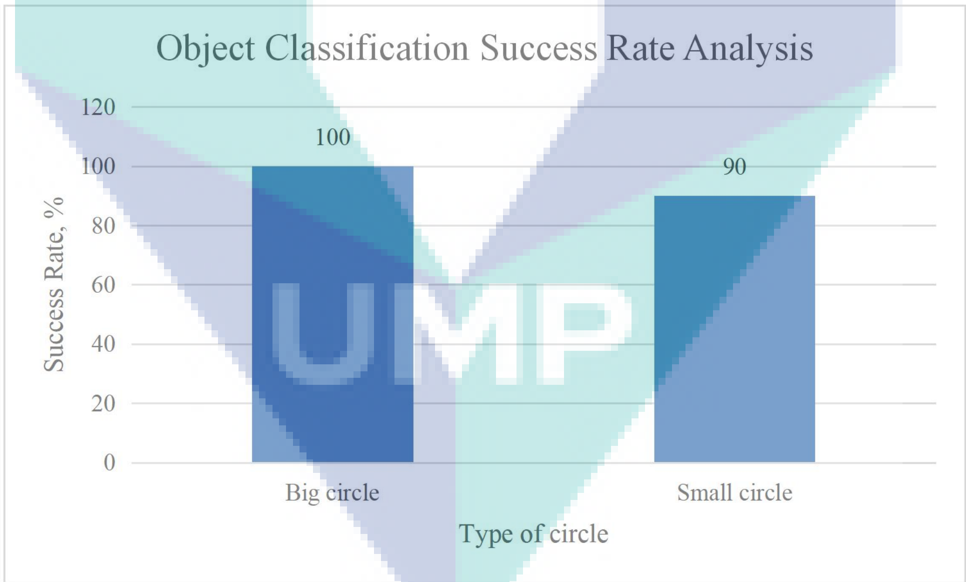

(b)

Figure 4.7 Object classification analysis (a) Data samples chart (b) Object classification success rate analysis

There are difficulties to detect SC for data samples V13, V14, V30 and V31. It is because the SC image is too small for detection purpose. Although it gives 90%

percentage for SC detection, it does not effect the system because the system needs to detect BC detection first followed by SC. The BC detection shows high percentage from 50-110 cm distance range which is 100%. For conclusion, the proposed system able to classify the spool at distance range 50-110 cm.

4.3 Results of Spool Detection

In this subchapter, the final output of detection algorithm is shown after implementing all methods mentioned in Chapter 3. The proposed method which is MCHT is compared with CHT method. All the results shown in grayscale filter. The red circle in the image represents the BC whereas the blue circle represents the SC. Figure 4.8 shows the results of spool detection using MCHT method. The system will detect the BC and SC within the radius range 35-65 pixel and 3-15 pixel. Additionally, the minimum value of distance the spool is detected within 50-110 cm distance range. Once the spool is detected, the estimated distance of camera to spool and the camera orientation are displayed on the screen. This results are taken by using real-time experiment. Figure 4.8 shows the MCHT method is able to detect the copper wire spool with various angles (0°-20°).

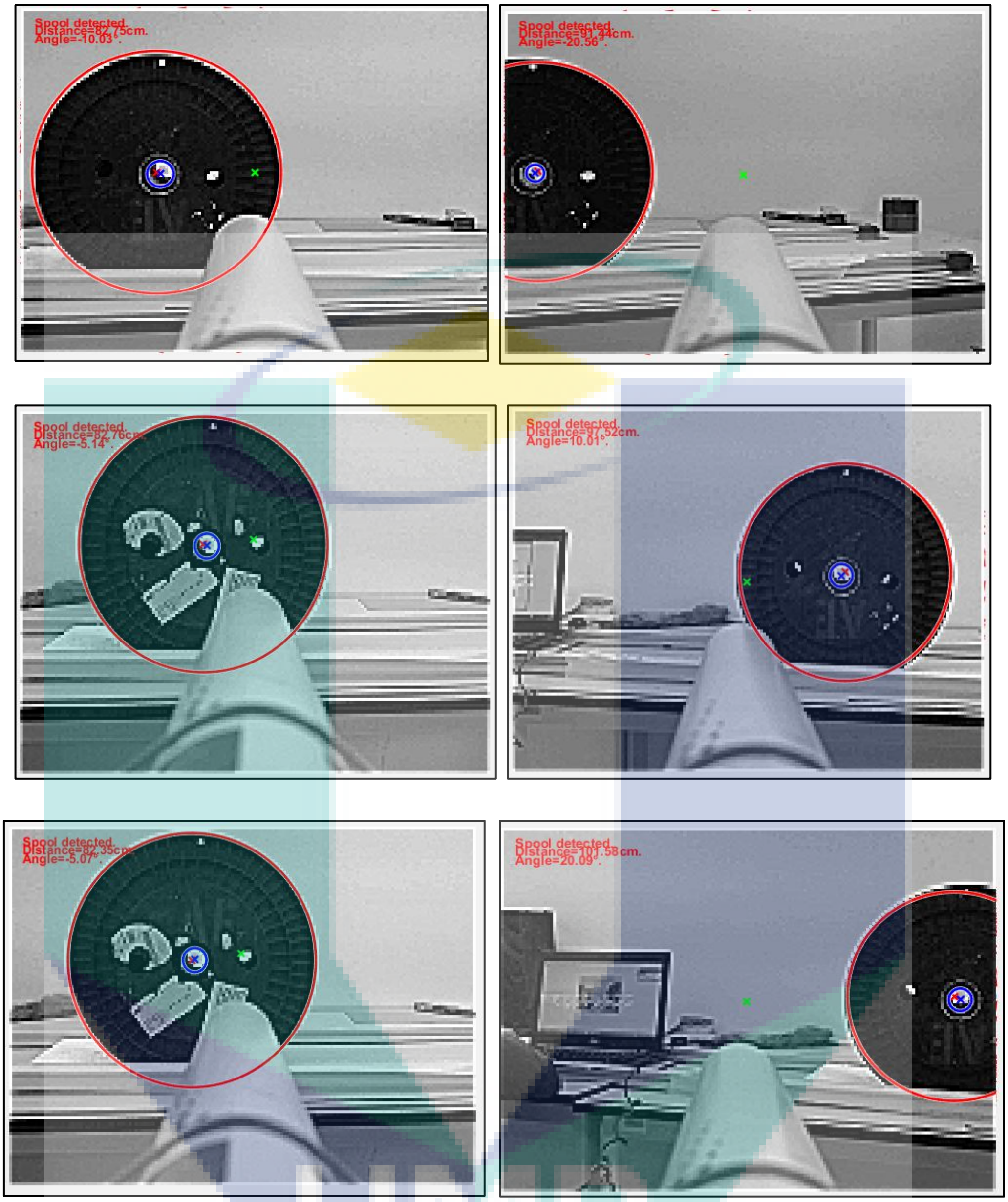

Figure 4.8 Spool detected in various angle and position

In other cases, the screen will not display anything when there is no detection. Therefore, the system will keep searching for the spool. Figure 4.9 shows the results when the system does not detect the spool which happened because of two factors. Firstly, the spool is out of the distance range of 50 cm to 110 cm. Secondly, camera orientation is more than 20°.

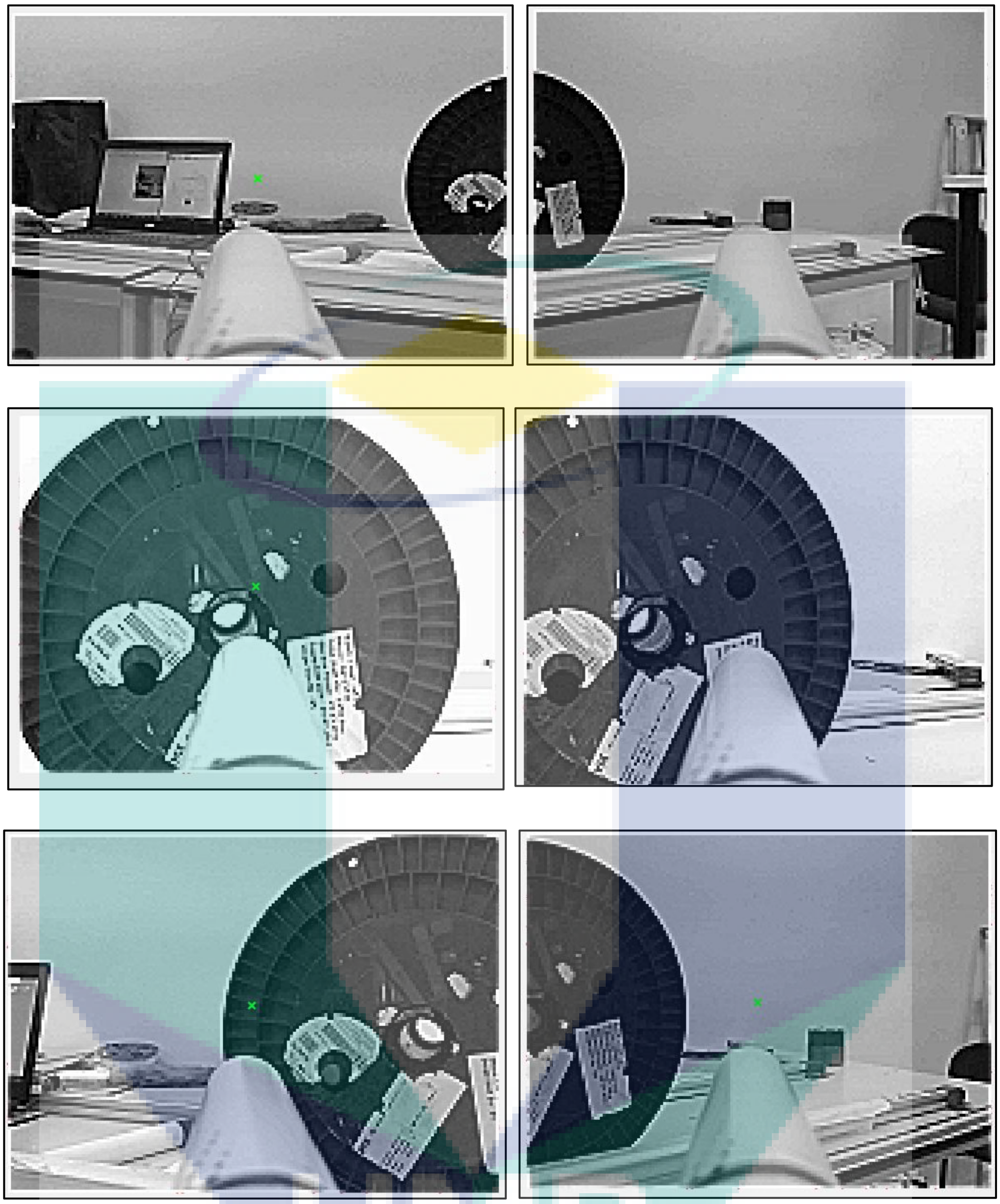

Figure 4.9 Spool is not detected in various angle

4.3.1 Comparison of CHT and MCHT method

Circular Hough Transform (CHT) is the original method for circle detection. Figure 4.10 shows the CHT method can detect the circular shape in the spool image. Moreover, it shows that by using CHT method only, it produces low accuracy for SC detection. There are false detections and outliers. However, CHT can detect BC accurately compared to SC. There are some input arguments need to be adjusted to produce high accuracy which are sensitivity and object polarity. The total samples used in this analysis is 100 samples taken by real-time experiment with various distance and angles. As mentioned in previous subchapter, the image of spool has a lot of noise that is hard to be removed. Thus, the MCHT method is an improvement from the CHT method to be able to classify the true circles. CHT method detect the BC and SC by using Rule 1 as mentioned in Subchapter 3.3.4.

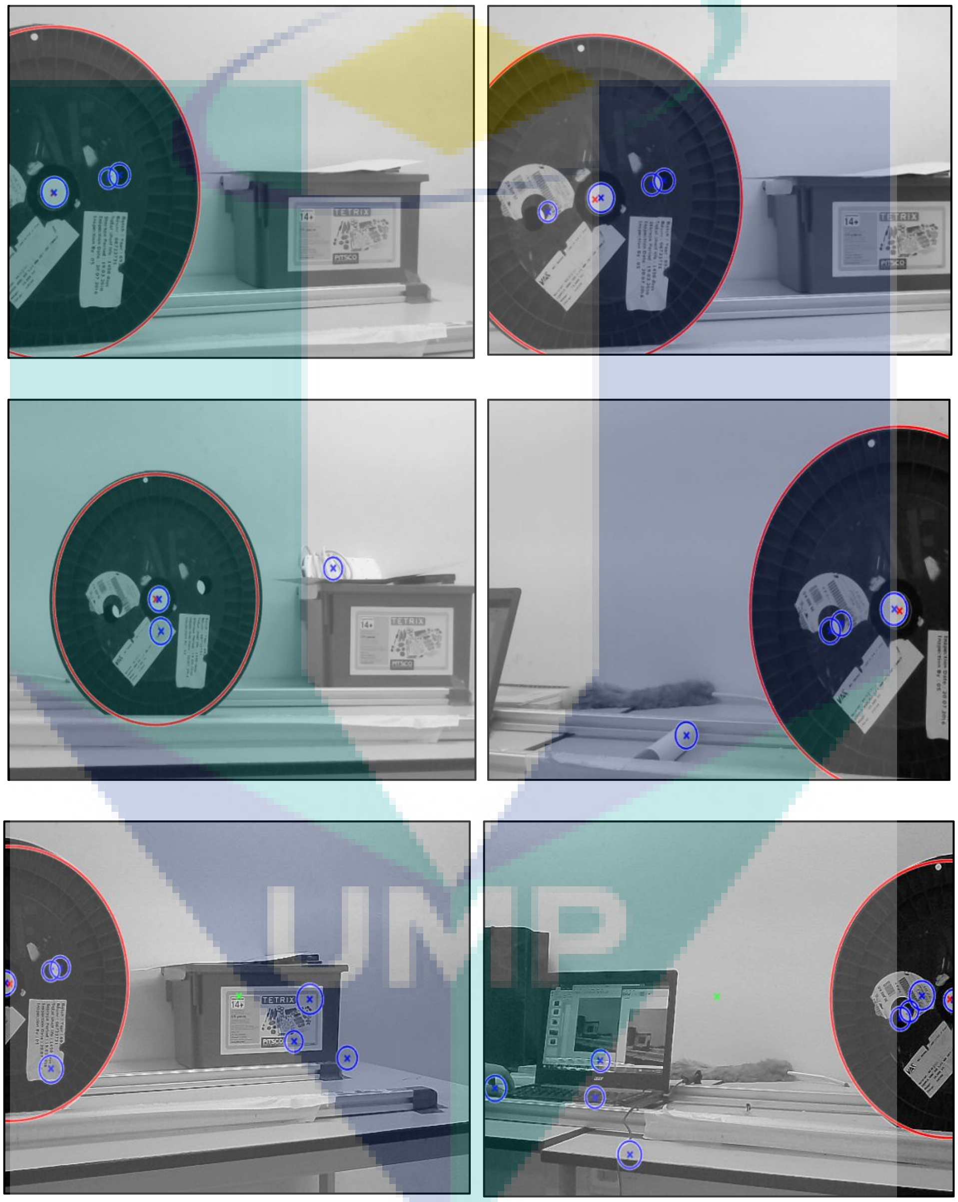

Figure 4.10 Spool detection by using CHT method

To increase the accuracy of SC detection, MCHT, an improved CHT is used. Figure 4.11 shows the results performed by using MCHT. It shows that there are no false SC detections and outliers compared to CHT method. Additionally, MCHT also can detect BC without false circles.

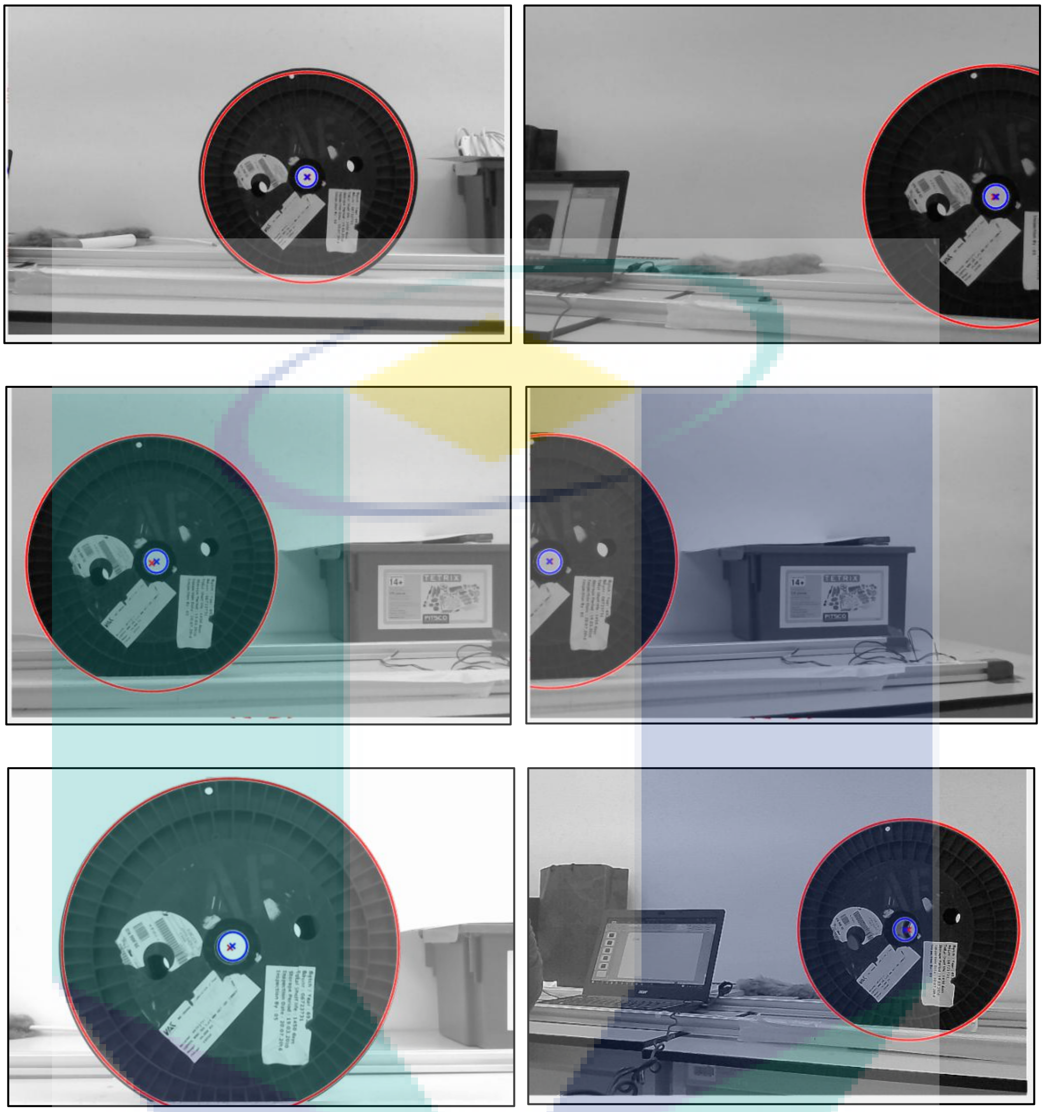

Figure 4.11 Spool detection by using MCHT method

The results are taken and shown in Figure 4.12 (a) for success rate analysis. The success rate between CHT and MCHT method is analyzed and shown in Figure 4.12 (b). There are 100 samples used in this analysis. Both methods can detect BC accurately compared to SC detection. Figure 4.12 (b) shows that both methods can detect BC accurately with a 100% success rate. However, the CHT method has a low success rate which is 48%. It is because CHT detects many false detections compared to MCHT. MCHT has a 96% success rate and the remaining 4% is because of false detections. From the analysis, it is proven that MCHT produce high accuracy and prevent false circle detections compared to CHT method with various angles and illumination conditions.

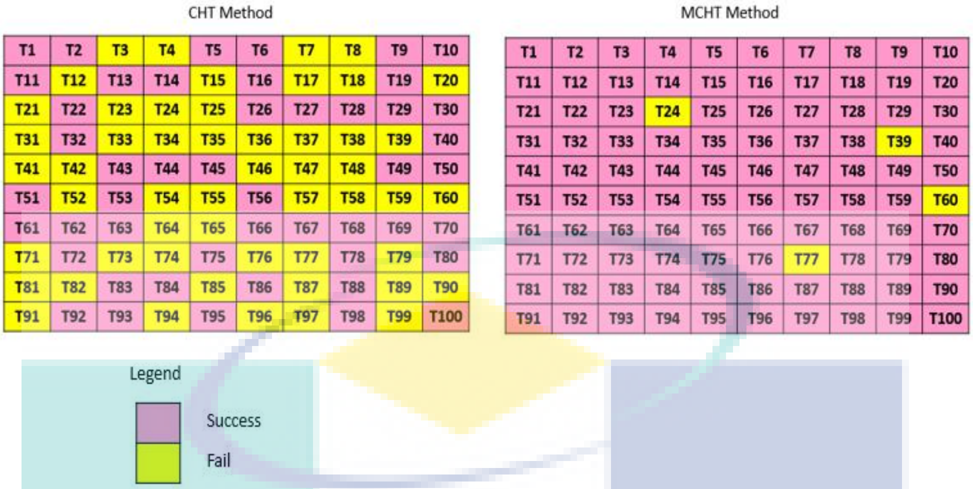

(a)

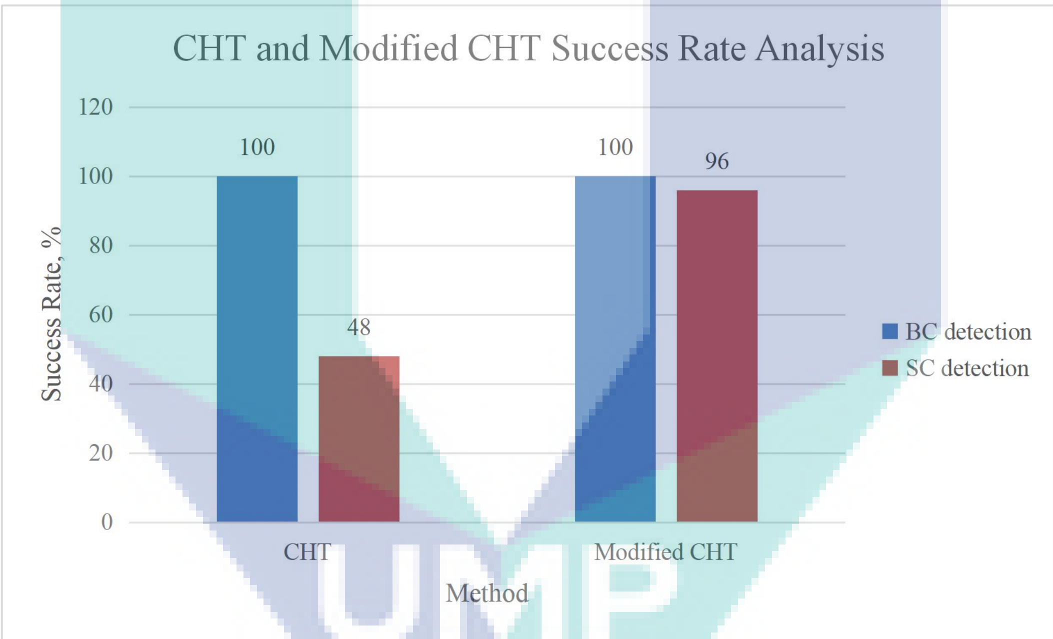

(b)

Figure 4.12 CHT and Modified CHT analysis (a) Data comparison chart (b) CHT and MCHT success rate analysis

4.3.2 Illumination Measurement Analysis

In this subchapter, the reliability of the spool detection system is analysed. The illumination factor is one of the common issues when it comes to image processing. There are few conditions to analyse the illumination factor. The reliability of the system is analysed to observe the illumination success rate in detecting spool in an indoor environment (Robotic Lab). Noted that this study has been done with default illumination where all switches are turned on. There are three switches, S1, S2, and S3. The illumination is measured by using Lux Meter application on Android. The analysis is shown in Figure 4.13, 4.14 and 4.15. It shows that the fourth condition are able to detect BC and SC almost accurate compared to other conditions. The results are taken in real-time experiment and shown in Figure 4.13 for success rate analysis calculation. There are 20 data samples used in this analysis. The illumination is analyzed in four conditions which are:

i. S1, S2 turn on (S3 turn off)

ii. S1, S3 turn on (S2 turn off)

iii. S2, S3 turn on (S1 turn off)

iv. S1, S2, S3 turn on

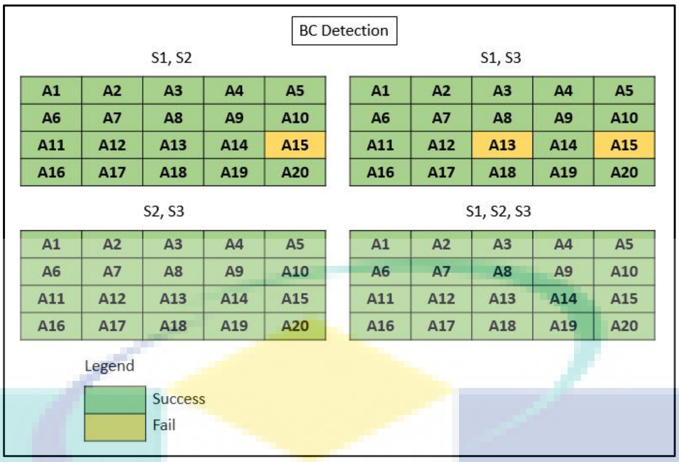

(a)

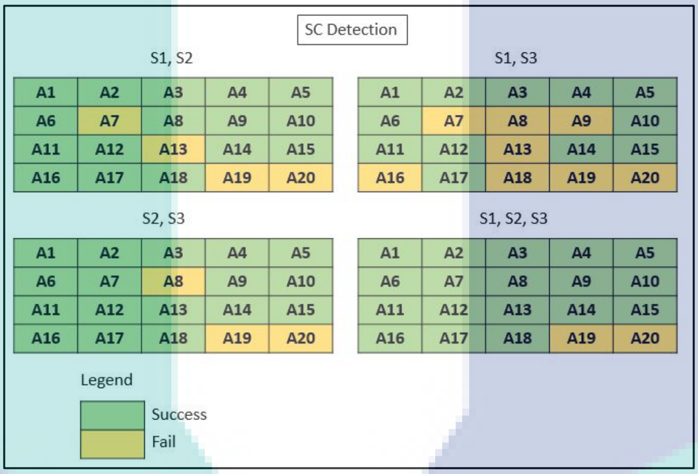

(b)

Figure 4.13 Comparison of illumination measurement analysis (a) BC data samples chart (b) SC data samples chart

Figure 4.14 shows that the system able to detect the spool whenever one of the switches is turn off. For second condition (S1, S3 turn on), it shows low percentage of SC detection which is 60% success rate. As information, second condition has the lowest illumination compared to other conditions. However, it is still able to detect BC with 90% success rate. The other conditions have high success rate for SC detection which are 80%, 85% and 90%. As for first condition (S1, S2 turn on), it has 95% success rate for BC detection and 80% success rate for SC detection. Next, the third condition (S2, S3 turn on) has high success rate for BC detection which is 100% and 85% for SC detection. All conditions have a high success rate for BC detection. Thus, the reliability of the system for different illumination for BC detection is proved. Lastly, the fourth condition the highest success rate among others which prove the illumination measurement analysis. The higher the illumination value, the higher the detection rate. However, the illumination is limited with 50-110 cm distance range. Therefore, this system is done by using the fourth condition to increase the accuracy detection of spool.

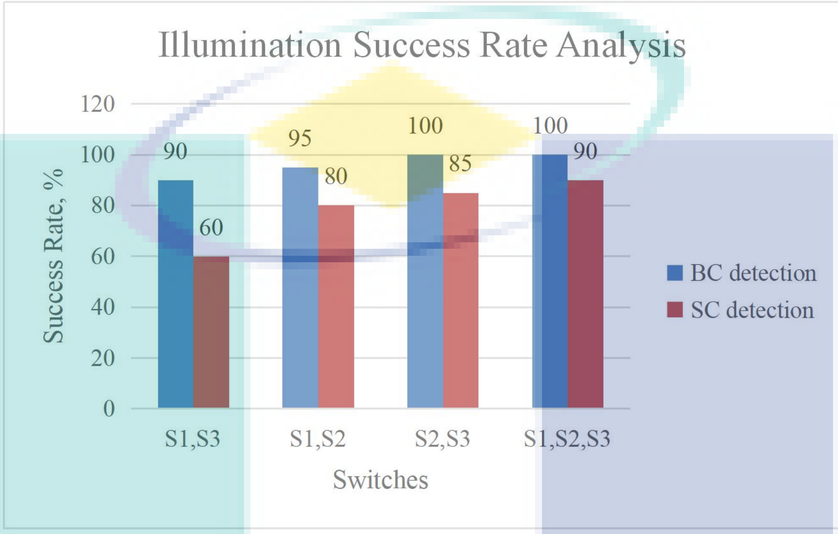

Figure 4.14 Illumination success rate analysis

From Figure 4.15, it shows the illumination measurement analysis for four switch conditions. For first condition, the minimum value of lux meter is 108 lx and the maximum value is 126 lx. Next, the minimum and maximum value lux meter for second condition are 98 lx and 121 lx. In addition, second condition has the lowest illumination lux meter compared to others. For third condition, the minimum and maximum value of lux meter are 140 lx and 170 lx. Lastly, by turn on all the switches, the minimum and maximum value of lux meter are 179 lx and 205 lx. It shows that the fourth condition has the highest value of lux meter compared to others. The detection success rate is analyzed in order to analyze which conditions is the most suitable for this system and the reliability of this system towards the illumination factor. The analysis is shown in Figure 4.15.

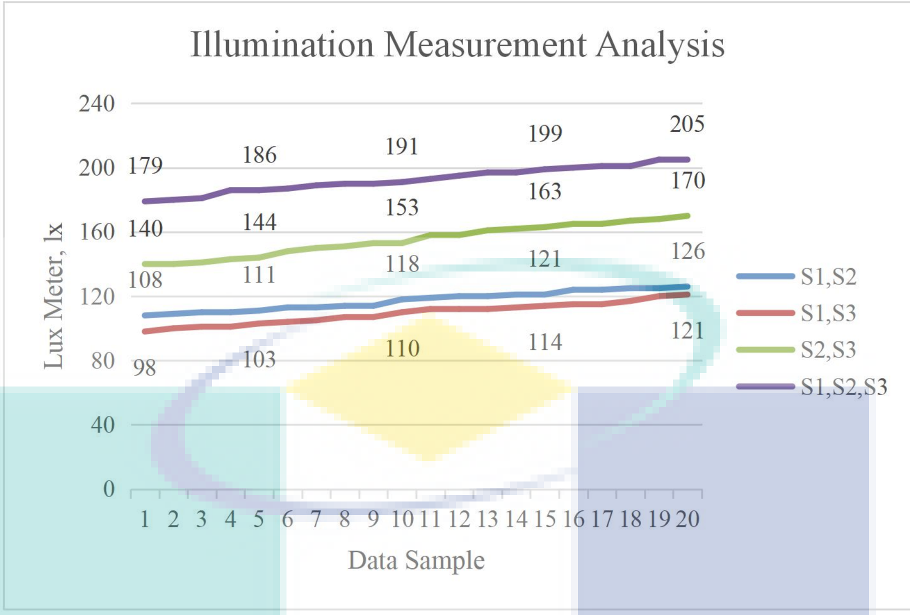

Figure 4.15 Illumination success rate analysis

4.4 Proposed Camera Orientation System Analysis

In this subchapter, the camera orientation analysis is shown to evaluate the success rate of the proposed method. Camera orientation analysis is including the distance calculation and yaw angle calculation. This chapter will discuss a detail analysis of the techniques used in the development of the proposed system.

4.4.1 Distance Calculation Analysis

The distance calculation used in this system is analyzed. By using Equation 3.2, the distance of camera to spool is calculated and compared with the real measurement by using measuring tape. The camera position is fix to 0°. The system will calculate the camera orientation once the system detects the spool. Hence, the camera position can be fix to 0°. The analysis results shown in the Figure 4.16. There are 30 samples taken from real-time experiment for distance calculation analysis. The real distance value is measured by using measuring tape and the calculated distance is calculated by using Equation 3.2. The table analysis is shown in Appendix C.

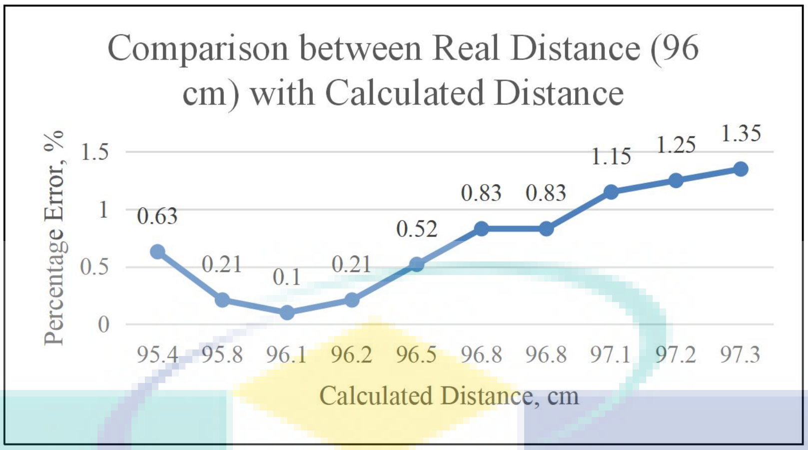

(a)

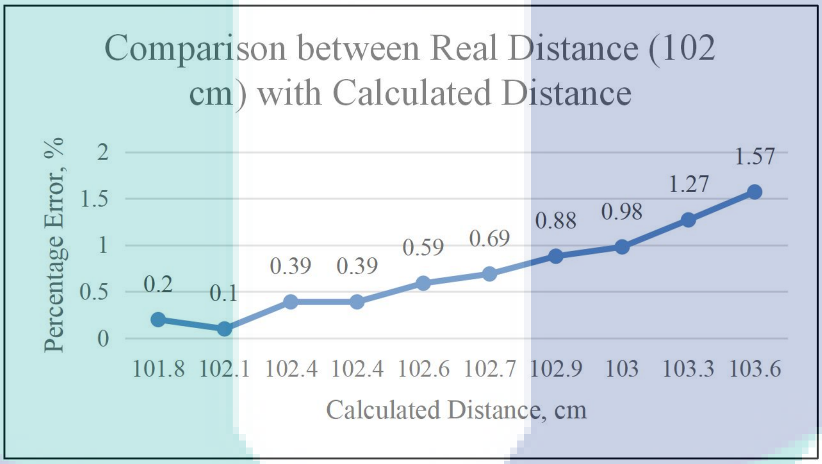

(b)

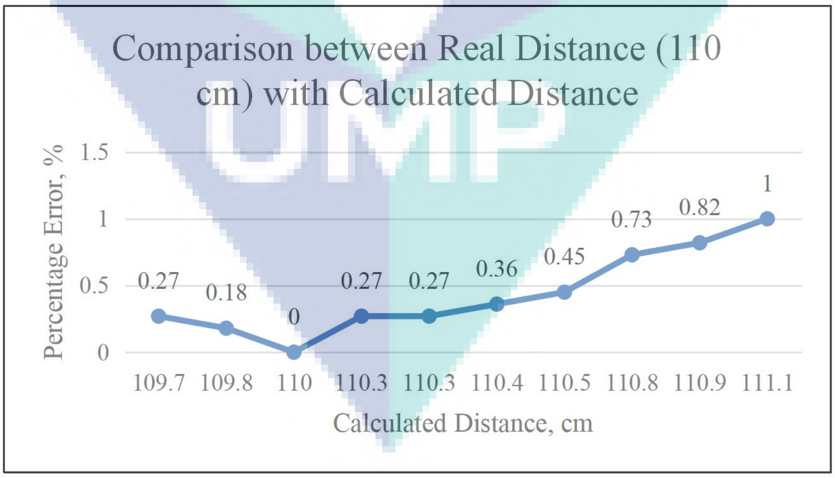

(c)

Figure 4.16 Distance calculation analysis compared to real distance value (a) 96 cm (b) 102 cm (c) 110 cm

From Figure 4.16, the calculated distance value is compared with real distance value by determining the percentage error value. From the figure, it shows that the results have low percentage error for the calculated distance compared to the real distance. The error rate for distance analysis is consistent except for 1.57%. It may be caused by image processing process when the camera cannot detect the spool correctly. The distance is calculated when the system detects the spool. From the analysis, the formula for distance calculation can be used because of the low percentage error.

4.4.2 Yaw Angle Analysis

In this subchapter, the yaw angle is analyzed to evaluate the performance of the distance calculation algorithm. The yaw angle is determined and compared with reference value and experimental value. The distance of camera to spool is measured by using measuring tape because it does not effect the yaw angle value. The yaw angle was analyzed in various distance from 80-100 cm. The calculated yaw angle is shown in Table 4.1 by using Equation 3.4 and 3.5 as mentioned in Subchapter 3.4.2.

Table 4.1 Yaw angle analysis

No.	Distance value (cm)	Yaw angle				
		Reference value (°)	Experimental value 1 (°)	Percentage error (%)	Experimental value 2 (°)	Percentage error (%)
1		-20.0	-19.98	0.10	-20.01	0.05
2		-15.0	-15.14	0.93	-15.57	3.80
3		-10.0	-10.08	0.80	-10.60	6.00
4		-5.0	-5.12	2.40	-5.05	1.00
5	100	0.0	-0.02	0.00	0.10	0.00
6		5.0	5.02	0.40	5.07	1.40
7		10.0	10.03	0.30	9.97	0.30
8		15.0	15.01	0.07	15.02	0.13
9		20.0	20.01	0.05	20.06	0.30
10		-20.0	-19.90	0.50	-20.13	0.65
11		-15.0	-15.22	1.47	-15.35	2.33
12		-10.0	-10.03	0.30	-10.09	0.90
13		-5.0	-5.02	0.40	-5.07	1.40
14	90	0.0	0.12	0.00	-0.25	0.00
15		5.0	5.01	0.20	4.94	1.20
16		10.0	10.02	0.20	9.94	0.60
17		15.0	15.08	0.53	14.97	0.20
18		20.0	20.17	0.85	20.08	0.40
19		-20.0	-20.64	3.20	-20.56	2.80
20		-15.0	-15.08	0.53	-15.46	3.07
21	80	-10.0	-9.93	0.70	-10.06	0.60
22		-5.0	-5.09	1.80	-5.03	0.60
23		0.0	-0.09	0.00	0.23	0.00

24	5.0	5.00	0.00	5.03	0.60
25	10.0	9.92	0.80	10.01	0.10
26	15.0	14.99	0.07	15.01	0.07
27	20.0	19.94	0.30	20.09	0.45

From Table 4.1, the yaw angle value is calculated from -5° to 20° angle. It is because the spool can be seen and detected clearly from that angle. There are two experimental values taken for this analysis. The results of the analysis are shown in percentage error between reference and experimental value as shown in Table 4.1. Most of the results give low percentage error which are from 0% to 1.47%. Although there is slightly high error rate, it is caused by the image processing analysis that unable to remove the noise in image perfectly. Generally, the camera and the spool are at the aligned position when the center of the spool overlapped with the center of the frame. The yaw angle must be at 0°. In Figure 4.17, the analysis has been done with two distance values which is 50 cm and 60 cm. Additionally, 60 cm is the maximum distance for puller to be inserted to the CHS. Hence, this analysis to prove that the camera is considered at aligned position whenever the yaw angle is at -0.25° to 0.25º theoretically. Next, this analysis is to ensure the tolerance between puller and SC is equal or less than 0.25 cm by using Equation 3.8 so that the puller is not scratch the spool.

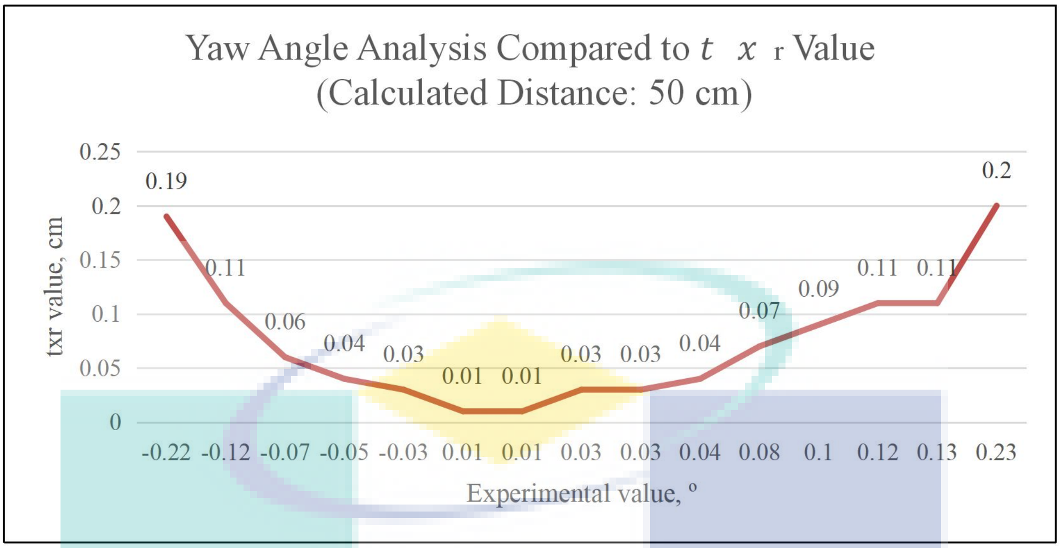

(a)

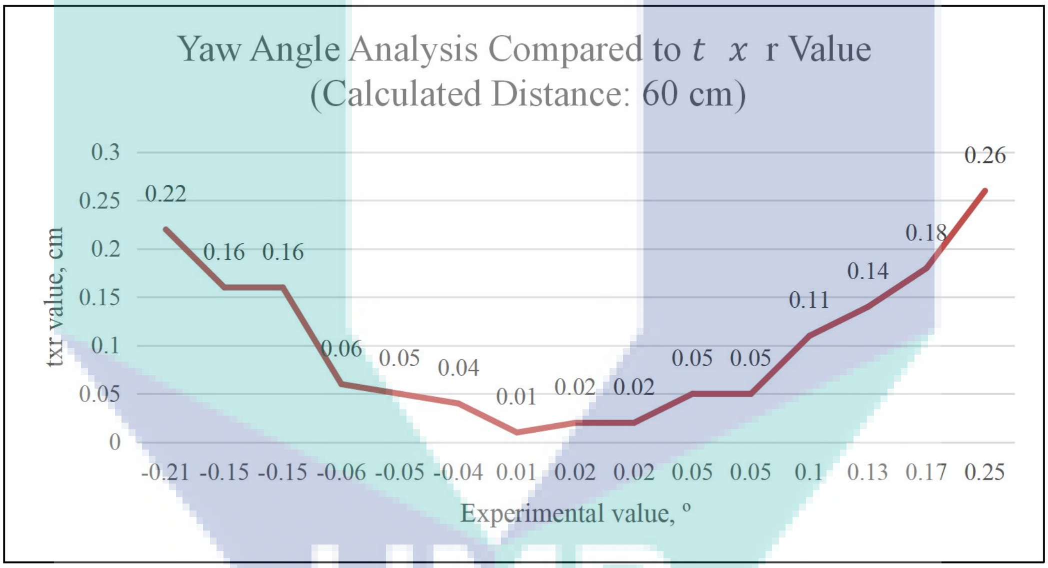

(b)

Figure 4.17 Analysis for yaw angle compared to tx_r value

Figure 4.17 shows that most of the tx_r value is less than 0.25 cm. In addition, at 0.25° angle and 60 cm distance, the tx_r value is 0.26 cm. However, the condition also can be accepted as aligned position. It is because at distance 60 cm, the tx_r value is 0.26 cm. From the analysis, it shows that the lower the distance, the lower the tx_r value. The camera will stop and move forward when the system detects the spool is aligned with the camera for the puller to be inserted to the CHS. Therefore, the tx_r value will be decrease and the angle value -0.25° to 0.25° can be accepted. From previous subchapter, it shows that the camera can detect the spool at 50-110 cm distance ranges whereas the puller's length is estimated around 50-60 cm. Therefore, at distance 50-60 cm, the puller can be insert to CHS.

4.5 Results of Camera Orientation System

In this subchapter, the experimental results of camera orientation system are presented. This stage began after spool is detected. The camera orientation to spool is calculated by using Equation 3.5 and 3.8 hence, the value is displayed on the screen. Next, the overlapping center is determined by using Rule 2 and display "Center overlapped" on the screen. In order to ensure the spool and camera are aligned with each other, the camera will move forward and focus on a SC which is in blue color. Lastly, the screen will display "Camera and spool aligned" once it fulfills the conditions. The conditions are:

i. Both centers overlapped the RC.

ii. The camera orientation angle is at -0.25° to 0.25° (theoretically at 0°).

iii. The distance between camera and spool is between 50-60 cm.

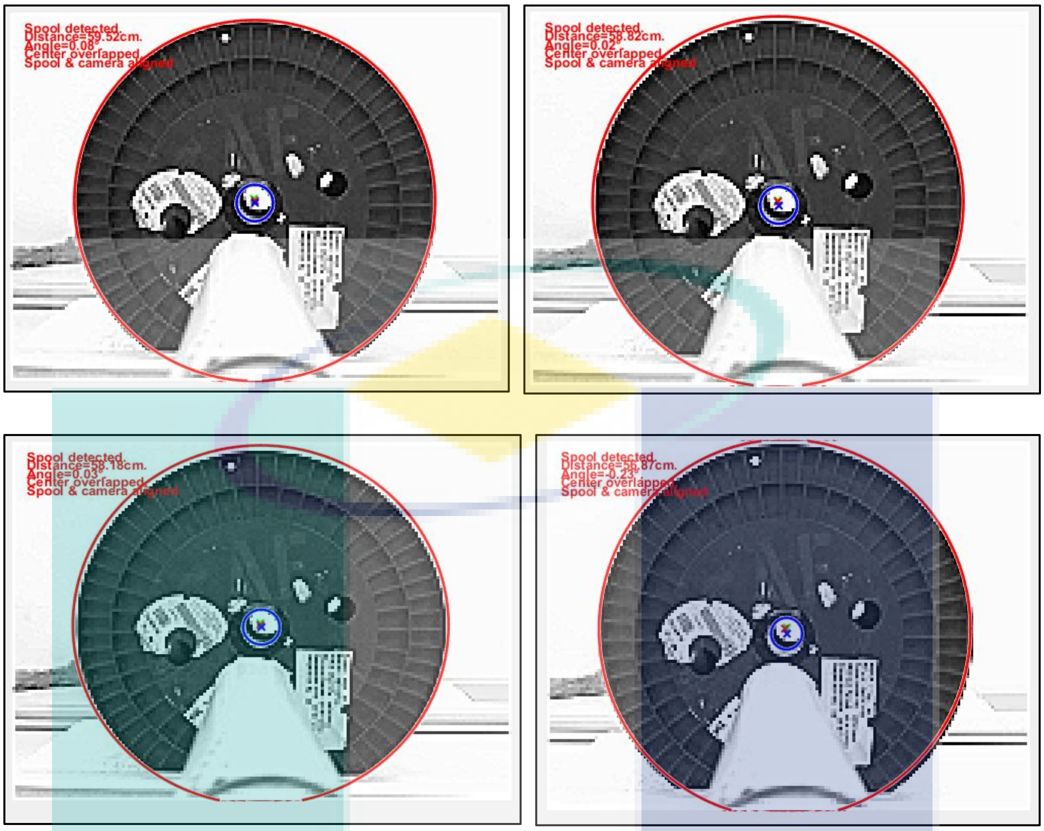

Figure 4.18 Camera and spool aligned in various situations

Figure 4.17 shows the results when the system detects the camera and spool aligned with each other. The puller can be insert to the CHS when the system detects the alignment of camera and spool.

4.6 Summary

This chapter has critically discussed the experimental results of proposed system. The aim of this study is to ensure the camera and spool orientation aligned each other by using image processing techniques so that the puller can be inserted perfectly into the CHS. The detection algorithm cannot provide better results by applied CHT method only. There are some errors due to illumination and noise that is hard to be eliminated at image processing stage especially for SC detections. The MCHT method is capable to detect the spool in different illumination factor. The illumination factor is tested with different illumination intensity and is analyzed in four conditions. However, the second conditions have low success rate for SC detection compared to others. Thus, it is proved that the proposed method is capable to detect the spool in any conditions for indoor performance except for second condition due to low error rate for SC detection. It will not be the cause of research failure because this research used the fourth condition. From the implementation of the detection algorithm, the accuracy of spool detection is achieved more than 90% compared to CHT method. The MCHT method is successfully proven. For camera orientation, the mathematical equation for camera's yaw angle is able to calculate the camera's yaw angle with 0% to 1.47% percentage error. The yaw angle is calculated from -5° to 20° compared with reference value. In order to calculate yaw angle at 0°, the tx_r value must less than 0.25 cm. The 0° angle value is calculated within 50-60 cm distance range. Therefore, the puller can be insert perfectly when the camera and spool is aligned at angle range -0.25° to 0.25°.

CHAPTER 5

CONCLUSION

5.1 Conclusion

The spool detection and camera orientation system by using image processing techniques in order to solve the peg-in-hole system is established in this study. The detection system is done through the Gaussian filter and Modified Circular Hough Transform (MCHT) for spool detection process. The performance of the detection rate by using this system achieved to 96% compared to existing method. This system is analyzed starting from the filtering, binarization and morphology by considering the issue of illumination, distance camera to the spool and camera orientation. The yaw angle is determined based on the spools' images conditions by using camera orientation system. The formula for tolerance between puller and small circle (SC) is derived in order to ensure the spool not scratch the spool hence, solve the peg-in-hole task. Next, this system is able to calculate the distance and yaw angle with low error rate. Therefore, the spool position can be determined based on image from camera without using Force/Torque sensor. This study accomplished the objectives through the experimental works carried out with acceptable error rate.

5.2 Summary of Contributions

MCHT method proves that it can be used to obtain camera's angle between camera and spool by only using simple algorithm with low cost camera and without any other sensors such as force sensor and torque sensor.

5.3 Future Research Directions

The results of this research highlight some improvement for future research that can be done. For detection, the future algorithm should be able to detect SC (hole of the spool) perfectly to increase the accuracy of detection. Secondly, the proposed future system should be implementing this proposed algorithm at outdoor environment so that, it covers all possibilities at indoor and outdoor environment. Finally, it is recommended that the proposed system algorithm to be integrated with a real-time robot in order to prove the system can be used with a real-time robot. Hence, the camera orientation can be verified.

REFERENCES

Abdullah, M. W., Roth, H., Weyrich, M., & Wahrburg, J. (2015). An approach for peg-in-hole assembling using intuitive search algorithm based on human behavior and carried by sensors guided industrial robot. *IFAC-PapersOnLine*, *28*(3), 1476–1481. https://doi.org/10.1016/j.ifacol.2015.06.295

Ali, H., Aizat, K., Yerkhan, K., Zhandos, T., & Anuar, O. (2018). Vision-based Robot Manipulator for Industrial Applications. *Procedia Computer Science*, *133*, 205–212. https://doi.org/10.1016/j.procs.2018.07.025

Azman, F. A., Daud, M. R., Mohamed, A. I., Irawan, A., & Ismail, R. M. T. R. (2017). Vision-based Object ' s Shape Determination for Robot Alignment. *Journal of Telecommunication, Electronic and Computer Engineering*, *10*(1), 111–115. Retrieved from http://journal.utem.edu.my/index.php/jtec/article/view/3330

Cai, W., Wen, X., Tu, Q., & Guo, X. (2019). Research on image processing of intelligent building environment based on pattern recognition technology. *Journal of Visual Communication and Image Representation*, *61*, 141–148. https://doi.org/10.1016/J.JVCIR.2019.03.014

Cangelosi, A., & Cangelosi, A. (2016). Stereo Vision based Object Tracking Control for a Movable Robot Head. *IFAC-PapersOnLine*, *49*(5), 155–162. https://doi.org/10.1016/j.ifacol.2016.07.106

Chang, W. C., & Wu, C. H. (2017). Automated USB peg-in-hole assembly employing visual servoing. *2017 3rd International Conference on Control, Automation and Robotics, ICCAR 2017*, 352–355. https://doi.org/10.1109/ICCAR.2017.7942717

Cho, K., Baeg, S., & Park, S. (2013). Real-time 3D multiple occluded object detection and tracking. *2013 44th International Symposium on Robotics, ISR 2013*, 1–5. https://doi.org/10.1109/ISR.2013.6695718

Czerniawski, T., Nahangi, M., Haas, C., & Walbridge, S. (2016). Pipe spool recognition in cluttered point clouds using a curvature-based shape descriptor. *Automation in Construction*, *71*(Part 2), 346–358. https://doi.org/10.1016/j.autcon.2016.08.011

Debortoli, L., Gallina, P., & Seriani, S. (2017). Peg-in-hole operation using a cobot without using external sensors. *Materials Today: Proceedings*, *5*(13), 1–3. https://doi.org/10.1016/j.matpr.2018.08.115

Deepu, R., Honnaraju, B., & Murali, S. (2015). Path Generation for Robot Navigation using a Single Camera. *Procedia Computer Science*, *46*, 1425–1432. https://doi.org/10.1016/j.procs.2015.02.061

Dong, W., Xiao, S., & Li, Y. (2018). Hyperspectral pansharpening based on guided filter and Gaussian filter. *Journal of Visual Communication and Image Representation*, *53*, 171–179. https://doi.org/10.1016/J.JVCIR.2018.03.014

Erkan, U., Gökrem, L., & Enginoğlu, S. (2018). Different applied median filter in salt and pepper noise. *Computers & Electrical Engineering*, *70*, 789–798. https://doi.org/10.1016/J.COMPELECENG.2018.01.019

Fu, Z., & Han, Y. (2012). A Circle Detection Algorithm Based on Mathematical Morphology and Chain Code. *2012 International Conference on Computing, Measurement, Control and Sensor Network*, 253–256. https://doi.org/10.1109/CMCSN.2012.61

Gandhi, N. J., Shah, V. J., & Kshirsagar, R. (2014). Mean shift technique for image segmentation and Modified Canny Edge Detection Algorithm for circle detection. *International Conference on Communication and Signal Processing, ICCSP 2014 - Proceedings*, (1), 246–250. https://doi.org/10.1109/ICCSP.2014.6949838

Gao, H., Hu, M., Gao, T., & Cheng, R. (2019). Robust detection of median filtering based on combined features of difference image. *Signal Processing: Image Communication*, *72*, 126–133. https://doi.org/10.1016/J.IMAGE.2018.12.014

Harada, K., Yoshimi, T., Kita, Y., Nagata, K., Yamanobe, N., Ueshiba, T., … Nakamura, O. (2014). *Project on Development of a Robot System for Random Picking – Grasp / Manipulation Planner for a Dual Arm Manipulator* –. 583–589. https://doi.org/10.1109/SII.2014.7028104

Hari, V. S., Jagathy Raj, V. P., & Gopikakumari, R. (2013). Unsharp masking using quadratic filter for the enhancement of fingerprints in noisy background. *Pattern Recognition*, *46*(12), 3198–3207. https://doi.org/10.1016/J.PATCOG.2013.05.014

Huang, S., Murakami, K., Yamakawa, Y., Senoo, T., & Ishikawa, M. (2013). Fast peg-and-hole alignment using visual compliance. *IEEE International Conference on Intelligent Robots and Systems*, 286–292. https://doi.org/10.1109/IROS.2013.6696366

Hussin, R., Juhari, M. R., Kang, N. W., Ismail, R. C., & Kamarudin, A. (2012). Digital image processing techniques for object detection from complex background image. *Procedia Engineering*, *41*(Iris), 340–344. https://doi.org/10.1016/j.proeng.2012.07.182

Jain, R. K., Majumder, S., & Dutta, A. (2013). SCARA based peg-in-hole assembly using compliant IPMC micro gripper. *Robotics and Autonomous Systems*, *61*(3), 297–311. https://doi.org/10.1016/j.robot.2012.12.001

Jasim, I. F., Plapper, P. W., & Voos, H. (2014). Position identification in force-guided robotic peg-in-hole assembly tasks. *Procedia CIRP*, *23*(C), 217–222. https://doi.org/10.1016/j.procir.2014.10.077

Jia, L. Q., & Peng, C. Z. (2012). A new circle detection method based on parallel operator. *Proceedings - International Conference on Machine Learning and Cybernetics*, *3*, 1085–1090. https://doi.org/10.1109/ICMLC.2012.6359506

Jiang, L., Wang, Z., Ye, Y., & Jiang, J. (2018). Fast circle detection algorithm based on sampling from difference area. *Optik*, *158*, 424–433. https://doi.org/10.1016/j.ijleo.2017.12.064

Kim, C., Han, D. S., Kim, J. K., & Kim, B. I. (2017). Automatic detection of defective welding electrode tips using color segmentation and Hough circle detection. *IEEE Region 10 Annual International Conference, Proceedings/TENCON*, 1371–1374. https://doi.org/10.1109/TENCON.2016.7848238

Kim, Y. L., Kim, B. S., & Song, J. B. (2012). Hole detection algorithm for square peg-in-hole using force-based shape recognition. *IEEE International Conference on Automation Science and Engineering*, 1074–1079. https://doi.org/10.1109/CoASE.2012.6386340

Landini, G., Galton, A., Randell, D., & Fouad, S. (2019). Novel applications of discrete mereotopology to mathematical morphology. *Signal Processing: Image Communication*, *76*, 109–117. https://doi.org/10.1016/J.IMAGE.2019.04.018

Lestriandoko, N. H., & Sadikin, R. (2017). Circle detection based on hough transform and Mexican Hat filter. *Proceeding - 2016 International Conference on Computer, Control, Informatics and Its Applications: Recent Progress in Computer, Control, and Informatics for Data Science, IC3INA 2016*, (1), 153–157. https://doi.org/10.1109/IC3INA.2016.7863041

Li, D., Nan, F., Xue, T., & Yu, X. (2017). Circle detection of short arc based on Randomized Hough Transform. *2017 IEEE International Conference on Mechatronics and Automation (ICMA)*, 258–263. https://doi.org/10.1109/ICMA.2017.8015824

Li, S., & Tie, Y. (2010). A robust high-precision circular target detection method based on Hough Transform. *ICCASM 2010 - 2010 International Conference on Computer Application and System Modeling, Proceedings*, *14*(Iccasm), 253–257. https://doi.org/10.1109/ICCASM.2010.5622319

Lin, L. L., Yang, Y., Song, Y. T., Nemec, B., Ude, A., Rytz, J. A., … Savarimuthu, T. R. (2015). Peg-in-Hole assembly under uncertain pose estimation. *Proceedings of the World Congress on Intelligent Control and Automation (WCICA)*, *2015-March*(March), 2842–2847. https://doi.org/10.1109/WCICA.2014.7053179

Lin, S. C. F., Wong, C. Y., Jiang, G., Rahman, M. A., Ren, T. R., Kwok, N., … Wu, T. (2016). Intensity and edge based adaptive unsharp masking filter for color image enhancement. *Optik*, *127*(1), 407–414. https://doi.org/10.1016/J.IJLEO.2015.08.046

Liu, N., Liu, Z., Wei, Q., & Cui, L. (2018). A containerized simulation platform for robot learning peg-in-hole task. *Proceedings of the 13th IEEE Conference on Industrial Electronics and Applications, ICIEA 2018*, 1290–1295. https://doi.org/10.1109/ICIEA.2018.8397908

Lo, R.-C., & Hsu, H.-C. (2016). A Circular Band Extraction Method Based on Extended Hough Transform. *International Journal of Pattern Recognition and Artificial Intelligence*, *30*(08), 1655021. https://doi.org/10.1142/S0218001416550211

Luo, J., Chen, X., & Hu, Y. (2017). *A fast circle detection method based on threshold segmentation and validity check for FPC images*. 3214–3217.

Luu, T. H., & Tran, T. H. (2015). 3D vision for mobile robot manipulator on detecting and tracking target. *ICCAS 2015 - 2015 15th International Conference on Control, Automation and Systems, Proceedings*, (Iccas), 1560–1565. https://doi.org/10.1109/ICCAS.2015.7364605

Meng, Y., Zhang, Z., Yin, H., & Ma, T. (2018). Automatic detection of particle size distribution by image analysis based on local adaptive canny edge detection and modified circular Hough transform. *Micron*, *106*(December 2017), 34–41. https://doi.org/10.1016/j.micron.2017.12.002

Mironov, K. (2017). Transport by robotic throwing and catching: Accurate stereo tracking of the spherical object. *2017 International Conference on Industrial Engineering, Applications and Manufacturing, ICIEAM 2017 - Proceedings*. https://doi.org/10.1109/ICIEAM.2017.8076490

Mohamed, A., Yang, C., & Cangelosi, A. (2016). Stereo Vision based Object Tracking Control for a Movable Robot Head. *IFAC-PapersOnLine*, *49*(5), 155–162. https://doi.org/10.1016/j.ifacol.2016.07.106

Ni, J., Khan, Z., Wang, S., Wang, K., & Haider, S. K. (2016). Automatic detection and counting of circular shaped overlapped objects using circular hough transform and contour detection. *Proceedings of the World Congress on Intelligent Control and Automation (WCICA)*, *2016-Septe*(Kylx15 0496), 2902–2906. https://doi.org/10.1109/WCICA.2016.7578268

Ortega-Aranda, D., Lopez-Juarez, I., Nath-Saha, B., Osorio-Comparan, R., Peña-Cabrera, M., & Lefranc, G. (2017). Towards learning contact states during peg-in-hole assembly with a dual-arm robot. *2017 CHILEAN Conference on Electrical, Electronics Engineering, Information and Communication Technologies, CHILECON 2017 - Proceedings*, *2017-Janua*, 1–6. https://doi.org/10.1109/CHILECON.2017.8229694

Park, H., Bae, J.-H., Park, J.-H., Baeg, M.-H., & Park, J. (2013). Intuitive peg-in-hole assembly strategy with a compliant manipulator. *IEEE ISR 2013*, 1–5. https://doi.org/10.1109/ISR.2013.6695699

Park, H., Park, J., Lee, D. H., Park, J. H., Baeg, M. H., & Bae, J. H. (2017). Compliance-Based Robotic Peg-in-Hole Assembly Strategy Without Force Feedback. *IEEE Transactions on Industrial Electronics*, *64*(8), 6299–6309. https://doi.org/10.1109/TIE.2017.2682002

Park, D. Il, Park, C., Do, H., Choi, T., & Kyung, J. (2012). Assembly phase estimation in the square peg assembly process. *Iccas*, 2135–2138.

Qu, J., Li, Y., & Dong, W. (2018). Fusion of hyperspectral and panchromatic images using an average filter and a guided filter. *Journal of Visual Communication and Image Representation*, *52*, 151–158. https://doi.org/10.1016/J.JVCIR.2018.01.006

Road, J., & District, Y. (2013). Circle And Circular Arc Detection Algorithm Research Based on Freeman Chain Code. *2013 IEEE 4th International Conference on Electronics Information and Emergency Communication*, 3–6. https://doi.org/10.1109/ICEIEC.2013.6835494

Rodrigues, É. O., Conci, A., & Liatsis, P. (2018). Morphological classifiers. *Pattern Recognition*, *84*, 82–96. https://doi.org/10.1016/J.PATCOG.2018.06.010

Schranzer, R., Rauscher, A., Haimburger, E., Bredies, K., Reishofer, G., & Grabner, G. (2018). Noise reduction in FLAIR2 images using total generalized variation, Gaussian and Wiener filtering. *Zeitschrift Für Medizinische Physik*, *28*(4), 286–292. https://doi.org/10.1016/J.ZEMEDI.2017.11.001

Scitovski, R., & Marošević, T. (2015). Multiple circle detection based on center-based clustering. *Pattern Recognition Letters*, *52*, 9–16. https://doi.org/10.1016/J.PATREC.2014.09.010

Shim, J.-H., & Cho, Y.-I. (2015). A Mobile Robot Localization using External Surveillance Cameras at Indoor. *Procedia Computer Science*, *56*, 502–507. https://doi.org/10.1016/j.procs.2015.07.242

Soans, R. V., Ranjith, Hegde, A., Singh, C., & Kumar, A. (2018). Object tracking robot using adaptive color thresholding. *Proceedings of the 2nd International Conference on Communication and Electronics Systems, ICCES 2017*, *2018-Janua*(Icces), 790–793. https://doi.org/10.1109/CESYS.2017.8321192

Šuligoj, F., Šekoranja, B., Švaco, M., & Jerbić, B. (2014). Object Tracking with a Multiagent Robot System and a Stereo Vision Camera. *Procedia Engineering*, *69*, 968–973. https://doi.org/10.1016/j.proeng.2014.03.077

Suzuki, Y., Koyama, K., Ming, A., & Shimojo, M. (2015). Grasping strategy for moving object using Net-Structure Proximity Sensor and vision sensor. *Robotics and Automation (ICRA), 2015 IEEE International Conference On*, 1403–1409. https://doi.org/10.1109/ICRA.2015.7139373

Takahashi, J., Fukukawa, T., & Fukuda, T. (2016). Passive Alignment Principle for Robotic Assembly between a Ring and a Shaft with Extremely Narrow Clearance. *IEEE/ASME Transactions on Mechatronics*, *21*(1), 196–204. https://doi.org/10.1109/TMECH.2015.2448639

Troppan, A., Guerreiro, E., Celiberti, F., Santos, G., Ahmad, A., & Lima, P. U. (2013). Unknown-color spherical object detection and tracking. *Proceedings of the 2013 13th International Conference on Autonomous Robot Systems, ROBOTICA 2013*, 1–4. https://doi.org/10.1109/Robotica.2013.6623533

Tsarouchi, P., Matthaiakis, S. A., Michalos, G., Makris, S., & Chryssolouris, G. (2016). A method for detection of randomly placed objects for robotic handling. *CIRP Journal of Manufacturing Science and Technology*, *14*, 20–27. https://doi.org/10.1016/j.cirpj.2016.04.005

Van Wyk, K., Culleton, M., Falco, J., & Kelly, K. (2018). Comparative Peg-in-Hole Testing of a Force-Based Manipulation Controlled Robotic Hand. *IEEE Transactions on Robotics*, *34*(2), 542–549. https://doi.org/10.1109/TRO.2018.2791591

Vishwakarma, A., Bhuyan, M. K., & Iwahori, Y. (2018). An optimized non-subsampled shearlet transform-based image fusion using Hessian features and unsharp masking. *Journal of Visual Communication and Image Representation*, *57*, 48–60. https://doi.org/10.1016/J.JVCIR.2018.10.005

Xu, J., Hou, Z., Wang, W., Xu, B., Zhang, K., & Chen, K. (2018). Feedback Deep Deterministic Policy Gradient with Fuzzy Reward for Robotic Multiple Peg-in-hole Assembly Tasks. *IEEE Transactions on Industrial Informatics*, *PP*(c), 1–1. https://doi.org/10.1109/TII.2018.2868859

Yadav, V. K., Batham, S., Acharya, A. K., & Paul, R. (2014). Approach to accurate circle detection: Circular Hough Transform and Local Maxima concept. *2014 International Conference on Electronics and Communication Systems, ICECS 2014*, 3–7. https://doi.org/10.1109/ECS.2014.6892577

Yao, Z., & Yi, W. (2016). Curvature aided Hough transform for circle detection. *Expert Systems with Applications*, *51*, 26–33. https://doi.org/10.1016/j.eswa.2015.12.019

Zhang, K., Xu, J., Chen, H., Zhao, J., & Chen, K. (2018). Jamming Analysis and Force Control for Flexible Dual Peg-in-hole Assembly. *IEEE Transactions on Industrial Electronics*, *0046*(c). https://doi.org/10.1109/TIE.2018.2838069

Zheng, Y., Zhang, X., Chen, Y., & Huang, Y. (2017). Peg-in-hole Assembly based on Hybrid Vision / Force Guidance and Dual-arm Coordination. *Proceedings of the 2017 IEEE International Conference on Robotics and Biomimetics, Macau*, 418–423.

LIST OF PUBLICATIONS

1. FA Azman, MR. Daud, AI Mohamed, A. Irawan & RM Taufika RM Ismail (2017). Vision-based Object's Shape Determination for Robot Alignment. *International Conference on Electrical, Control & Computer Engineering, INECCE 2017, Langkawi, Malaysia.*

2. A. Irawan, MA Yaacob, FA Azman, MR Daud, AR Razali & SN Sheikh Ali (2018). Vision-based Alignment Control for Mini Forklift System in Confine Area Operation. *International Symposium on Agents, Multi-Agent Systems and Robotics, ISAMSR 2018, Putrajaya, Malaysia.*

APPENDIX A
IMPORTANT CODING FOR PROPOSED ALGORITHM

```
while (true)
    trigger(vid);

    %get a single image frame
    image = getdata(vid);
    fill = imgaussfilt(image, 2);
    bw=im2bw(fill,0.35);
    se2=strel('disk',[2]);
    op=imopen(bw,[se2]);
    c=bwareaopen(op,30);

%reference circle center
imageCenter = [80, 50];


%range radius big and small circle(diff range)
[center, radii] = imfindcircles(c,[35 65],'ObjectPolarity','dark','Sensitivity',0.89);%as
[center2, radii2] = imfindcircles(c,[3 15],'ObjectPolarity','bright','Sensitivity',0.89);
```

```
plot(imageCenter(:,1),imageCenter(:,2),'yx','LineWidth',2,'Color','g');
%find big circle
if (radii)
      plot(center(1,1),center(1,2),'yx','LineWidth',2,'Color','r');
      viscircles(center, radii,'EdgeColor','r');
      message = sprintf('Spool detected.');
      text(5,5,message,'Color','r','FontWeight','bold');

%find small circle (all)
if (radii2)

     %Define every center in system
       circleCenterX = center(1,1);
       circleCenterY = center(1,2);

      circleCenterX2 = center2(:,1);
       circleCenterY2 = center2(:,2);

       imageCenterX = imageCenter(1,1);
       imageCenterY = imageCenter(1,2);
```

```
%calculate the distance between center
 distanceX = circleCenterX - imageCenterX;
 distanceY = circleCenterY - imageCenterY;

 distanceX2=circleCenterX2-imageCenterX;
 distanceY2=circleCenterY2-imageCenterY;

distanceXX=circleCenterX-circleCenterX2;
distanceYY=circleCenterY-circleCenterY2;


%Calculate distance between camera and object
a=(0.4*35.0*120);    %a=(focal,cm x real height-diameter spool,cm x in
b=((radii*2)*0.24); %b=(object height,px x sensor height,cm)
totaldistance=a/b;
message =sprintf('\nDistance=%.2fcm.',...
                      totaldistance);
 text(5,5,message,'Color','r','FontWeight','bold');
```

```
%calculate camera angle
m=60/(sqrt((120^2+160^2)));  %60deg (FOV) %120x160 (resolution)
n=distanceX ;                %center-center besar
totalangle=m*n;
message =sprintf('\n\nAngle=%.2f°.',...
                     totalangle);
text(5,5,message,'Color','r','FontWeight','bold');


%find small circle (real)
 if (distanceXX>=-5)&(distanceXX<=5)&(distanceYY>=-5)&(distanceYY<=5)
p2=plot(center2(:,1),center2(:,2),'yx','LineWidth',2,'Color','b');
v2=viscircles(center2, radii2,'EdgeColor','b');


%calculation for center overlapped
if (distanceX>=-2)&(distanceX<=2)&(distanceY>=-2)&(distanceY<=2)&...
   (distanceX2>=-2)&(distanceX2<=2)&(distanceY2>=-2)&(distanceY2<=2)
   message = sprintf('\n\n\nCenter overlapped.');
   text(5,5,message,'Color','r','FontWeight','bold');
```

```
if (distanceX>=-2)&(distanceX<=2)&(distanceY>=-2)&(distanceY<=2)&...
(distanceX2>=-2)&(distanceX2<=2)&(distanceY2>=-2)&(distanceY2<=2)&...
(totaldistance<=60)&(totalangle>=-1)&(totalangle<=1)
message =sprintf('\n\n\n\nSpool & camera aligned');
text(5,5,message,'Color','r','FontWeight','bold');

pause (1);
```

APPENDIX B
SENSOR HEIGHT ANALYSIS

Measured distance (cm)	Object height (pixel)	Sensor height (cm)
133.0	53.09	0.24
	52.83	0.24
	52.95	0.24
	53.10	0.24
117.0	61.40	0.23
	61.15	0.23
	60.98	0.24
	61.05	0.24
109.0	62.98	0.24
	62.85	0.25
	63.01	0.24
	63.05	0.24
102.0	69.56	0.24
	69.61	0.24
	69.50	0.24
	69.68	0.24
98.0	71.32	0.24
	71.22	0.24
	71.27	0.24
	71.24	0.24
94.0	74.02	0.24
	74.05	0.24
	73.96	0.24
	73.91	0.24

APPENDIX C
DISTANCE CALCULATION ANALYSIS

No.	Real distance (cm)	Calculated distance (cm)	Percentage error (%)
1	96.0	96.1	0.10
2		96.2	0.21
3		95.8	0.21
4		96.5	0.52
5		95.4	0.63
6		96.8	0.83
7		96.8	0.83
8		97.1	1.15
9		97.2	1.25
10		97.3	1.35
11	102.0	102.1	0.10
12		101.8	0.20
13		102.4	0.39
14		102.4	0.39
15		102.6	0.59
16		102.7	0.69
17		102.9	0.88
18		103.0	0.98
19		103.3	1.27
20		103.6	1.57
21	110.0	110.4	0.36
22		110.3	0.27
23		110.5	0.45
24		111.1	1.00
25		110.0	0.00
26		110.9	0.82
27		110.8	0.73
28		109.7	0.27
29		110.3	0.27
30		109.8	0.18

APPENDIX D
YAW ANGLE ANALYSIS COMPARED TO tx_r VALUE

No.	Calculated distance (cm)	Experimental value (°)	tx_r value (cm)
1		0.01	0.01
2		0.03	0.03
3		-0.05	0.04
4		-0.12	0.11
5		0.13	0.11
6		0.01	0.01
7		-0.22	0.19
8	50.0	0.12	0.11
9		0.04	0.04
10		0.1	0.09
11		-0.03	0.03
12		0.03	0.03
13		0.08	0.07
14		0.23	0.20
15		-0.07	0.06
16		0.01	0.01
17		-0.04	0.04
18		0.05	0.05
19		0.05	0.05
20		0.1	0.11
21		0.13	0.14
22		-0.05	0.05
23	60.0	0.02	0.02
24		0.17	0.18
25		-0.15	0.16
26		-0.06	0.06
27		0.25	0.26
28		0.02	0.02
29		-0.15	0.16
30		-0.21	0.22

APPENDIX E
40 DATA SAMPLES (V1-V40)

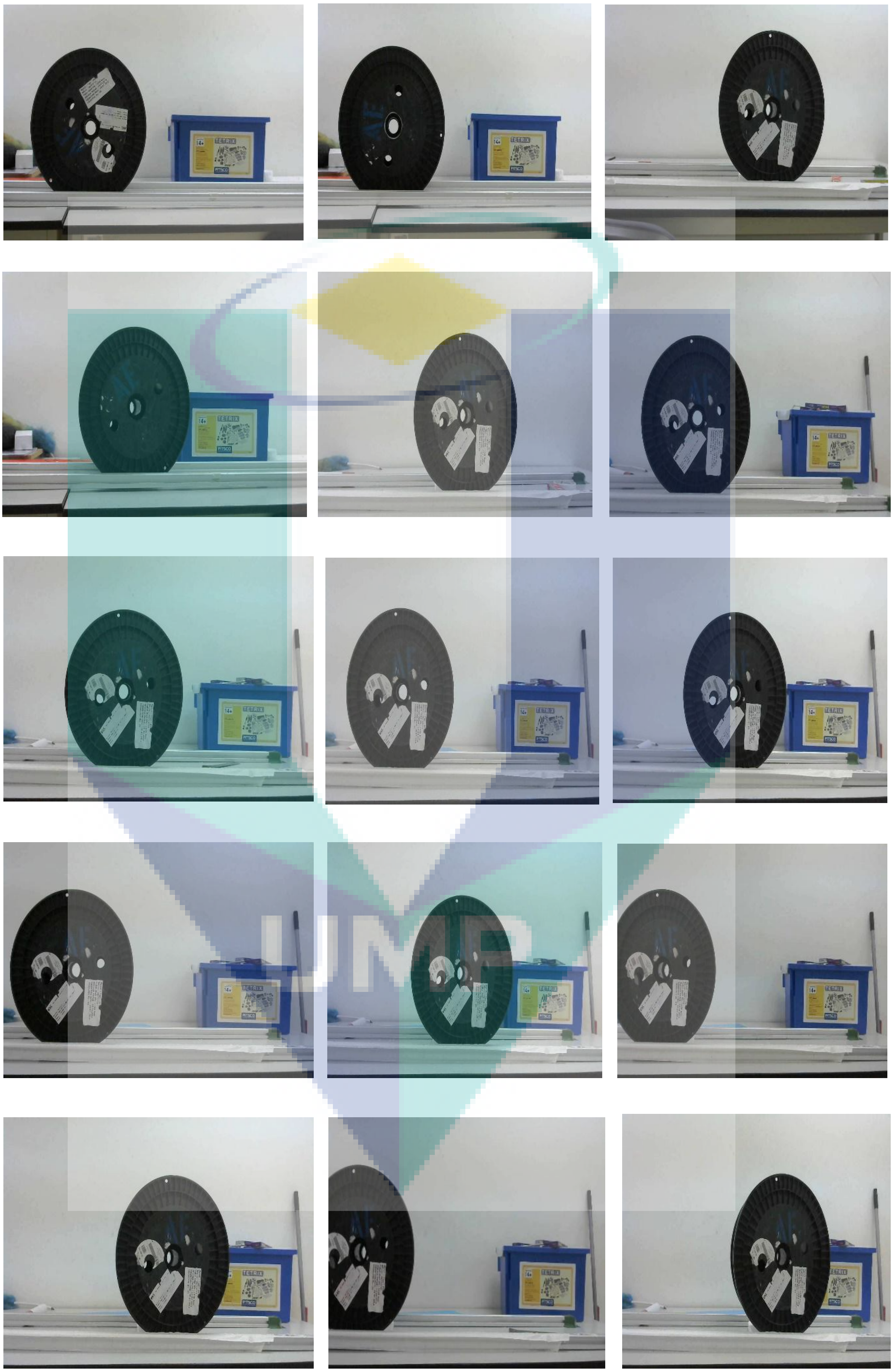

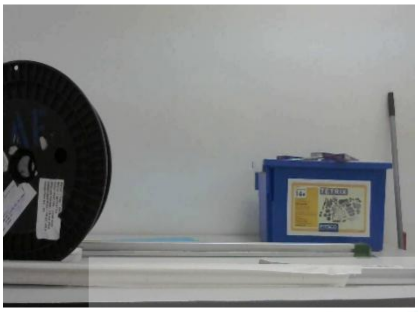








APPENDIX F
BINARY THRESHOLDING ANALYSIS